Structural Evolution of the Kohat and Potwar Fold and Thrust Belts of Pakistan

Dissertation

Von

Humaad Ghani

zur Erlangung des akademischen Grades

DOCTOR RERUM NATURALIUM

»DR. RER. NAT.«

in der Wissenschaftsdisziplin

Geologie

eingereicht an der

Mathematisch-Naturwissenschaftlichen Fakultät

der Universität Potsdam

Potsdam, im June 2019

Datum der Disputation: 20.11. 2019

Supervisors

apl Prof. Edward Sobel

Dr Gerold Zeilinger
Institute of Geosciences, University of Potsdam, Germany

Referees

1: **Dr Gerold Zeilinger**
Institute of Geosciences, University of Potsdam, Germany

2: **Prof. Delores Robinson**
Department of Geological Sciences, University of Alabama, USA

3: **Prof. Peter van der Beek**
ISTerre Université Grenoble Alpes, France

Published online at the
Institutional Repository of the University of Potsdam:
https://doi.org/10.25932/publishup-44077
https://nbn-resolving.org/urn:nbn:de:kobv:517-opus4-440775

To my father

who left, when I started to understand him

Table of Contents

List of Figures

Chapter 4

Chapter 5

Appendix 1 (Chapter 4)

Appendix 2 (Chapter 5)

List of Tables

Abstract

Fold and thrust belts are characteristic features of collisional orogen that grow laterally through time by deforming the upper crust in response to stresses caused by convergence. The deformation propagation in the upper crust is accommodated by shortening along major folds and thrusts. The formation of these structures is influenced by the mechanical strength of décollements, basement architecture, presence of preexisting structures and taper of the wedge. These factors control not only the sequence of deformation but also cause differences in the structural style.

The Himalayan fold and thrust belt exhibits significant differences in the structural style from east to west. The external zone of the Himalayan fold and thrust belt, also called the Subhimalaya, has been extensively studied to understand the temporal development and differences in the structural style in Bhutan, Nepal and India; however, the Subhimalaya in Pakistan remains poorly studied. The Kohat and Potwar fold and thrust belts (herein called Kohat and Potwar) represent the Subhimalaya in Pakistan. The Main Boundary Thrust (MBT) marks the northern boundary of both Kohat and Potwar, showing that these belts are genetically linked to foreland-vergent deformation within the Himalayan orogen, despite the pronounced contrast in structural style. This contrast becomes more pronounced toward south, where the active strike-slip Kalabagh Fault Zone links with the Kohat and Potwar range fronts, known as the Surghar Range and the Salt Range, respectively. The Surghar and Salt Ranges developed above the Surghar Thrust (SGT) and Main Frontal Thrust (MFT). In order to understand the structural style and spatiotemporal development of the major structures in Kohat and Potwar, I have used structural modeling and low temperature thermochronolgy methods in this study. The structural modeling is based on construction of balanced cross-sections by integrating surface geology, seismic reflection profiles and well data. In order to constrain the timing and magnitude of exhumation, I used apatite (U-Th-Sm)/He (AHe) and apatite fission track (AFT) dating. The results obtained from both methods are combined to document the Paleozoic to Recent history of Kohat and Potwar.

The results of this research suggest two major events in the deformation history. The first major deformation event is related to Late Paleozoic rifting associated with the development of the Neo-Tethys Ocean. The second major deformation event is related to the Late Miocene to Pliocene development of the Himalayan fold and thrust belt in the Kohat and Potwar. The Late Paleozoic rifting is deciphered by inverse thermal modelling of detrital AFT and AHe ages from the Salt Range. The process of rifting in this area created normal faulting that resulted in the exhumation/erosion of Early to Middle Paleozoic strata, forming a major unconformity between Cambrian and Permian strata that is exposed today in the Salt Range. The normal faults formed in Late Paleozoic time played an important role in localizing the Miocene-Pliocene deformation in this area. The combination of structural reconstructions and thermochronologic data suggest that deformation initiated at 15±2 Ma on the SGT ramp in the southern part of Kohat. The early movement on the SGT accreted the foreland into the Kohat deforming wedge, forming the range front. The development of the MBT at 12±2 Ma formed the northern boundary of Kohat and Potwar. Deformation

propagated south of the MBT in the Kohat on double décollements and in the Potwar on a single basal décollement. The double décollement in the Kohat adopted an active roof-thrust deformation style that resulted in the disharmonic structural style in the upper and lower parts of the stratigraphic section. Incremental shortening resulted in the development of duplexes in the subsurface between two décollements and imbrication above the roof thrust. Tectonic thickening caused by duplexes resulted in cooling and exhumation above the roof thrust by removal of a thick sequence of molasse strata. The structural modelling shows that the ramps on which duplexes formed in Kohat continue as tip lines of fault propagation folds in the Potwar. The absence of a double décollement in the Potwar resulted in the preservation of a thick sequence of molasse strata there. The temporal data suggest that deformation propagated in-sequence from ~ 8 to 3 Ma in the northern part of Kohat and Potwar; however, internal deformation in the Kohat was more intense, probably required for maintaining a critical taper after a significant load was removed above the upper décollement. In the southern part of Potwar, a steeper basement slope ($\beta \geq 3°$) and the presence of salt at the base of the stratigraphic section allowed for the complete preservation of the stratigraphic wedge, showcased by very little internal deformation. Activation of the MFT at ~4 Ma allowed the Salt Range to become the range front of the Potwar. The removal of a large amount of molasse strata above the MFT ramp enhanced the role of salt in shaping the structural style of the Salt Range and Kalabagh Fault Zone. Salt accumulation and migration resulted in the formation of normal faults in both areas. Salt migration in the Kalabagh fault zone has triggered out-of-sequence movement on ramps in the Kohat.

The amount of shortening calculated between the MBT and the SGT in Kohat is 75±5 km and between the MBT and the MFT in Potwar is 65±5 km. A comparable amount of shortening is accommodated in the Kohat and Potwar despite their different widths: 70 km Kohat and 150 km Potwar. In summary, this research suggests that deformation switched between different structures during the last ~15 Ma through different modes of fault propagation, resulting in different structural styles and the out-of-sequence development of Kohat and Potwar.

Zusammenfassung

Falten- und Überschiebungsgürtel sind charakteristische Merkmale von Kollisionsorogenen, die sich im Laufe der Zeit als Reaktion auf konvergente Spannungen in das Vorland vorbauen. Die Deformationsausbreitung in der oberen Kruste erfolgt durch die Verkürzung entlang von Falten und Überschiebungen. Die Bildung dieser Strukturen wird durch die mechanische Eigenschaft des Décollements (Abscherhorizonts), dem Aufbau des Grundgebirges, der strukturellen Vorprägung und der Geometrie des Verfomungskeils beeinflusst. Diese Faktoren steuern nicht nur die Verformungsabfolge, sondern führen auch zu unterschiedlichen Strukturen im Falten- und Überschiebungsgürtel.

Der Himalaya Falten- und Überschiebungsgürtel zeigt signifikante Unterschiede im strukturellen Bau von Ost nach West. Die äußere Zone des Himalaya Falten- und Überschiebungsgürtel, auch Subhimalaya genannt, ist hinsichtlich der zeitliche Entwicklung und des strukturellen Baus in der Region von Bhutan, Nepal und Indien gut untersucht. Im Gegensatz dazu ist die Geologie des pakistanischen Subhimalayas erst in groben Zügen verstanden. Der Kohat- und der Potwar- Falten- und Überschiebungsgürtel (im Folgenden einfach Kohat und Potwar genannt) sind Teil der externe Sedimentationszone des Himalaya-Falten- und Überschiebungsgürtel in Pakistan. Die „Main Boundary Thrust“ (MBT) markiert ihre nördliche Grenze und zeigt, dass beide, sowohl Kohat als auch Potwar, trotz ihres unterschiedlichen strukturellen Baus durch eine gemeinsame, ins Vorland gerichteten Verformung des Himalaya-Orogens entstanden sind. Der Kontrast im strukturelle Bau wird nach Süden ausgeprägter, wo die aktive Kalabagh Seitenverschiebung die frontalen Deformationszonen Kohats und Potwars verbindet, die als „Surghar Range“ bzw. „Salt Range“ bekannt sind. Die „Surghar Range“ und die „Salt Range“ entwickeln sich oberhalb der Surghar Überschiebung (Surghar Thrust, SGT) und der frontalen Hauptüberschiebung (Main Frontal Thrust, MFT). Ziel dieser Studie ist es, die Deformationsentwicklung und den strukturellen Bau Kohats und Potwars als Beispiel für die Vielfalt der Entwicklung im frontalen Bereich von Orogenen zu entschlüsseln. Um den strukturellen Stil und die räumlich-zeitliche Entwicklung der Hauptstrukturen in Kohat und Potwar zu untersuchen, werden in dieser Studie Strukturmodellierungs- und Niedertemperatur-Thermochronologie-Methoden verwendet. Die Strukturmodellierung basiert auf der Erstellung bilanzierter Profile, deren Grundlage die Kombination von Oberflächengeologie, seismischen Reflexionsprofilen und Bohrlochdaten bildet. Die Niedertemperatur-Thermochronologie-Methoden gründen einerseits auf Apatit (U-Th-Sm)/He (AHe) und andererseits auf Apatit-Spaltspur (AFT) Datierungen. Die Resultate beider Methoden erlauben die zeitliche Rekonstruktion von Kohat und Potwar vom Paläozoikum bis zur jüngsten Geschichte.

Die Ergebnisse dieser Studie deuten auf zwei Hauptereignisse in der Verformungsgeschichte hin. Das erste große Deformationsereignis steht im Zusammenhang mit der spätpaläozoischen Riftbildung im Zuge der Öffnung der Neotethys. Das zweite große Deformationsereignis steht im Zusammenhang mit der spätmiozänen bis pliozänen Entwicklung des Himalaya Falten- und Überschiebungsgürtel. Die spät-paläozoische Riftbildung wird mittels einer inversen thermischen Modellierung der Apatit-AFT und AHe-

Alter aus der „Salt Range“ rekonstruiert. Der Prozess des Riftbildung verursachte Abschiebungen, die zur Exhumierung bzw. Erosion früh- bis mittelpaläozoischer Schichten führte und eine bedeutende Diskordanz zwischen kambrischen und permischen Schichten ausbildet, die heute in der „Salt Range“ aufgeschlossen ist. Diese im Spätpaläozoikum entstandenen Abschiebungen wurden dann während der miozän-pliozänen Bildung des Falten- und Überschiebungsgürtel reakiviert.

Die Rekonstruktion der Strukturen, kombiniert mit der Datierung (AFT, AHe), deutet darauf hin, dass die Verformung um ca. 15±2 Ma auf der SGT-Rampe im südlichen Teil Kohats aktiv war. Diese erste Deformation entlang der SGT hat das Vorland an den Kohat-Verformungskeil geschweisst und bildet damit die neue Verformungsfront. Die MBT bildete um ca. 12±2 Ma die nördliche Grenze von Kohat und Potwar. Die Deformation breitete sich in südlicher Richtung von der MBT aus in Kohat auf zwei Décollements aus, während sich in Potwar ein einziges basales Décollement bildete. Die beiden parallelen Décollements in Kohat formten aktive Dachüberschiebungen aus, die zum disharmonischen Stil im oberen und unteren Teil des Profils führten. Die inkrementelle Verkürzung formte Duplex-Strukturen zwischen den beiden Décollements und Schuppen oberhalb der Dachüberschiebung. Auf die tektonische Verdickung durch die Duplex-Strukturen folgte die Abkühlung bzw. Exhumation oberhalb der Dachüberschiebung durch die Abtragung mächtiger Molasseschichten. Die Rekonstruktion der Strukturen zeigt, dass die Rampen, auf denen die Duplex-Strukturen in Kohat gebildet wurden, sich in Potwar als Frontallinien der frontalen Knickung fortsetzen. Das Fehlen der beiden parallelen Décollements in Potwar führte zur Erhaltung dicker Molassenschichten in der stratigraphischen Abfolge.

Die Ergebnisse der Datierung deuten darauf hin, dass sich die Verformung dann von ca. 8 bis 3 Ma normal im nördlichen Teil von Kohat und Potwar in Richtung Süden ausbreitete. Die Verformung in Kohat war intensiver durch die Bildung eines kritischen Winkels im Deformationskeil, als die signifikante Auflast über dem oberen Décollement entfernt wurde. Der südliche Teil Potwars dagegen ist durch eine geringe interne Verfomung gekennzeichnet, hervorgerufen durch eine geringere Neigung der basalen Überschiebung ($\beta \geq 3°$) und das Vorhandensein von Salz an der Basis der stratigraphischen Abfolge. Dabei ist stratigraphische Abfolge innerhalb des Deformationskeils erhalten. Mit der Deformation entlang der MFT um ca. 4 Ma begann die Entwicklung der „Salt Range“ als frontale Deformationszone von Potwar. Die Abtragung dicker Molassenschichten über der MFT-Rampe verstärkte die Rolle des Salzes bei der Deformation der „Salt Range“ und der Kalabagh-Störungszone. In beiden Gebieten kam es zu Abschiebungen duch Salzakkumulation und Salzmigration. Die Salzmigration in der Kalabagh- Störungszone hat durchbrechende Überschiebungen entlang der Rampen in Kohat ausgelöst.

Der Verkürzungsbetrag zwischen MBT und SGT beträgt für Kohat 75±5 km und für Potwar zwischen MBT und MFT 65±5 km. Sowohl Kohat und Potwar haben trotz ihrer unterschiedlichen räumlichen Ausdehnung (70 km Kohat und 150 km Potwar) eine vergleichbare Verkürzung erfahren. Zusammenfassend lässt sich sagen, dass diese Studie aufzeigt, wie die Verformung zwischen den einzelnen Strukturen in den letzten ~15 Ma, verursacht durch unterschiedliche Deformationsausbreitung, gesprungen ist und damit für die

unterschiedlichen spezifischen Struktur-Stile und durchbrechende Deformationssequenzen in Kohat und Potwar verantwortlich ist.

Preface

Education is to some people and societies a basic right, to some it is a privilege and to many of them it is still a dream today. I was born at Mansehra, a small beautiful town in the Himalaya. I lived with my six siblings. When my parents had to decide which of six children will get the better education, obviously my brothers and I were preferred over our sisters, as is common in the developing world. This was the first privilege I got and ultimately my two elder sisters' education was sacrificed, as I used their part of the money for a better school. Today I am happy that we realized this mistake; their daughters now go to the same school as their sons.

The decision of moving to Germany and getting a PhD was not the only primary goal. I moved to Germany to broaden my vision and exposure of the world, especially after spending twenty-eight years in the same country. When I look back today, I see a very clear transformation in my views about society, I understood how society begins to transform for the better by accepting and safeguarding equal human rights, women's empowerment, multiculturalism and tolerance.

The last two decades in Pakistan have proved to be disastrous for the culture of research in geology, mainly because of the political situation. The renowned Himalayan geologists didn't get a chance of going to this region, which adversely affected the capacity of Pakistani researchers due to the lack of collaborations. Today when you look at maps and graphs they are populated with tons of information from the Indian and Nepalese side but little is known about the Pakistan Himalaya. This is a huge burden on my generation - to fill up this gap of two decades by building new collaborations and convincing people to travel back to Pakistan. In this thesis project, I put forward my efforts to explain the complex geology of Pakistan in a simple way.

I tried to give my best as my part of paying back the privilege I received, although someone else much better than I deserved this opportunity. How well I succeeded in my effort I leave to your fine sense of judgement.

Humaad Ghani

Potsdam 25.06.2019

Acknowledgements

I am very thankful to my PhD supervisors, Ed Sobel and Gerold Zeilinger, for their help, support and guidance that played a key role in the completion of this research. Their support outside of academics helped me overcome the crises I faced during the tenure of this PhD, especially Ed who remained very kind and extended his helping hand always. I really appreciate the lowest level of power distance you keep with the students, so that anyone can approach at any time and discuss any matter. I am thankful to Gerold for the trust and support you showed at the starting point of my PhD. I appreciate both of you for supporting my initiatives if it was applying for funds to attend conferences or an application for teaching projects. I will not forget discussions we had aside from academics, on music, social issues, cultures, and politics that always helped to broaden my perspective.

I am very thankful to the German Academic Exchange service (DAAD) and the people of Germany for my fellowship, coming from public funds, that helped me to complete this research at Potsdam. I am very thankful to Dagmar Beerwerth and Dagmar Hosseini Razi for the support during this period. I gratefully acknowledge Potsdam Graduate School (POGS) for funding to attend international conferences. I pay my thanks to couple of people in Potsdam who supported me in different capacity during the project, Martina Heidemann, Ines Muench, Heiko Pingel and Christina Fischer for the help in bureaucratic issues and help in the labs making things lot easier. I pay special thanks to Tanja Klaka-Tauscher who was so kind in her dealings and always helped with every problem. I am very happy you came back to Potsdam. Claudia Roessling and Caroline Sawitala are gratefully acknowledged for their help and support finding accommodation, kindergarten for my child and visa procedures during my stay in Potsdam. I really appreciate Manfred Strecker for creating a nice environment in the department and research group through his leadership.

I am thankful to Tahseenullah Khan, Muhammad Zafar, Imtiaz Hussain, Asif Javed, Imtiaz Khan and Muhammad Ashfaq for their support from Bahria University. I am grateful to Hamid Hussain, Khurram Durrani, Mubashar Khattak, Uzair Safi, Saleem Shahzad, Sardar Umer Farooq and Kaleem Niazi for helping in the fieldwork and hosting me at their homes that helped to save lot of time and money. I am thankful to Muhammad Sajid, Suleiman Khan, Irfan Hashmi, Asim Akbar, Nowrad Ali, Wajahat Khan, Yasir ayub, Muhammad Arsalan, Imran Ahmed, Raees Amjad, Kaleem-ullah and other students of Bahria and Peshawar Universities for help in the fieldwork. Directorate General of Petroleum Concession (DGPC) Pakistan is thanked for providing seismic and well bore data for research. There are couple of people I would like to pay thanks for their moral support, among them are Muhammad Javed Khan, Saad Rauf, Khalid Iqbal, Abdul Rauf, Muhammad Fayyaz, Muhammad Faisal, Muhammad Sajid, Arshad Ali, Khurram Shahzad, Muhammad Shahbaz Asif, Muhammad Naveel, Umair-ullah Jameel, Fahad Mehmood, Asad Taimur, Fahdi-al-Houmoush, Debopam Das, Shewta Bhattachariya, Xia Wang, Sebastian Zapata Henao, Ghasem Haiderzadeh, Mian Irfan, Hafiz Rabnawaz and Armughan Faisal.

I would like to say special thanks to my wife Irum who will be busy now doing the formatting of this thesis while I am writing this acknowledgement. I am very thankful to you and Arhaan for filling my life with colors that give me motivation and energy to excel in my life and career. I say special thanks to my family members, Imtiaz Ahmed, Khanzeb Khan, Fawad Ghani, Zawar Khan, Farjad Khan, Yasmeen bibi, Tamkeen bibi, Maria Ghani, Khushbo Khan, Samreen Jamal, Muhammad Baber zaib, Amir shahzad, and Sajjad Wali for their love and support.

To whom I could never pay thanks in words for their unconditional love and support are my parents, I wish you were alive to see my success to which you have contributed so much. My prayers may ALLAH give you a place in Jannah-tul-Firdous and give me strength to contribute my best to society. That would be a real thanks for your hardships and efforts spent on raising me to become a responsible person in society.

Chapter 1. Introduction

1.1 Research statement

Fold and thrust belts have been extensively studied to understand the structural style and timing of the development of orogenic belts (e.g., Dahlen et al., 1984; Davis et al., 1983; McClay et al., 2004; Poblet and Lisle, 2011; Pfiffner, 2006). The in-sequence structural evolution of a fold and thrust belt is defined as the propagation of deformation from the hinterland by emplacement of thrust sheets on top of younger ramps toward the foreland (e.g., Dahlstrom, 1969; Suppe, 1983). In contrast, out-of-sequence development of a fold and thrust belt suggests that deformation is distributed more on the hinterlandward thrusts in the belt at a given time; deformation is not always focused on the structure closest to the foreland (e.g., Davis et al., 1983; Dahlen, 1988; Burbank and Beck, 1989; Wobus et al., 2005). Structural geologic models can be coupled with geochronologic and thermochronologic data to constrain the temporal evolution of fold and thrust belts from their origin in undeformed sedimentary basins (e.g., Lock and Willet, 2008; Robinson and McQuarrie, 2012; Castelluccio et al., 2015; McQuarrie and Ehlers, 2015; Mora et al., 2015; Gavillot et al., 2018). Over the past two decades, detailed structural, stratigraphic, geo- and thermo-chronologic studies have shown the difference in the structural style, shortening, exhumation and sequence of structural evolution along the strike in the Himalayan fold and thrust belt (e.g., DiPietro and Pogue, 2004; Yin, 2006; Deekan et al., 2011; Gavillot et al., 2018). The debate continues today in the Himalaya: has deformation propagated in-sequence or out-of-sequence in the fold and thrust belt and what is controlling the deformation pattern, climate or tectonics?

The closure of the Neo Tethys Ocean and collision of India with Asia resulted in the development of the Himalayan foreland basin. The Himalayan fold and thrust belt has propagated into this basin (e.g., Searle et al, 1987; Najman et al, 2010) (Fig. 1.1). The fold and thrust belt is subdivided into four distinct tectonic terrains in the Central Himalaya (DiPietro and Pogue, 2004 and references therein). The South Tibetan Detachment (STD), Main Central Thrust (MCT), Main Boundary Thrust (MBT) and Main Frontal Thrust (MFT) separate the Tethyan, Higher, Lesser and Subhimalayan tectonic terrains, respectively (Fig. 1.1). The Subhimalaya in the Central Himalaya of Nepal is a narrow belt (~30 km) between the MBT and MFT. This belt widens toward the west. In Pakistan, the MFT is located 150

km south of the MBT (Fig. 1.1). The MFT in Pakistan thrusts Precambrian to Pliocene age rocks over Quaternary deposits of the Indo-Gangetic plains. This is different from the Subhimalaya in the Central Himalaya of India and Nepal, where predominantly Neogene strata is exposed at the surface (e.g., Bakers et al, 1988; Van der Beek et al., 2006; Ghani et al., 2018) except some mapped units of Permian and Eocene strata exposed in the south of Shimla and north-west of Jammu in India. Structural models constructed in the Central Himalaya of India, Nepal and Bhutan by combining balanced cross-sections with geochronologic and thermochronologic data have contributed to constraining the structural evolution, sequence of thrusting, shortening and exhumation rates involved in the Cenozoic history of fold and thrust belt development (e.g., Bollinger et al 2006; Gavillot et al., 2018; Robinson and McQuarrie, 2012; McQuarrie and Ehlers, 2015). The high Holocene shortening rate of 20 mm/yr calculated for the MFT in Nepal is considered to accommodate nearly all of the convergence (~20 mm/yr) between India and Asia in the Central Himalaya (Lave and Avouac, 2000; van der Beek et al., 2006).

In the northwestern Subhimalaya of India, the sequence of thrusting in the Kangra Reentrant and Kashmir regions shows that deformation is accommodated out-of-sequence in different parts of the fold and thrust belt. The out-of-sequence movement in the interior of the fold and thrust belt resulted in the reactivation of the MBT and the Jawal Mukhi Thrust (JMT) in the Kangra Reentrant (Theide et al., 2017; Dey et al., 2017) (Figs. 1.1, 2.1). MFT movement at 4 Ma in the Kashmir Himalaya and the development of the Lesser Himalayan Duplex in the region between 2-4 Ma illustrate out-of-sequence development in this area (Gavillot et al., 2018). The Subhimalayan fold and thrust belt west of the Hazara Kashmir syntaxis in the Pakistan Western Himalaya has an internally varied structural style; this is quite different from the style of the Subhimalaya of India and Nepal. The previous geochronologic and thermochronologic studies conducted in the Pakistan Western Himalaya were mainly focused on understanding the timing of the MBT and MFT. Detailed studies on how deformation propagated within the foreland, shortening and exhumation processes, or the temporal development of structural style have not been conducted south of the MBT in this region.

We have studied the spatio-temporal structural evolution of the Kohat and Potwar fold and thrust belts (herein called Kohat and Potwar), also called the Subhimalaya in Pakistan (Fig. 1.1). The structural style of the Kohat is very different from the structural style of the rest of the Subhimalaya and especially the Potwar, located towards the east. The structural

style of the Kohat results from deformation along double décollements, causing intense internal deformation of the stratigraphic wedge; in comparison, the Potwar has a simpler structure and is less internally deformed (Abbasi and McElroy, 1991; McDougall and Hussain, 1991; Pivnik and Sercombe, 1993; Qayyum et al., 2015; Faisal and Dixon, 2015; Ghani et al., 2018). In the Kohat, molasse strata has been removed from the surface but in the Potwar, a large amount of molasse is preserved in the stratigraphic wedge. Previous studies in the Kohat and Potwar were mainly focused on examining the structural style and constraining the amount of shortening.

To constrain the onset and duration of slip along structures, previous paleomagnetic studies investigated the activity of the MFT in the Salt Range and the MBT in the Western Axial Belt (Burbank and Beck, 1989; Meigs et al., 1995). An older group of studies proposed the development of the MBT at 5 Ma, and the MFT and SGT at 2 Ma (Yeat and Hussain., 1987; McDougall and Hussain, 1991; McDougall and Khan, 1993); these results implied that deformation propagated through Kohat in the time duration of 3 Ma. Redating the development of the MBT as a major Himalayan thrust active at ~10 Ma (Meigs et al., 1995; Turab et al., 2017) and the development of MFT at 4 Ma (Burbank and Beck., 1989) revised the structural chronology in this region.

1.2 Aim and objectives of the research

Previous studies investigated the Kohat and Potwar separately, so important details about the contemporaneous structural style evolution were missing. There are significant uncertainties about the timing and sequence of the structural evolution and the driving mechanisms of exhumation in Kohat and Potwar. Therefore, we undertook to check and synthesize the spatial and temporal evolution of major structures, the role of preexisting structures, and the influence of décollements that govern the structural style variation in the Subhimalaya of Pakistan.

1.3 Research methods

The project consists of three subprojects aimed at understanding different aspects of the temporal structural evolution of Kohat and Potwar. The subprojects include modeling the structural style of Kohat and Potwar, examining the long term history of the Salt Range development from northern Indian Passive margin to Himalayan range front, and constraining the timing for the development of MBT and the sequence of deformation propagation in the Kohat. I prepared a revised geological map of the area by integrating previous maps and

newly acquired field data. A balanced cross-sections and 3D model were constructed by integrating seismic profile interpretations, outcrop orientation data and petroleum exploration wells data. The balanced sections were restored to calculate the amount of shortening accommodated by different structures. Low temperature thermochronologic (U-Th-Sm/He (AHe) and Apatite Fission Track (AFT)) analysis was conducted on detrital apatite to predict the time-temperature thermal history of samples and constrain episodes of exhumation in the basin. The cooling ages of samples were coupled to structural models in order to constrain the timing and sequence of deformation in the Kohat and Potwar.

1.4 Significance of the research

This research provides new temporal constraints on the development of the Kohat and Potwar in Pakistan. My structural model shows how deformation propagation from a double décollement to a single décollement can lead to marked differences in the structural style of contemporaneously evolving portions of a fold and thrust belt. The visualization of the structural style in a 3D model helps us to understand the structural compatibility and kinematics of transfer zones. We have produced a significant AFT and AHe age dataset that has a large amount of dispersion. Better age resolution is obtained by correlating AFT ages with kinetic parameters (e.g. Dpar) and the structural position of the samples. This approach could help thermochronologists understand the significance of structural controls on their data in other areas. A new low temperature thermochronology modeling approach is adopted that helps to constrain the long term thermal history of the Pre-Himalayan tectonics in the basin. The constraints on the timing of development of major thrusts in the Kohat and Potwar has helped in the construction of a new structural evolution model. The shortening and exhumation rates are calculated for major structures, thus providing new constraints on the sequence of deformation in this region. The results of this study help us to understand the role of tectonics in shaping structural style and controlling pattern of exhumation in this region. The temporal constraints on the structures in the area provide an opportunity for the petroleum exploration industry to understand the timing of structural development of the reservoirs and look for new targets in the poorly studied areas along the boundary zone of Kohat and Potwar. The pattern and rate of exhumation, long- and short-term shortening rates involved in structural evolution of this region could be used to understand the similarities and differences of fold and thrust kinematics along the Himalayan Orogen.

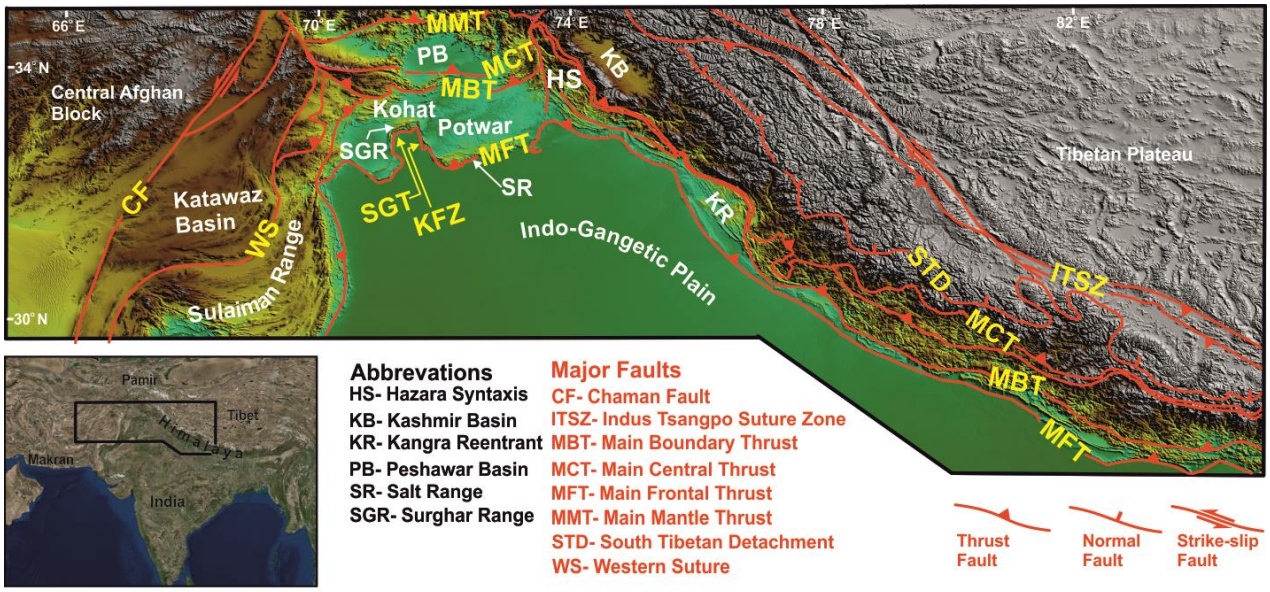

Figure 1.1. Regional tectonic map of the Himalaya and surrounding regions (modified after Beck et al., (1995); Badshah et al., (2000); DiPietro and Pogue, (2004)).

1.5 Thesis outline

Chapter 2

Chapter 2 focuses on the regional tectonic framework of northwestern Pakistan. The chapter briefly introduces the main tectonic terrains and their boundaries. The details provided in the chapter are helpful to understand the position of the Kohat and Potwar in a regional tectonic perspective. The details in the chapter provide a review about the timing of structural development in the region that help to understand the temporal evolution of different tectonic terrains.

Chapter 3

This chapter exclusively deals with the structural style of Kohat and Potwar, taken as a linked structural system. Previous work in the region explained the structural style of Kohat and Potwar as separate cases of deformation, so details about how the structural style changes from Kohat to Potwar were not known. The chapter includes seven new balanced cross-sections along the strike of the belt; together, these are used to visualize a 3D structural model. All of these are used to explain changes in structural style and their compatibility. The cross-sections show that the variation in structural style between Kohat and Potwar is strongly influenced by the presence of a double décollement in the Kohat compared to a

single décollement in the Potwar. The structural modeling explains the kinematics of the transfer zone between Kohat and Potwar which is known as the Kalabagh Fault Zone. We have shown through the structural model that the amounts of shortening in the Kohat and Potwar are similar despite differences in their structural style. The kinematic nature of the Kalabagh Fault Zone is investigated. We suggested that it is a rotational fault zone that connects out-of-sequence thrusting in Kohat with normal faulting in the Kalabagh Fault Zone. The role of salt is proposed to produce normal faulting in the Salt Range, salt diapirs in the Kalabagh Fault Zone, gentle folding in the Potwar, and the formation of curved fault traces and axial surfaces of folds in the Western Salt Range and Southern Kohat.

Chapter 4

The Himalayan range front in Pakistan is known as the Salt Range in the Potwar. The unique feature of the Salt Range is that it contains a Precambrian to Pliocene stratigraphic succession compared to the range front in India and Nepal, where predominantly Miocene to Pliocene strata are exposed. In this chapter, we describe the pre-Himalayan history of the basin and development of the range front. We have collected samples from different sections of the Salt Range. We coupled AHe and AFT dating with balanced cross-section. The AFT and AHe ages are dispersed between 2 to 350 Ma. The AFT age dispersion can be understood by analyzing kinetic proxy data (Dpar) and the structural position of the samples. We have adopted a new thermochronology modeling approach using the program QTQt to combine different age detrital samples into a single thermal model. The model results suggest that samples experienced two major exhumation events in the Late Paleozoic and Early Pliocene. The Late Paleozoic exhumation is interpreted to reflect rifting that was a consequence of formation of the Neo-Tethys. The rifting event has also been reported in the adjoining areas of Zanskar, Kashmir and Peshawar Basin. The Early Pliocene event is coupled to a balanced cross-section of Cenozoic deformation to constrain the development of the Salt Range in Pakistan. Structural reconstructions confirm that the MFT maintained a constant shortening rate between 5 - 6 mm/yr after 4 Ma and a maximum exhumation rate of 2 – 2.5 mm/yr on the MFT ramp.

Chapter 5

Chapter 5 deals with the past 15 Ma of structural evolution of the Kohat. The previous structural model in the region explained development of structural style in the Kohat completed in the past 5 Ma (Yeats and Hussain., 1987; McDougall and Khan, 1993). The

evidence that the MBT developed at 10 Ma (Meigs et al., 1995) requires new structural models that explain the sequence of deformation in this area. In the last two decades, no such structural model has been developed which could constrain the timing and sequence of deformation. Our study couples newly acquired AFT and AHe data from the Kohat with a balanced cross-section and a structural forward model; we present a new structural model with an active roof thrust. The results suggest that deformation propagated to the range front at ~14 Ma; this accreted the foreland into the deforming wedge. The earlier development of the range front is correlated with an angular unconformity on the range front. The deformation propagated out-of-sequence after ~11 Ma in Kohat on a double décollement, resulting in extensive exhumation of strata above the upper décollement. The tectonic thickening of the section between the two décollements is achieved by formation of duplexes.

Chapter 6

Chapter 6 summarizes the discussions and conclusions of chapters 3, 4, and 5, providing a summary about the overall structural evolution of Kohat and Potwar in Pakistan.

Chapter 2. Tectonic framework of northwestern Pakistan

The geology of north and northwestern Pakistan comprises the Hindukush, the Karakoram and the Kohistan Arc, which accreted to Asia during Paleozoic- Mesozoic times, and the Himalayan and Himalayan western axial fold and thrust belts, which formed by the Cenozoic India-Asia collision (Fig. 2.1). Below, these tectonic zones are presented separately from north to south.

2.1. Hindukush and Karakoram

The Hindukush is comprised of Paleozoic to Mesozoic plutonic, metasedimentary and sedimentary rocks separated from the Central Pamir by the Rushan-Pshart Suture (Fig. 2.1). The block contains Paleozoic slates that are overlain by Permo-Triassic clastic sedimentary and platform carbonate rocks (Hildebrand et al., 2000; Zanchi et al., 2000). Mantle ultramafic rocks along the Tirich Mir Fault Zone (TMFZ) implies that this boundary between the Hindukush and the Karakoram is a suture. The Karakoram is composed of metamorphic basement intruded by granitoids and overlain by a Middle Paleozoic to Cretaceous sedimentary succession. The mid-Cretaceous Tirchmir Pluton intruded both the Hindukush and the Karakoram, indicating that the two blocks accreted in Mesozoic time. The evolution of the Hindukush and the Karakoram began with Late Paleozoic rifting in Gondwana due to opening of the Neo-Tethys. These rifted blocks accreted to Asia during the Late Triassic to Early Jurassic Cimmerian Orogeny (e.g., Zanchi et al., 2000; Faisal et al., 2018). The collision of India with Asia resulted in crustal thickening, metamorphism and emplacement of Miocene granitic plutons in the Hindukush and Karakoram region (Faisal et al., 2018).

2.2 Kohistan Arc

The Kohistan Arc is separated from the Eurasian Plate (Karakoram and Hindukush) by the Main Karakoram Thrust (MKT) in the north and from the Indian Plate by the Indus Suture, also called the Main Mantle Thrust (MMT) (Gansser, 1980; Searle et al., 1999; Burg, 2011) in the south. The Kohistan Arc is regarded as an obducted island arc formed by intra-oceanic subduction in the Tethys, which started in the Late Jurassic- Early Cretaceous (Tahirkheli et al., 1979; Schaltegger et al., 2002; Burg 2011). Late Cretaceous rifting within the Kohistan block resulted in the emplacement of extensive magmatic intrusions (Khan et al., 1993; Schaltegger et al., 2002). The closure of the Tethys and collision of India with Asia

was completed by suturing of the Kohistan Arc to India and Asia during Eocene to Miocene time (Zeilinger et al., 2007; Khan et al., 2009; Burg, 2011).

2.3 Himalaya

The Western Himalaya is located in Pakistan; this covers the region between the Nanga Parbat - Hazara syntaxes and the Himalayan western axial fold and thrust belt (Fig. 2.1). The Central Himalaya in India and Nepal is subdivided into distinctive tectono-stratigraphic segments that are bounded by major faults (e.g., Hodges, 2000; Yin, 2006). As the structural style varies along strike, a simple scheme of tectonic subdivision of the Western Himalaya was outlined by DiPietro and Pogue (2004). The Western Himalaya is divided into three different tectono-stratigraphic zones (Fig. 2.1) from north to south: 1) the Western Hinterland (metamorphic zone), 2) the Lesser Himalaya, and 3) the Subhimalaya.

2.3.1 Western Hinterland (metamorphic zone)

The Western Hinterland is thrust to the north by the Indus Suture or MMT and on the south by the Panjal- Khairabad, also called the Main Central Thrust (MCT). This zone is comprised of Lower Proterozoic to Paleozoic age rocks of the Indian Plate (Calkins et al., 1975; Pogue et al., 1992b; Dipietro et al., 1999). Lower Proterozoic medium-grade metamorphic rocks are exposed in the antiformal Indus Syntaxis that divides the area into the Hazara and Swat synformal nappes (Treloar et al., 1989). The Upper Proterozoic metasedimentary rocks are intruded by Ordovician granites in the Hazara and Swat areas. The area in the northeastern part of the Peshawar basin is comprised of a Cambrian to Triassic platform sequence lying above Upper Proterozoic meta-sedimentary rocks (Pogue et al., 1992b). Two important tectonic events are reported from the area: A Late Cambrian to Early Ordovician alpine-type orogeny that resulted in intrusion of granitic rocks, and Carboniferous to Permian extension that resulted in the removal of older rocks from different areas (Pogue et al., 1992a; Sajid et al., 2018).

2.3.2 Nanga Parbat Syntaxis

The Nanga Parbat Syntaxis is a north-south-trending domal structure located between the Kohistan and Ladakh Arcs. The Nanga Parbat syntaxis is bounded almost entirely from east to west by the MMT, which thrust Kohistan and Ladakh Arcs southward onto the Indian Plate (Treloar et al., 2000). The Nanga Parbat syntaxis is comprised of Indian Plate rocks that were metamorphosed to high pressure and temperature conditions, and the emplacement of

young granitic intrusions (Zeitler et al., 2001). The core of the structure is characterized by high uplift and erosion rates (Zeitler et al., 1985; Wilke et al., 2012). The position of the MCT is not fully established in the southern part of syntaxis; however, the Main Boundary Thrust (MBT) separates the Nanga Parbat Syntaxis from the Hazara Syntaxis.

2.3.3 Lesser Himalaya

The Lesser Himalaya in Pakistan is bounded by the MCT and MBT. This zone is comprised of imbricates that stack Precambrian to Eocene stratigraphic thrust sheets to the west of Hazara Syntaxis (Fig. 2.1). The hanging wall of the MBT is comprised of an intensely deformed Mesozoic to Eocene sedimentary succession. The MBT continues as a major structure to the west of the Hazara syntaxis towards the western part of the Subhimalaya (Yeats and Hussain, 1987; Meigs et al., 1995; Turab et al., 2017).

2.3.4 Subhimalaya and Hazara Syntaxis

The Subhimalaya of Pakistan is the region located between the MBT and the Main Frontal Thrust (MFT) the west of the Hazara Syntaxis (Fig. 2.1). The area is comprised of the Kohat and Potwar fold and thrust belts, Bannu Basin, Salt and Trans Indus Ranges. The Kohat and Potwar show significant variations in structural style along strike (Abbasi and McElroy, 1991; Faisal and Dixon, 2015; McDougall and Hussain, 1991; Pivnik and Sercombe, 1993; Qayyum et al., 2015). The surface structural style in the Kohat is comprised of asymmetric and box-shaped folds developed above Eocene age evaporites that are cut at fold limbs by steeply-dipping to overturned thrusts (Ghani et al., 2018). The Potwar has a simple structural style that is less internally deformed and is translated as a single thrust sheet above the MFT ramp; this structure forms the Salt Range (Baker et al., 1988; Ghani et al., 2018). The Trans Indus Ranges from the range front of the Kohat and the Bannu Basin, while the Salt Range forms the range front of the Potwar. The range front of the Kohat and Potwar is not a single linear feature; rather, the Central Salt Range is located 90 km south of the Surghar Range; the two segments are connected by the Kalabagh Fault Zone. The Salt Range contains Precambrian to Pliocene age strata that are comprised of sediment eroded from cratonic basement exposed in the southern part of India and sediments originally deposited in the Tethys (Hughes et al., 2019). The molasse strata in the Subhimalaya is comprised of sediments eroded from the Himalaya (Burbank et al., 1996; Najman et al., 2003). The Hazara Syntaxis is an anticlinal structure that contains folded Neogene molasse strata in the core.

2.4 Himalayan western axial fold and thrust belt

The north-south trending Himalayan western axial fold and thrust belt was formed by the collision of India in the west with the Asian Plate (Beck et al., 1995). The belt is bordered on the west by the Katawaz and Makran Basins (Fig. 2.1). The obduction of the Waziristan and Bela ophiolitic complexes delineate the Late Paleocene India Asia suture (Beck et al., 1995; Qayyum et al., 1996; Badshah et al., 2000). The structural style of the fold and thrust belt results from contractile tectonism that was strongly overprinted by transpressional tectonism since the development of the left-lateral Chaman Fault in Miocene time (Badshah et al., 2000).

2.5 Development of the Himalayan fold and thrust belt

The collision of India with Asia in northern Pakistan has been estimated to have occurred between 55 to 40 Ma (e.g., Najman et al., 2001; Khan et al., 2009; Ding et al., 2016). There have been several recent ideas that challenge this view. One new concept is that an intra-cratonic rift basin developed within India during the Cretaceous. The northern part of India accreted to Asia at 50 Ma, followed by subduction of the rift-formed oceanic basin and then the final collision of India with Asia occurred at 25 – 20 Ma (van Hinsbergen et al., 2012, 2018). Deformation propagated to the interior of Indian plate after this collision along major thrusts such as the MCT, MBT and MFT. The Eocene timing for motion of the MMT is reported to be almost synchronous with the collision; the fault is reported to be reactivated later, in the Pliocene (Zeilinger et al., 2007). There are no direct age constraints available for the activation of the MCT in Pakistan; however, it is accepted that motion was synchronous with the Early Miocene development in the north of the Hazara Syntaxis and in the Central Himalaya of India and Nepal (e.g., Robinson et al., 2003; Bollinger et al., 2004; Turab et al., 2018; Gavillot et al., 2018). The MBT is a major structure that developed synchronously along the Western and North-western Himalayan range of Pakistan and India around 10 Ma (Meigs et al 1995; Turab et al., 2017) and reported to developed at 5 Ma in Nepal (Robinson and McQuarrie, 2012). The MFT in Pakistan is developed at 4-5 Ma (Burbank and Beck, 1989). A similar age of 4 Ma is reported for the MFT in India and 2 Ma in Nepal (Gavillot et al., 2018; Van der Beek et al., 2006).

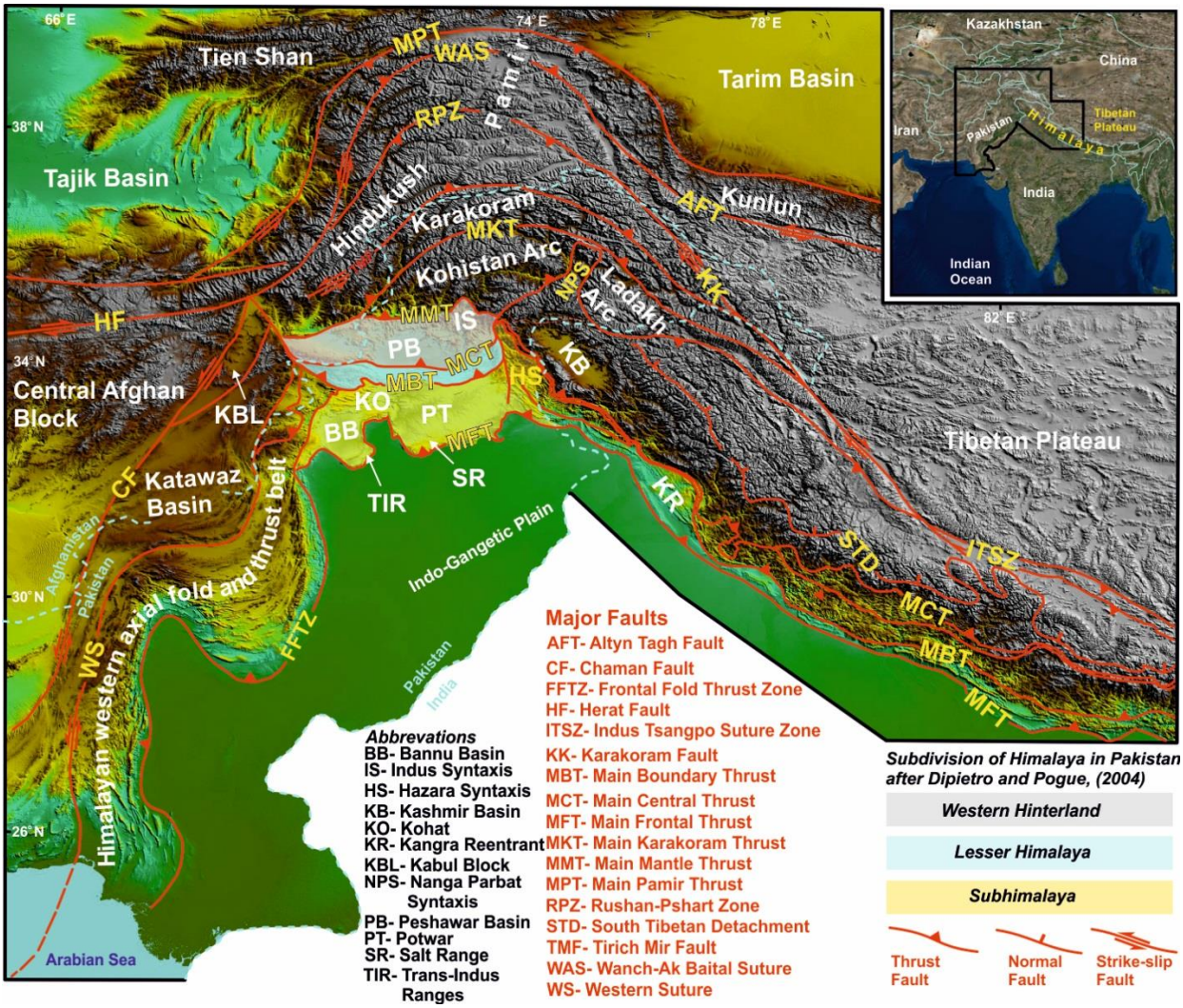

Figure 2.1. Regional tectonic map of the Himalaya and surrounding regions. The inset shows the geographic location. Western Hinterland, Lesser Himalaya and Subhimalaya are shown by a colored polygon bounded by the MMT, MCT, MBT and MFT (modified after Beck et al. (1995); Badshah et al. (2000); Dipietro and Pogue (2004); Faisal et al. (2018)).

Chapter 3. Structural variation within the Himalayan fold and thrust Belt: A case study from the Kohat and Potwar fold and thrust belts of Pakistan

Abstract

The Kohat and Potwar fold and thrust belts (KP-FTB) in Pakistan exhibit structural variations over 250 km along strike within the Himalayan fold and thrust system. The 3D deformation model shows that Kohat surface structures evolved above an active roof thrust in Eocene evaporites. The ramp-forming duplexes in the Kohat were stacked and passively transported toward the foreland above new ramps, resulting in up to 5 km of thickening between the two décollements. Ramps from the Kohat extend into the Potwar as thrust tips of fault propagation folds. The basement slope changes from flat ($\beta < 1°$) below the northern part to north-dipping ($\beta > 1°$) below the southern part, corresponding to the change in structural style and complexity. The Kalabagh Fault Zone, linking the two belts, is interpreted as a zone of complex dextral strike slip rotational faulting. Salt expulsed from the hanging walls of normal faults and under synclines in the Kalabagh fault zone moved toward the footwall of normal faults, accumulated in the cores of anticlines, and formed lobe structures at the deformation front. The fundamental reasons for the variable structural styles are changes in décollement strength, basement slope, preexisting normal faulting, presence of a secondary décollement and spatially-variable salt mobility and accumulation.

3.1 Introduction

Fold and thrust belts (FTB) are a characteristic feature of orogenic systems and have been extensively studied to elucidate fold and thrust kinematics, thin and thick skinned style of deformation and their hydrocarbon potential (e.g., Davis et al., 1983; Dahlen et al., 1984; McClay et al., 2004; Poblet and Lisle, 2011; Pfiffner, 2006). FTB often show structural variation along and across strike resulting from difference in mechanical strength and number of décollements, basement architecture, pre-existing normal faulting, and thickness and rheology of the wedge. Physical, numerical and classical structural geologic models have been constructed to understand the role of these factors in causing structural variation in FTB (e.g., Chapple, 1978; Davis and Engelder, 1985; Cotton and Koyi, 2000; Costa and Vendeville, 2002; Couzens-Schultz et al., 2003; Bonini, 2007).

The ongoing collision of India with Asia started in the Eocene, forming the Himalayan fold and thrust belt, which records the deformation history of the Himalayan Orogeny (e.g., Searle, 1987; Najman et al., 2010). The age of collision in Pakistan is reported in the range of 40-55 Ma (Najman et al., 2001; Ding et al., 2016; Qasim et al., 2018). The Kohat Fold and Thrust Belt (herein called Kohat) and Potwar Fold and Thrust Belt (herein called Potwar) in Pakistan represent the external zone of the Himalayan fold and thrust belt. The Main Boundary thrust marks their common northern boundary (Yeats and Hussain, 1987; Yeats et al., 1984; McDougall et al., 1993; Meigs et al., 1995), yet the two FTBs show significant variations in structural style along strike (Abbasi and McElroy, 1991; McDougall and Hussain, 1991; Pivnik and Sercombe, 1993; Faisal and Dixon, 2015; Qayyum et al., 2015). The range front of the Kohat-Potwar Fold and Thrust Belt (denoted in text combined as KP-FTB) is not a single linear feature; rather, the Central Salt Range is located 90 km south of the Surghar Range (Fig. 3.1). The causes of structural variations in the KP-FTB is described separately in different models, including 1) it is linked to presence of salt in the Potwar compared to the Kohat (Cotton and Koyi, 2000) 2), presence of double décollement in the Kohat compared to single décollement in the Potwar (Abbasi and McElroy, 1991), 3) taper of the wedge and presence of salt in the Potwar (Davis and Engelder, 1985; Smith et al, 2003), 4) transpressional strike-slip faulting in the Kohat (Pivnik and Sercombe, 1993) compared to coherent thrust sheet deformation in the Potwar. The structural styles of the Kohat and the Potwar have always been discussed separately through one or two cross-sections which are insufficient to explain the interrelationship between the role of salt, double décollements, basement slope and preexisting normal faulting on the fold and thrusts kinematics along strike and especially explaining the structural style transition from the Kohat to the Potwar.

In this paper, for the first time we present a structural model at the southern boundary zone of the Kohat and Potwar by constructing balanced cross-sections using Midland Valley Move software. The cross-sections are constrained using industrial seismic reflection lines, petroleum well data and outcrop orientations of structures mapped in the field. We have also studied previous structural models of the KP-FTB (Baker et al., 1988; Butler et al., 1987; Abbasi and McElroy, 1991; McDougall and Hussain, 1991; Pivnik and Sercombe, 1993; Jaswal et al., 1997; Cotton and Koyi, 2000; Faisal and Dixon, 2015; Khan et al., 2012; Qayyum et al., 2015) and adopted parts that are similar to our interpretations. The overall structural model is a reinterpretation and integration of previous models with our new

findings. In this paper we discuss 1) the structural style of the Kohat and Potwar, 2) causes of structural variation, 3) the structural transition from the Kohat to Potwar, 4) comparison of shortening in the Kohat and Potwar, 5) the evolution of structures in the Kalabagh Fault Zone and 6) the contemporary evolution of the KP-FTB.

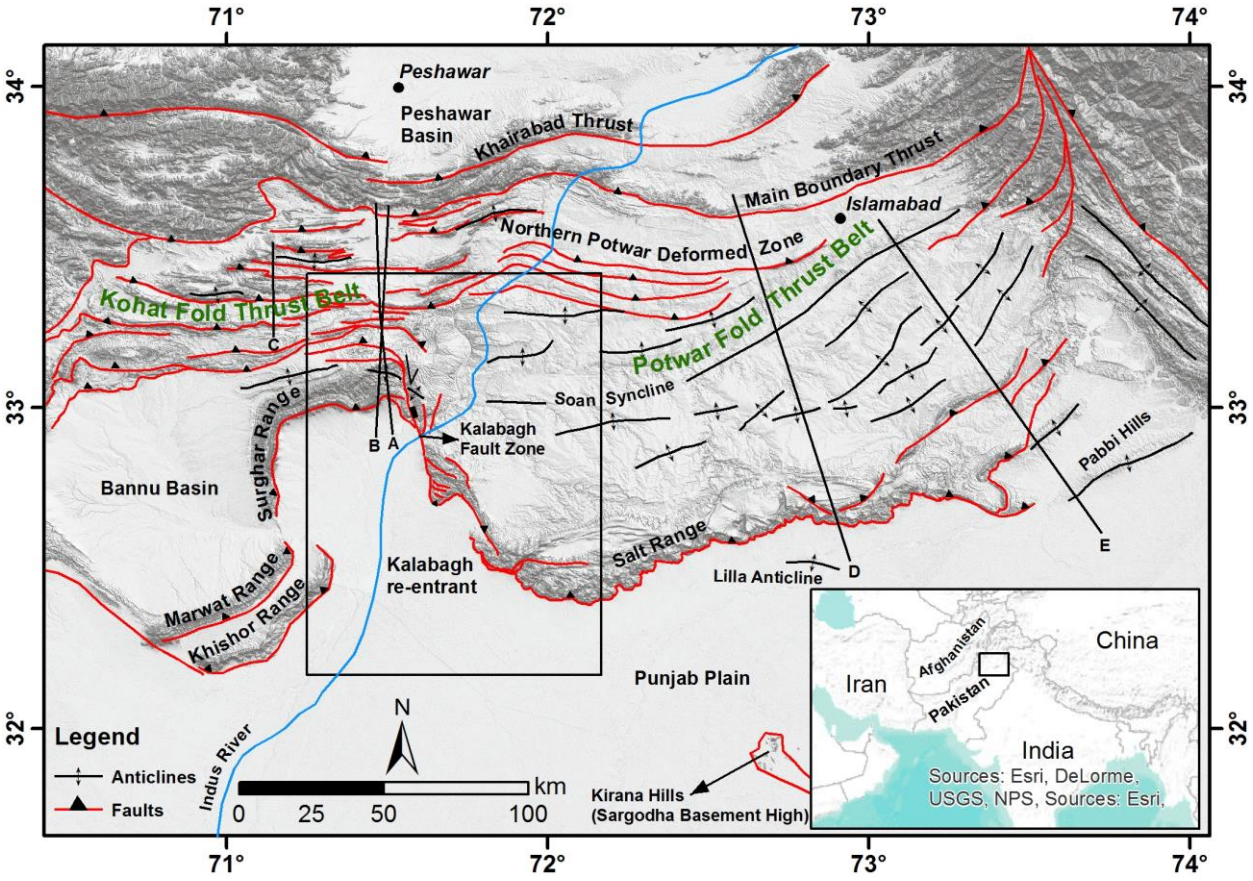

Figure 3.1. Generalized tectonic map of northern Pakistan, showing major geological features. Inset box shows location of this study. Kirana Hills are comprised of Indian basement shield rocks. Cross-sections A-E are shown in Figure 2. Map is modified after Baker et al (1988), Pennock et al (1989), Jaswal et al (1997), Faisal and Dixon (2015), and Meissner et al (1974).

3.2 Tectonic framework and previous structural interpretations

The approximately 250 km wide KP-FTB formed due to deformation of the Himalayan foreland basin. The northern and western border of the KP-FTB is marked by the Main Boundary Thrust (MBT) (called the Kurram thrust to the west of Kohat by some authors), which formed around ~10 Ma (Meigs et al., 1995). The MBT places intensely deformed Mesozoic sedimentary strata and ophiolite on Cenozoic and younger strata of the KP-FTB (Yeats and Hussain, 1987; McDougall et al., 1993; Burbank et al., 1996). The range front of Kohat and Potwar are known as the Surghar Range and Salt Range, respectively

(Figs. 3.1-3.3). The area between the range fronts is the Kalabagh Fault Zone, which is a zone of strike slip deformation and salt tectonics (Yeats et al., 1984; McDougall and Khan, 1990; Chen and Khan, 2010; Khan et al., 2012). Folds in the Kohat are symmetric to asymmetric, tight to overturned and box shaped structures cut at the limbs by steeply dipping to overturned thrusts. Anticlinal cores are occupied by Eocene shales and evaporites. On the surface, some thrusts can be traced from the Kohat into the Potwar. Along the boundary between the Kohat and the Potwar, the trends of fault traces and axial trend of folds are deflected from east west to north south (Fig. 3.1). The western segment of the Surghar Range is the frontal range for the Bannu basin.

McDougall and Hussain (1991) explain the structural style of the Kohat using a balanced cross-section that shows thrust sheets translated above partially emergent thrusts, forming duplexes, fault bend folds and décollement folds throughout the Kohat (Fig. 3.2a). Abbasi and McElroy (1991) explain the structural evolution using a double décollement model. Surface structures are interpreted as a passive roof sequence above Eocene shales and evaporites. The EoCambrian to Paleocene stratigraphy is modeled as a hinterland-dipping duplex structure between a sole thrust at the base of sedimentary strata and a passive roof thrust beneath Eocene strata (Fig. 3.2b). Pivnik and Sercombe (1993) and Sercombe et al. (1998) explain deformation of the Kohat in two stages, achieved through typical fold and thrust geometries, which were subsequently overprinted by transpressive deformation in the western and northwestern part of the Kohat (Fig. 3.2c).

The Potwar is structurally divided into two zones: The Northern Potwar Deformed Zone (NPDZ) and the Soan syncline (Fig. 3.1). At the surface in the NPDZ, the Miocene molasse is exposed; however, seismic data suggest that this is the surface expression of an intensely deformed passive roof duplex structure (Jadoon and Frisch, 1997; Jaswal et al., 1997) (Fig. 3.2d). The Khair-e-Murat thrust marks the boundary between the NPDZ and the Soan syncline. To the south of the NPDZ, a zone of open folds is present at the surface (Fig. 3.2d). In the eastern Potwar, structures at the surface are NE-SW oriented, which differs from the E-W orientation of structures in the central and western part of the Potwar. North and south verging thrusts bound upright folded structures in the eastern part of the Potwar (Drewes, 1995; Pennock, 1989; Jaumé and Lillie, 1988; Faisal and Dixon, 2015) (Fig. 3.2e).

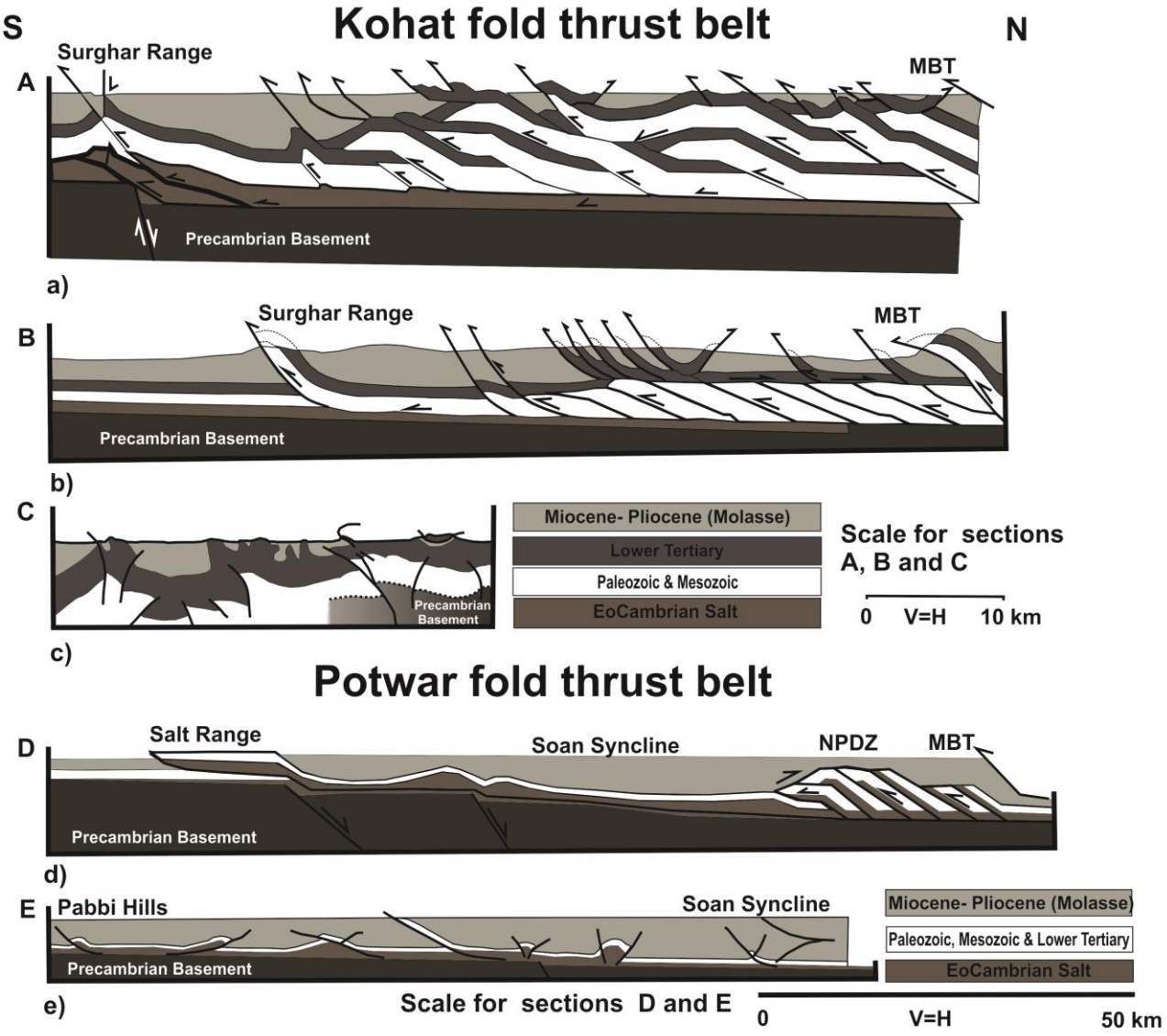

Figure 3.2. Evolutionary models of the Kohat and Potwar. a) Balanced section A by McDougall and Hussain (1991) suggests that extensive thrust tectonics below the molasse was responsible for 86 km of shortening in the Kohat. b) Section B by Abbasi and McElroy (1991) shows that the deformation style was controlled by a double detachment in the Kohat, accounting for 56 km of shortening. c) Section C by Pivnik and Sercombe (1993) shows structures that evolved through transpressional tectonics in the Kohat. d) Regional cross-section D by Baker et al. (1988) shows major structural features of the Potwar and Salt Range. Note basement normal faults beneath the Salt Range. e) Section E by Pennock et al (1989) shows structures in the eastern Potwar between the Soan syncline and Pabbi Hills. Note the vergence of structures toward the north and south and the slope of basement. See fig. 3.1 for location of the sections. Abbreviations: MBT-Main Boundary Thrust, NPDZ- Northern Potwar Deformed Zone. Section A, C and E are reprinted by permission of the AAPG whose permission is required for further use.

To the south of the Potwar, a major ENE-WSW trending structural and topographic feature known as the Salt Range marks the thrust front. Precambrian to Pliocene strata are thrust above Quaternary sediments along the emergent Salt range thrust (SRT) (Yeats et al., 1984; Butler et al., 1987; Baker et al., 1988; Qayyum et al., 2015) (Figs. 3.1-3.3). Precambrian salt, interpreted on seismic profiles beneath the southern Potwar, forms the décollement horizon over which Cambrian to Pliocene strata glided in a single coherent thrust sheet (Baker et al., 1988; Qayyum et al., 2015). Thrusting along the Salt Range ramp started at 5 Ma followed by the 2 Ma final stage of displacement (Yeats et al., 1984; Yeats and Hussain 1987; Burbank et al., 1986, Burbank and Raynolds, 1988, Burbank and Beck, 1989, 1991). In the central part of the Salt Range, a normal fault is interpreted on the seismic profiles that provided a ramp for the basal décollement to form an upper flat in the Pliocene strata (Baker et al., 1988; Faisal and Dixon, 2015; Qayyum et al., 2015) (Fig. 3.2d). In the western Salt Range, a basement normal fault has not been described (Leathers, 1987; Qayyum et al., 2015). The Kalabagh Fault Zone is a complex network of faults joining the Kohat and Potwar. It is interpreted as a lateral ramp for the Potwar (Butler et al., 1987) and a right lateral tear fault (McDougall and Khan, 1990). To the south of the Salt Range, igneous rocks of the Indian basement shield are exposed in the Kirana hills (Fig. 3.1).

3.3 Stratigraphy and décollements

The stratigraphic section is known from excellent outcrops in the Salt Range, Surghar Range, KP-FTB and wells drilled for hydrocarbon exploration. The sedimentary succession unconformably overlies the Precambrian crystalline basement of the Indian craton. The sedimentary sequence is subdivided into three major units: 1) the Precambrian Salt Range Formation (SRF), 2) the Cambrian to Eocene siliciclastic, carbonate and evaporite sequence of the Tethyan domain, and 3) the Miocene to Pliocene molasse sequence related to erosion of the Himalayan orogeny (Figs. 3.3-3.4) (Shah, 1977; Gee, 1980; Khan et al., 1986; Kazmi and Abbasi, 2008).

The SRF is composed of salt, gypsum and marl (Gee, 1980), which forms the décollement horizon for the Potwar and Salt Range (Butler et al., 1987; Baker et al., 1988; Richards et al., 2015). The SRF is 830 m thick in the central Salt Range; it is entirely exposed along the Salt Range. It forms salt dome and diapirs toward the west near the town of Kalabagh. In the Kalabagh Reentrant, the SRF is not penetrated in the Kundian well (McDougall and Hussain, 1991). South of the Salt Range, the thickness of the SRF in the

Lillah and Warnali wells is 219 and 96 m, respectively. These provide evidence that the SRF thins toward the south and southwest of the Potwar (Figs. 3.3, 3.4). The spatial distribution of the SRF has a dramatic effect on the location of the décollement horizon that controls the structural style of the KP-FTB.

The Paleozoic succession is composed of Cambrian strata at the base and Permian strata on the top, separated by an Ordovician-Carboniferous unconformity (Gee, 1980; Shah, 1977; Kazmi and Abbasi, 2008). These strata are the Cambrian age Jhelum Group and the Permian age Nilawahan and Zaluch Groups (Fig. 3.4). The Jhelum Group consists of the Khewra, Kussak, Juttana and Baghanwala Formations, which are sandstone interbedded with shale, claystone and dolostone. The Group is well exposed in the eastern Salt Range, pinches toward the central Salt Range and is absent in the western Salt Range. The Tobra, Dandot, Warcha and Sardai Formations form the Permian Nilawahan Group. It consists entirely of clastic rocks, with a conglomeratic unit at the base overlain by thin to thick bedded sandstone, and siltstone interbedded with shale and clay. It is well exposed in the eastern and central Salt Range whereas in the western Salt Range, only the conglomeratic unit (Tobra Formation) and the middle clastic sequence (Warcha Formation) unconformably overlie the SRF. The Upper Permian Zaluch Group is a platform carbonate sequence comprised of the Amb, Wargal and Chiddru Formations. It is well exposed at the surface in the western and central Salt Range; however, it is absent in the eastern Salt Range (Shah, 1977; Gee, 1980; Kazmi and Abbasi, 2008). In the Surghar Range, Upper Permian strata are only exposed within some gorges and are difficult to map as lateral units. The Mesozoic succession is comprised of the Mianwali, Tredian, Kingriali, Datta, Shinawri and Samanasuk Formations. They contain shale, white sandstone (quartz arenite), dolostone and carbonate. The Mesozoic succession is best exposed in the west, lying unconformably over the Upper Permian strata separated by the Permo-Triassic Boundary. The Mesozoic succession thins towards the east and is absent in the eastern Salt Range and Potwar. In the Surghar Range, the 500 m thick unit is well exposed in the core of an anticlinal structure and has been penetrated in several wells in the Kohat. The Paleocene Lockart and Patala Formations are comprised of carbonate overlain by shale. The formations are exposed in the Surghar Range and reported from wells in the Kohat and Potwar. In the Salt and Surghar Ranges, they maintain the same thickness and gradually thin toward the east where only the shale unit is exposed unconformably over the Permian strata (Figs. 3.3-3.4) (Shah, 1977; Gee, 1980; Kazmi and Abbasi, 2008).

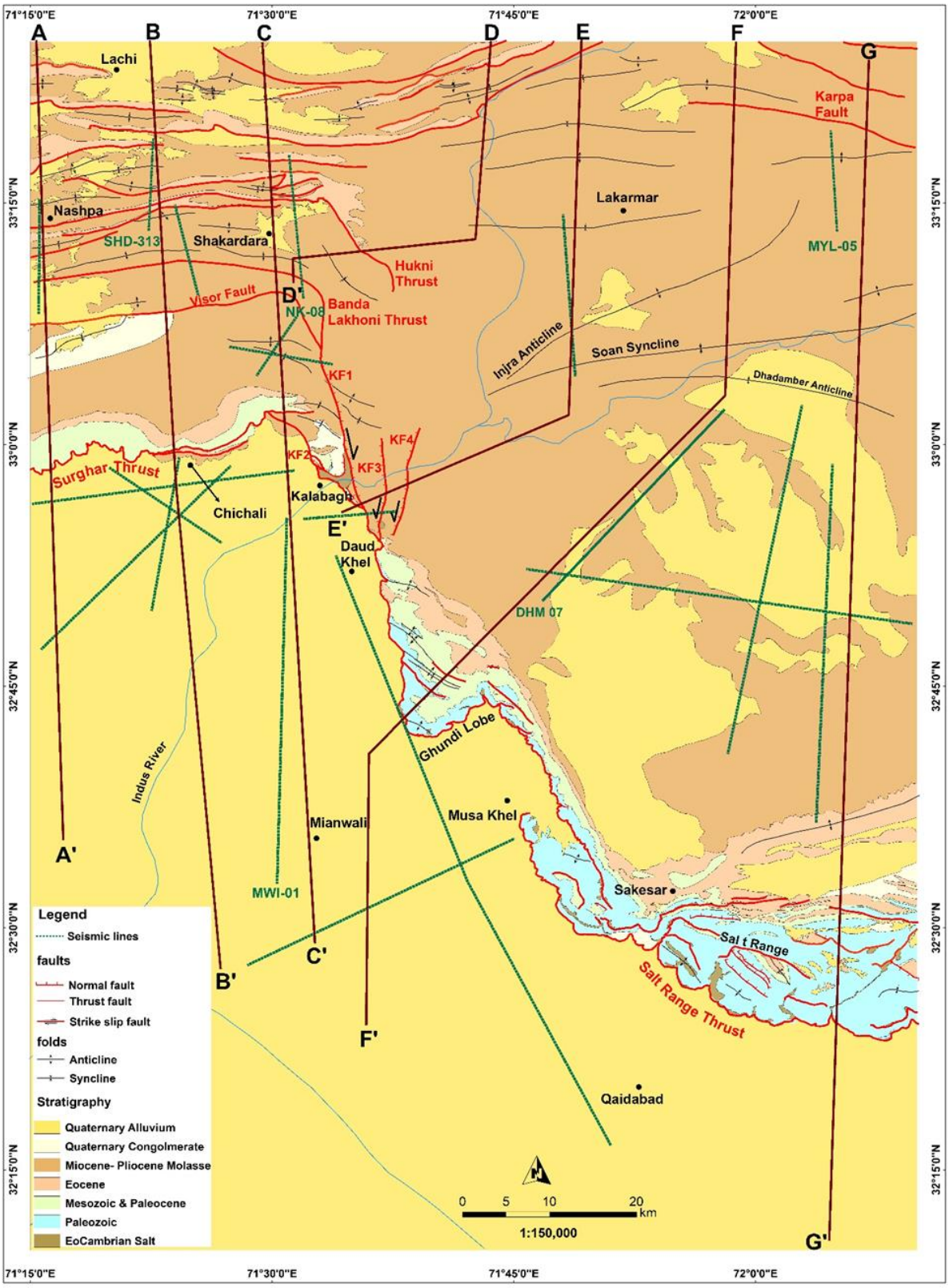

Figure 3.3. Geological map of the study area revised after Meissner et al. (1974) and Gee (1980). See figures 3.5 and 3.7 for seismic profiles (only 5 out of 20 interpreted seismic profiles shown in the map as green lines are presented in this paper). See figure 3.6 for cross-sections AA'-CC' and figure 3.8 for DD'-GG'.

The Eocene sequence in the Kohat is comprised of carbonate and evaporite deposited in a restricted marine basin (Meissner et al., 1974; Khan et al., 1986; Pivnik and Wells, 1996). The Bahadar Khail salt, Jatta gypsum, Sheikhan, Kuldana and Kohat formations represent the Eocene stratigraphy in the Kohat (Figs. 3.3-3.4). This evaporite belt is of prime importance because it forms a secondary décollement within the KP-FTB. In the Potwar, Surghar Range and Salt Range, the Eocene succession is comprised of the Nammal, Sakesar and Chorgali Formations, which contain carbonate interbedded with shale.

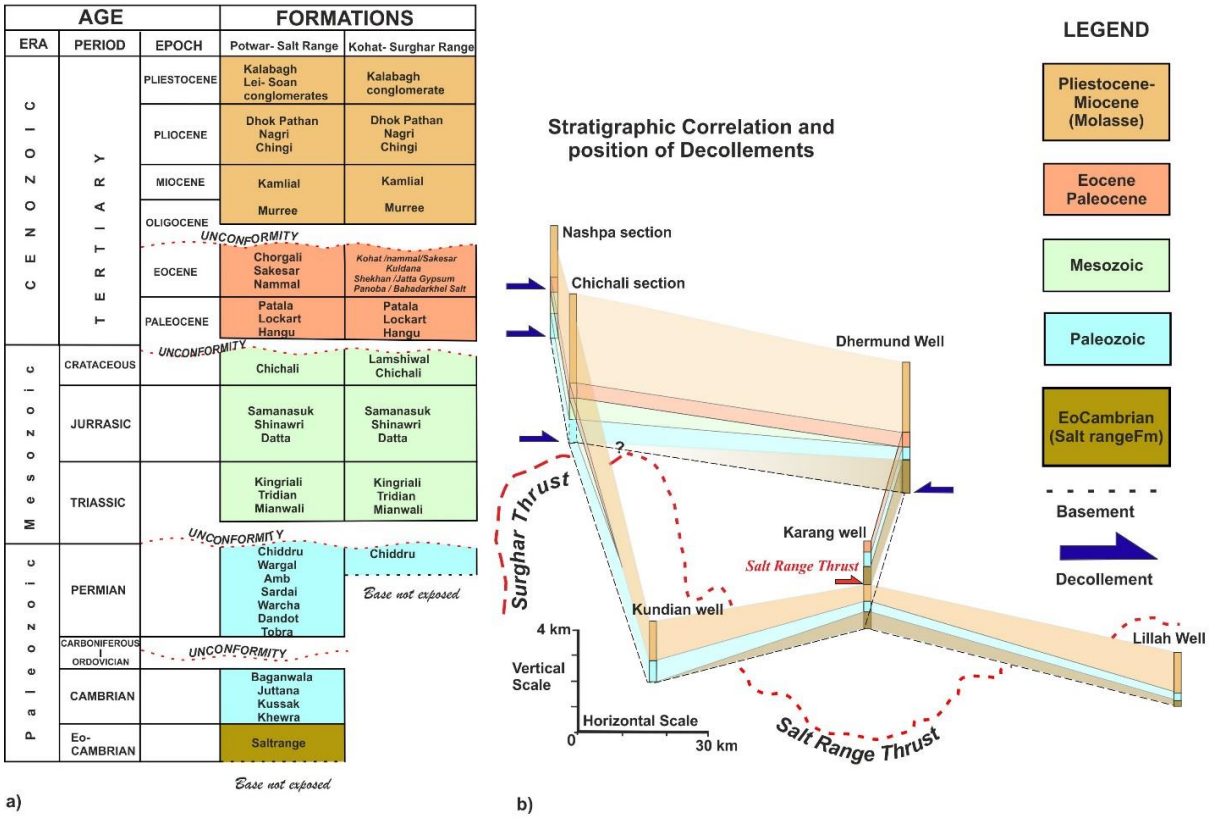

Figure 3.4. Stratigraphic column and correlation chart showing north to south thickness variations of different stratigraphic packages. Horizontal scale for location of sections and vertical scale for thickness of sections. Stratigraphic column and chart is modified after Qayyum et al. (2015), Gee (1980), Meissner et al. (1974) and Pivnik and Wells. (1996).

The molasse sequence is comprised of non-marine, syn-orogenic clastic sedimentary rocks. It is divided into two groups: the Miocene Rawalpindi Group, comprised of the Murree and Kamlial Formations and the Pliocene-Pleistocene Siwalik Group, consist of the Chingi, Nagri and Dhokpathan Formations. In the Kohat and the northern part of the Potwar, the molasse sequence is up to 5 km thick and lies unconformably over Eocene carbonate. It thins

toward the south. In the Kundian and Lillah wells, the thickness of the molasse is 1478 m and 1400 m, respectively (Fig. 3.4) (McDougall and Hussain, 1991; Qayyum et al., 2015).

3.4 Structural style of KP-FTB

Seven cross-sections have been constructed to show the structural style of the Kohat and Potwar. Cross-sections are constructed using map patterns, dip and strike orientations, seismic and well data using the structural modeling software MOVE. Twenty seismic profiles are interpreted to understand subsurface structural style; however, only five, representative of the structural style, are presented here. The locations of cross-sections and seismic lines are shown on the geological map (Fig. 3.3). Four sections are oriented north-south, parallel or sub-parallel to the tectonic transport direction deduced from the strike of fold axial traces and surface traces of faults. Three sections trend oblique and perpendicular to the tectonic transport direction. The purpose of the bent sections is to show the structural style in the subsurface across lateral ramps and rotated structures. Template beds in Move, termed as marker beds in the classical manual cross-section technique, are constructed from the surface dip data using parallel-type folds (Ramsay, 1967). These beds have kink-shaped geometries. In order to show the box fold and overturned fold geometries that are exposed at the surface in the Kohat, the shapes are modified (similar fold style) in the upper 2 km of sections. The equal parallel thickness method is mostly used to construct stratigraphy from template beds; however, the thickness of beds is reduced manually to deal with stratigraphic tapering from north to south. Mismatches between deformed and restored lengths of beds less than 20 m are ignored and considered acceptable for sections with length between 70 and 100 km.

Depth to basement is calculated to be 7 km in the Kohat and the northern part of the Potwar using undeformed stratigraphic thickness, seismic profiles, well data and previous sections by Abbasi and McElroy (1991), Jaswal et al (1991) and McDougall and Hussain (1991). A double décollement is interpreted in the Kohat at the base of the sedimentary cover and in the Eocene. A single décollement under the southern part of the Potwar and the Salt Range is interpreted in the SRF. Three sections are restored using fault parallel flow movement algorithms and the classical method of line-length balancing for competent lithologies and area-balance method for incompetent lithologies (Dahlstrom, 1969; Elliott, 1983) in Move. The cross-sections are integrated to develop a 3D model (Fig. 3.11) that shows structural style variation along and across the strike of the KP-FTB.

3.4.1 Kohat- Surghar

3.4.1.1 Seismic profiles

Ten seismic reflection profiles were used to interpret the subsurface structural style; however, only two lines representative of structural style are shown in this paper. The location of seismic lines is shown on Figure 3.3. Seismic data was collected during the 1980's and 1990's and the overall quality is poor in the Kohat (Fig. 3.5). A clear prominent reflector marking the basement on NK-8 and SHD-313 is not present on these lines; our interpretation of basement is based on the assumption of flattening of reflectors near 4.0 second two-way travel time (TWT) (Fig. 3.5) and the seismic interpretation of McDougall and Hussain (1991) in the Kohat. In the southern part of the Kohat, interpretation of seismic lines SHD-313 and NK-8 (Fig. 3.5) shows two décollement levels: below the Eocene and directly above basement. Folds and faults exposed at the surface are interpreted to continue down to only 1.5 second TWT. Surface folds and faults involving Eocene and molasse strata are interpreted to develop above the Eocene décollement. The strata reflections between 1.5 and 4.0 second can best be interpreted as north-dipping duplexes involving strata of Paleozoic to Paleocene age bounded by thrusts emanating from the basal décollement and merging with the roof thrust in the Eocene décollement (Fig. 3.5). Interpretation of seismic profile shows that the secondary décollement in the Eocene ends south of the Banda Lakhoni thrust; further south, the reflection patterns seem to be concordant from top to bottom. Below the Banda Lakhoni thrust, the duplex is breached by ramp in the southern part of line SHD-313 and NK-8.

3.4.1.2 Cross-sections

Three parallel sections, AA', BB' and CC', are oriented north-south and spaced ~20 km apart (Fig. 3.6). The basement slope on all sections change from nearly flat under the Kohat to 2-3° north-dipping under the undeformed foreland in the Kalabagh Reentrant. Strata tapering toward the south on the sections is interpreted from seismic profile MWI-01 (Fig. 3.7) and the well data of Kundian-01 (Fig. 3.4), indicating that Permian strata is overlain by molasse. The basement high in the southern part of section is the WNW projection of the Sargodha high (Fig. 3.1). Paleozoic to Pleistocene strata are folded in the hanging wall of the Surghar thrust (SGT), forming the frontal range of the Kohat. In section BB', two thrusts splay out from the SGT and join the main fault trace toward the east and west. The slip on the

thrusts resulted in a 2 km deflection in the Surghar Range front at Chichali section (Figs. 3.3, 3.6).

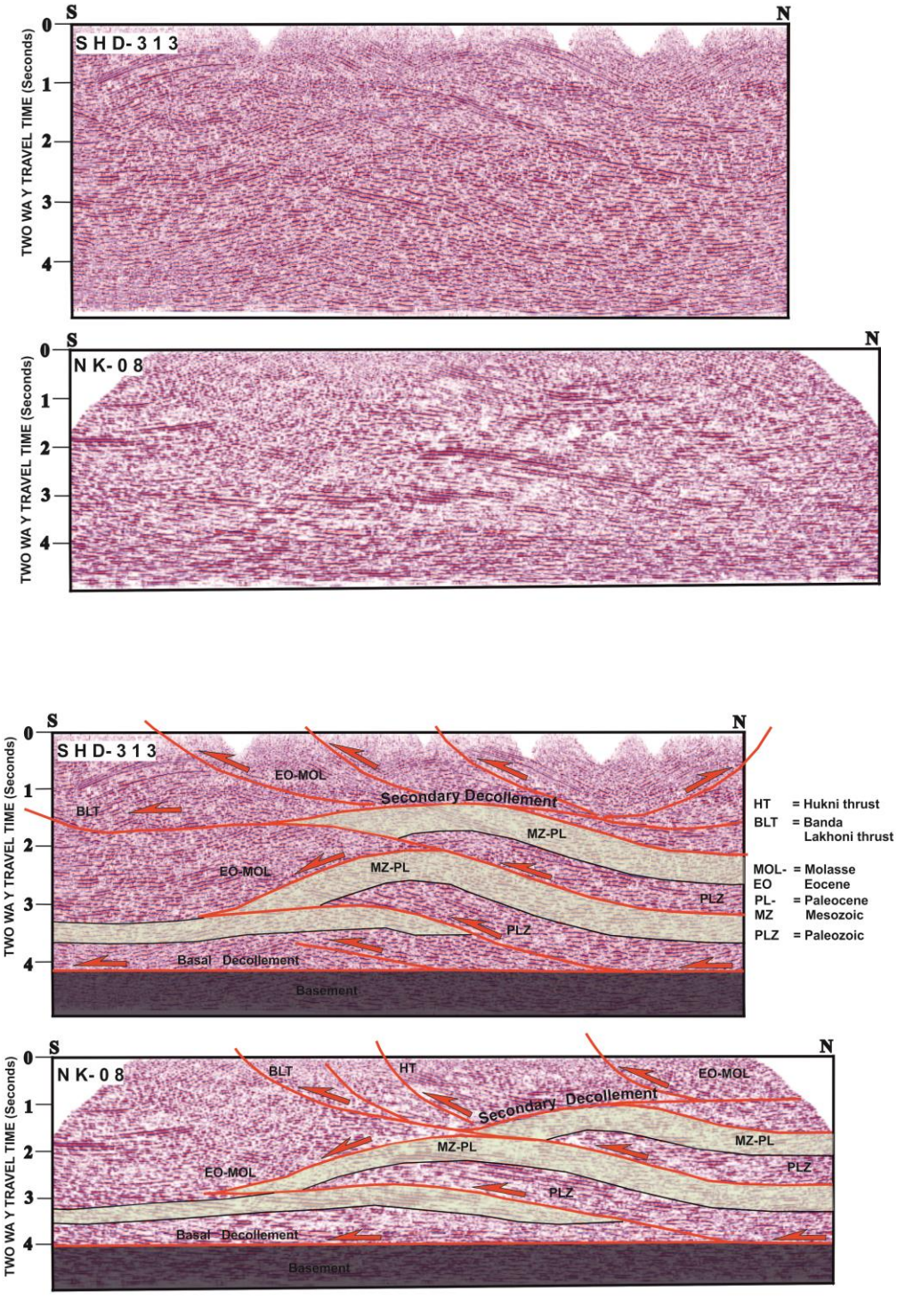

Figure 3.5. a) Un-interpreted seismic profiles from the Kohat (see fig. 3.3 for location of lines). b) Interpreted seismic profiles. Lines NK-08 and SHD-313 show surface faults that originated above the

roof thrust in a secondary detachment. Duplexes are located between basal and secondary décollements. Note breached duplex under the Banda Lakhoni thrust.

Map patterns and sections show that the upper 1.5 to 2 km in the northern part of Kohat is comprised of box folds with overturned limbs cut by thrust faults developed above Eocene salt and gypsum. Constructing sections from surface dip data and the thickness of different stratigraphic units show that these surface folds cannot be projected much deeper into the section than pre-Eocene stratigraphic units as this would produce a significant gap between the section and basement. This shows that surface structures originated from a décollement in Eocene evaporites. Hinterland-dipping duplexes comprised of Paleozoic to Paleocene strata are interpreted on seismic profiles to be present between the sole thrust at the base of the sedimentary cover and the roof thrust in the Eocene (Fig. 3.6). Duplexes are formed on ramps that develop from a sole thrust above the basement and merge with a roof thrust in the Eocene. Out-of-sequence movement is interpreted on the duplex ramp present below the Banda Lakhoni and Hukni thrusts (Fig. 3.6, 3.9).

A fault bend fold in the footwall marks the limit of the secondary décollement in the Kohat. The roof thrust reaches its southern limit at this structure. The Visor fault is an out-of-sequence reverse fault in the Kohat (Abbasi and McElroy 1991, McDougall and Hussain 1991). South of the Visor fault, a fault propagation fold is present on a blind thrust in sections BB’ and CC’. On the surface, this anticline structure is present is cut and displaced about 7 km to the south in the hanging wall of KF1 (Figs. 3.1, 3.3). Ten kilometer south of the Surghar Range, a blind thrust fault is forming a new structurally controlled range front (Figs. 3.6, 3.12).

3.4.1.3 Restored sections

Sections AA’ and BB’ are fully restored whereas section CC’ is partially restored due to out of section strike-slip movement in the Kalabagh Fault Zone. The restored section AA’ and BB’ show ~13 to 14 km of slip on the SGT (Fig. 3.6). Duplexes are restored using a fault-parallel flow algorithm to calculate slip on the fault ramps. Line length method is used to restore line-parallel shortening in the horizons; that is less than 1 km observed in all section for strata older than Eocene. There was 7 to 13 km of slip on the ramps, including 1.5 km of out-of-sequence slip on the ramp of the breached duplex beneath the Banda Lakhoni thrust. The restored length of the duplex in sections AA’, BB’ and CC’ accommodated between 21 to 24 km of shortening. Strata above the Eocene are restored using the line-length

balancing method north of the Banda Lakhoni thrust. The restored lengths on the top Eocene and molasse stratigraphic sequence indicate that cumulative shortening of about ~ 32 km in section AA' and ~ 25 km in section BB' resulted from buckling and fault related folding of the Eocene décollement. The complete area restoration of section AA' and BB' shows a difference of 4 and 10 km^2 between the deformed and restored sections. The difference is less than 2% of the total section area; this is acceptable assuming a 10% error on the shortening. The 10% error is assumed to account for the difference in shortening between sections, uncertainty in depth to décollement, stratigraphic thickness for the Paleozoic strata and molasse strata, eroded cutoff angles and difference in area restoration.

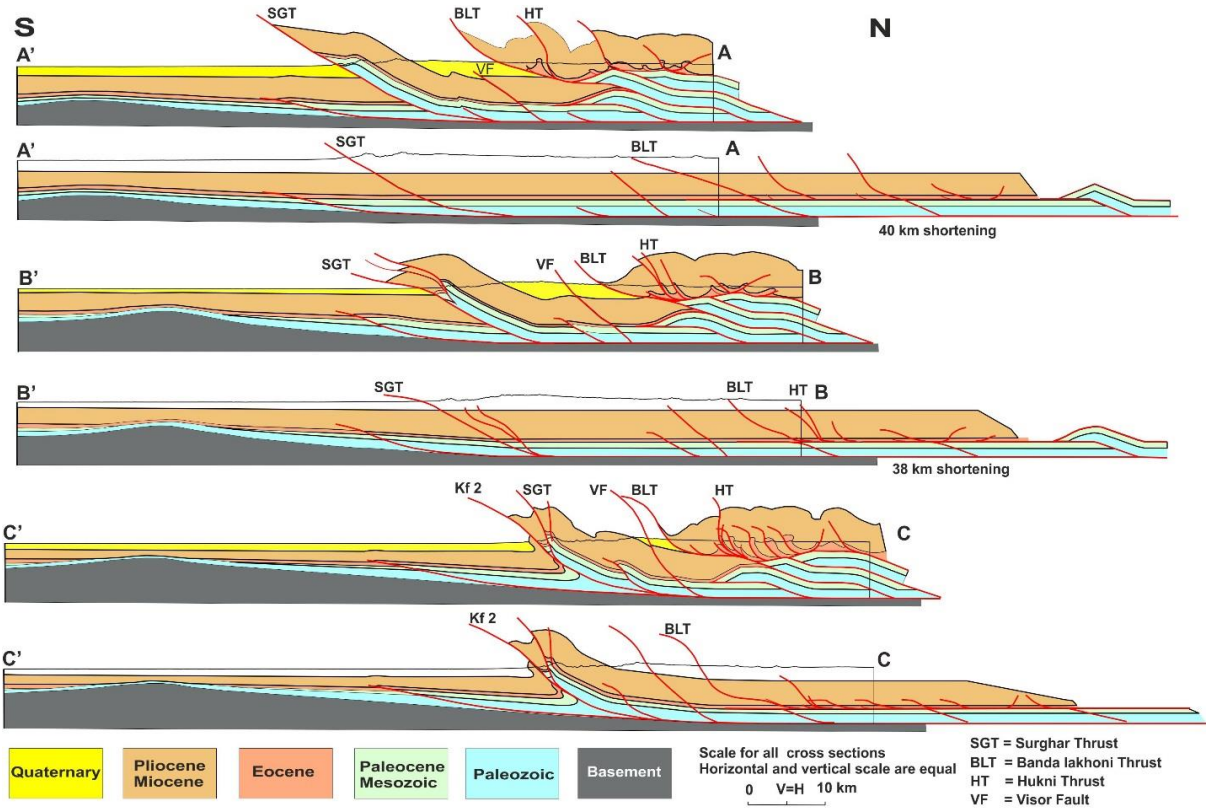

Figure 3.6. Cross-sections traversing the Kohat (see fig. 3.3 for location of sections). Deformed sections show the structural style above the double detachments. Box folds at the surface above Eocene strata are cut by faults originating from an active roof thrust. Duplexes in Paleocene and older strata cause tectonic thickening of the northern part of the section. A breached duplex cuts the upper detachment below the Banda Lakhoni thrust. The Surghar Range is located above the emergent SGT that ramps up from the basal detachment. Note imbrication in the SGT hanging wall in section BB' and fanning of thrust and normal faults in section CC' in the Kalabagh Fault Zone. In the footwall of the SGT, a younger thrust marks the new range front. Fault trajectories in the restored section AA' and BB' are admissible. Note length differences below and above roof thrust.

The overall shortening is 38 ± 4 km below and 28 ± 3 km above the Eocene décollement. The difference in shortening across the Eocene décollement is due to the additional lengths of duplexes incorporated into the complete section, uncertainty in thickness of Eocene strata, eroded Eocene and molasse strata above present topography and depth to upper décollement. The final restored geometries are admissible and satisfy the criteria for balanced sections (Fig. 3.6).

3.4.2 Potwar, Salt range and Kalabagh fault zone

3.4.2.1 Seismic profiles

Ten seismic reflection profiles were used to interpret the subsurface structural style; however, only 3 lines representative of different structural styles are shown (Fig. 3.3). Interpretations take into account the surficial structural geology and previous interpretations (Lillie et al., 1987; Jaswal et al., 1997; Khan et al., 2012; Qayyum et al., 2015; Leathers, 1987). Seismic profiles in the southern Potwar, Salt Range and Kalabagh Reentrant are divided into four seismic stratigraphic units. 1) The molasse is identified by semi-continuous, parallel reflectors of moderate amplitude. 2) The Cambrian-Eocene stratigraphic package exhibits a series of strong, parallel, continuous reflections of moderate to high amplitude. 3) The Precambrian SRF is characterized by a semitransparent zone with discontinuous reflectors. 4) Crystalline basement of the Indian Shield is usually the prominent reflector at the base of the stratigraphic section (McDougall and Hussain, 1991; Jaswal et al., 1997; Khan et al., 2012; Qayyum et al., 2015).

The top of basement is interpreted at 4.0s two-way travel time (TWT) on seismic line MYL-05 (Fig. 3.7) based on the assumption of flattening of reflectors near 4.0s TWT. The basement on seismic line DHM-07 is a prominent reflector dipping northward on the time section between 2.0s to 3.0s TWT (Fig. 3.7). In the Kalabagh Re-entrant on seismic line MWI-01, a basement high is interpreted (Fig. 3.7), which is probably the west-northwest projection of the Sargodha high, located to the south of Salt Range (Fig. 3.1) (Leathers, 1987; McDougall and Hussain, 1991). The seismic data show basement dips toward the north and west in the southern Potwar and Kalabagh Re-entrant and gradually flattens under the Kohat and in the northern Potwar at 4.0s TWT. The gently-dipping basement represents the foredeep of the Himalayan foreland; the basement high represents the forebulge.

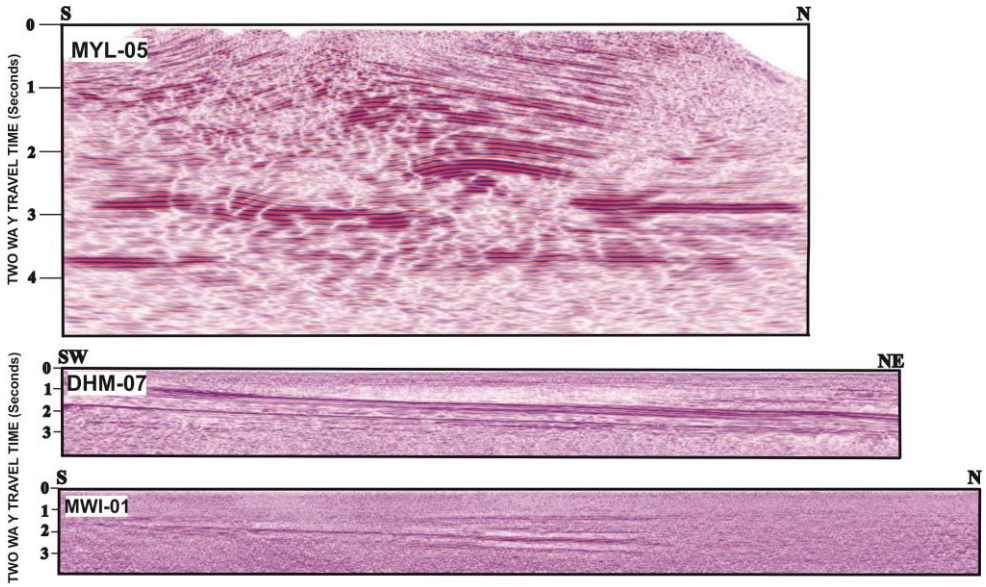

a)

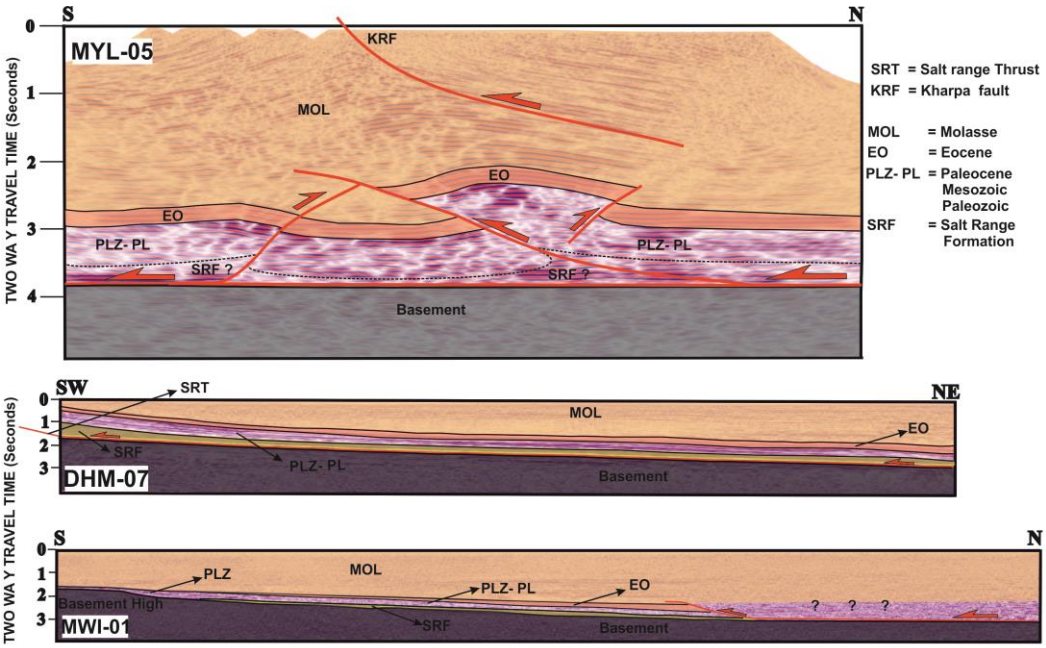

b)

Figure 3.7. a) Un-interpreted seismic profiles from the Potwar and the Kalabagh re-entrant (see fig. 3 for location of lines). b) Interpreted seismic profiles. Line MYL-05 shows the structural style at the southern end of the NPDZ A pop-up structure and a triangle zone in the footwall is interpreted. Line DHM-07 shows gentle folds in the southern Potwar. Note the accumulation of salt in the core of gentle anticlines and under the Salt Range ramp. Line MWI-01 in the Kalabagh re-entrant shows the southward taper of the stratigraphic wedge; the basement high in the southern part is the NW projection of a Sargodha basement high formed of Indian shield rocks exposed in the Kirana hills (see fig. 3.1). Fault in the middle of line MWI- 01 delineates the new range front.

The SRF as a semi-transparent zone of discontinuous reflectors that can be easily identified in the southwestern part of the Potwar above a north-dipping prominent basement reflector on lines DHM-07 and MWI-01. The thickness of salt varies in the northern part of line DHM-07 due to salt expulsion beneath the gentle synclines into the core of the gentle anticlines (Fig. 7). Line MYL-05 shows pop-up structure above the tip of blind thrusts emanating from the basal décollement (Fig. 3.7). A triangle zone is interpreted in the footwall of a pop-up structure. Line DHM 07 shows gentle folding in the Cambrian to molasse strata above the SRF. The SRT is interpreted as a sole thrust in the southern Potwar (Fig. 3.7).

3.4.2.2 Cross-sections

Three of the four Potwar sections (DD', EE', and FF') have bends in the section trace to show the structural style of the Salt Range and the Kalabagh Fault Zone; section GG' is straight. Three major structural styles are interpreted from north to south on sections EE', FF' and GG' (Fig. 3.8). In the southern part of the section FF' and GG', the Precambrian to Pleistocene strata are transported above a frontal ramp and a lateral ramp, forming a fault bend fold known as the Salt Range that is bounded on the south by the emergent SRT. The dips of exposed strata above the ramp are 20-30° in the central Salt Range to 45-55° in the western Salt Range. The crestal portion of this fault bend fold structure contains asymmetrical tight folds with curved axial traces bounded by thrusts and normal faults (Figs. 3.3, 3.8).

In the central part of sections FF' and GG', the Cambrian to molasse stratigraphic sequence is gently folded as a single slab above the SRF in kilometric scale folds such as the Soan syncline (Figs. 3.1, 3.3 and 3.8). Salt accumulation in the core of anticlines are present in the sections. Interpretation and time to depth conversion of seismic data suggest that the dip of the basement increases from nearly flat to 2-3° south of the Soan syncline. In the northern part in all sections, thrust fault ramps from the basal décollement terminate into fold core in the molasse. These thrust faults are the continuations of ramps in the Kohat duplexes. A pop-up structure is developed between fore-thrust and back-thrust in the northern part of section GG'. A triangle zone is interpreted to underlie the footwall of the blind fore thrust. The basement in the northern part is flat and at a depth of 7 km, similar to the Kohat.

The southern part of section EE' is roughly perpendicular to the Kalabagh Fault Zone (Fig. 3.8). The frontal thrust has a steeply dipping (70-80°) ramp and hosts three major normal faults in its hanging wall. The faults have a dextral and sinistral component of shear

along their fault planes (Fig. 3.3). Salt has moved in the footwall of these normal faults and salt diapirs are seen in the molasse in the field along the footwall (Fig. 3.10). A half graben is interpreted between normal faults KF1 and KF3 (Fig. 3.8). The KF1 is the main lineament of the Kalabagh fault zone; the map pattern and our section suggests right lateral transtensional movement of ~7 km and active expulsion of salt under the hanging wall toward the footwall (Figs. 3.3, 3.10).

Section DD' is constructed between the Kohat and Potwar. In the northern part near the surface, molasse strata are intensely folded and faulted above the Eocene décollement. In the subsurface, ramps of blind thrusts shown in sections EE', FF' and GG' becomes 10-15° steeper, molasse strata are sandwiched between these ramps and the upper Eocene décollement; they thin towards the west and eventually disappears under the secondary décollement in the Kohat section CC'. The accumulation of salt beneath the blind thrust footwall is modelled based on the presence of the SRF in this part of the Potwar and the occurrence of a ~5 km^2 area gap in the section. The fault bend fold and surface structures from sections AA', BB', and CC' change their orientation to north-south as shown on the map and model (Figs. 3.1, 3.3 and 3.11). The eastern limit of the Eocene décollement is modeled above the fault bend fold. The Banda Lakhoni thrust and Visor thrusts are close together and eventually join further south into the KF1. The displacement of the fault that forms a fault bend fold ends 10 km SE in the Potwar.

3.4.2.3 Restored sections

Section GG', parallel to the tectonic transport direction, is restored in order to calculate shortening in the western Potwar and Salt Range. Section DD', EE' and FF' are not restored due to out of section strike-slip movement related to the Kalabagh Fault Zone. Retro deforming the SRT shows ~30 km of slip in section GG' including shortening related to faults and folds in the Salt Range. Five km of slip is documented on blind thrusts in the northern part and the rest of the shortening is achieved by folding above its tip. A 10% error is assumed to account for the uncertainty in depth to décollement, thickness of SRF, changes in stratigraphic thickness from north to south, position and cutoff angle of SRT, salt diapiric movement and normal faulting in the Salt range. The difference in area restoration is less than 2% for the complete section. The overall shortening is 40 ± 4 km in section GG'.

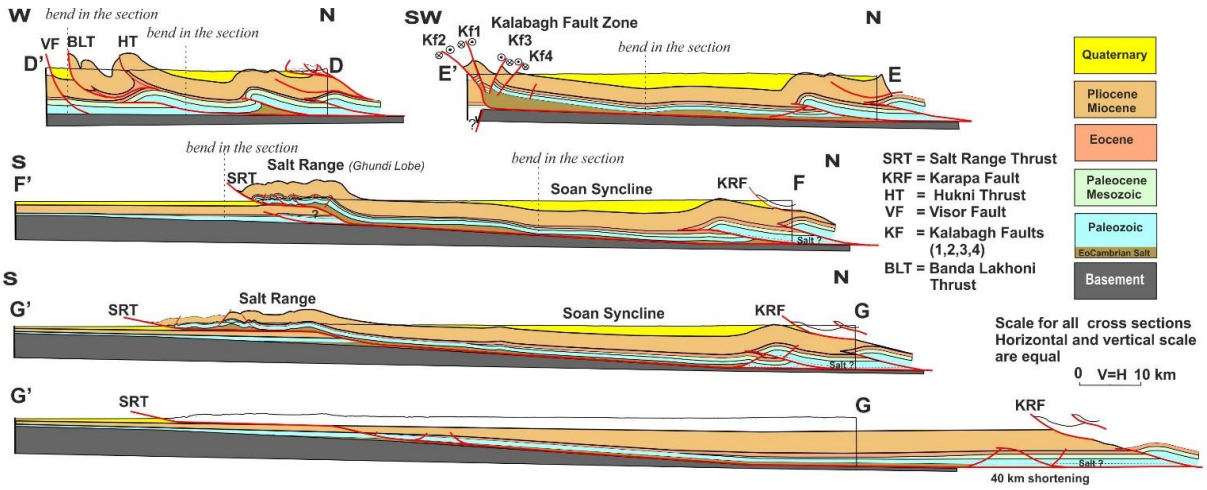

Figure 3.8. Cross-sections through the Potwar, Kalabagh Fault Zone and the Kohat (see fig. 3.3 for location of sections). Section DD' shows the boundary zone of the Kohat and the Potwar. In the northern part of the upper detachment in the Eocene, asymmetric folds and faults are depicted. The upper detachment is shifted from the Eocene to the molasse in the boundary zone. The Karapa Fault (KRF) originated above the molasse. The accumulation of salt below the blind thrust was expelled from the adjacent syncline and triangle zones. In the Kohat section, section DD' shows the anatomy of structures that were rotated at the surface from EW to NS. Note the branching point of the Eocene detachment depicted by the facies change. Cross-section EE' shows parts of the Potwar and Kalabagh Fault Zone. The northern part of section EE' shows a fault propagation fold above a triangle zone and gentle folding in the middle part. In the southern part, it shows the structural style of the Kalabagh Fault Zone. The steeply dipping KF2 is an extension of the SRT from the Potwar. The hanging wall is collapsed by normal faults. All faults in this part have a dextral shear component. In the southern part of cross-section FF', the section runs through the Ghundi lobe. Fore-thrusts and back thrusts with asymmetric folds can be seen in the crestal part of the Salt Range. The ramp of the SRT is steeper in this part and salt accumulation is thick compared to section GG'. Deformed and restored section GG' shows a pop-up structure and triangle zone in the northern part and gentle folding above the SRF. The Salt Range is a fault bend fold structure bounded on the south by the emergent SRT.

3.5 Discussion

Fold and thrust belts (FTB) show structural variations along and across strike due to changes in the mechanical strength of the décollement, basement architecture, presence of preexisting structures and varying wedge thickness. The structural style of the Potwar and Salt Range is explained here quite similarly to previous research. It consists of three zone

from north to south, 1) NPDZ, 2) Soan syncline, and 3) Salt Range. The basic common characteristic of all the previous cross-sections constructed in the Potwar and cross-sections constructed in this study show, that the dip of the basement changes from <1° in the north to 2-3° under Soan syncline and Salt Range and the décollement is located in the SRF. Thrusting along the Salt Range ramp started in the first stage of deformation around 5 Ma (Burbank et al., 1986, Burbank and Raynolds, 1988, Burbank and Beck, 1989, 1991). The formation of duplexes in the NPDZ around 2 Ma (Jaswal et al., 1997) is contemporaneous with a second phase of southward propagation of deformation that resulted in the expulsion of salts beneath part of the competent strata, forming the Soan syncline and the accumulation of salt in the cores of the Injra and Dadhmber anticlines (Figs. 3.3, 3.7 and 3.8). The displacement in the eastern and central Salt Range is measured to be 20 to 27 km in balanced cross-sections (Baker et al. 1988, Qayyum et al., 2015). Cross-section GG' suggest 30 km of displacement at the boundary between the central and western Salt Range (eastern boundary of map in figure 3.3). In the northern part of Potwar sections, fault propagation folds and a pop-up structure are developed above blind thrusts. These blind thrusts are continuations of ramps branching from a duplex system beneath the Kohat (Fig. 3.11). These thrusts have similar spacing in the Kohat and Potwar in restored sections, cutting up stratigraphic section from the basal décollement at the sedimentary rock-crystalline boundary; however, in the Kohat they join the upper décollement in Eocene strata and in the Potwar they terminate in the molasse strata (Fig. 11). It is uncertain whether the décollement in the Kohat and northern Potwar is present in the salt or the brittle clastic sedimentary rocks. In our cross-section, a passive roof thrust is not shown in molasse as was previously by Jaswal et al (1997). The fold geometries in the northern part consistently show a complete stratigraphic sequence compared to the Kohat, where Eocene strata is decoupled above the upper décollement. The surface structures in the Potwar do not show a north vergence, which should be exhibited if there is a passive roof thrust. Baker et al (1988) reported 65 ± 5 km overall shortening in the Potwar from the MBT to the Eastern Salt Range; however, Jaswal et al (1997) reported only 55 km of shortening in the NPDZ. Our shortening estimates of 40 ± 4 km in the western Potwar is 10 km more than earlier reported and comparable to the 26 km width of Salt Range fault bend fold in this area. The structure is 15 and 18 km wide in central and eastern Salt Range, respectively. If our sections were extended to the MBT, they might yield ~ 75 ± 5 of shortening.

The reasons for the simple structural style of the Potwar and Salt Range is compared in physical analogue models to wedges deforming above ductile décollements (Davis and Engelder, 1985; Cotton and Koyi, 2000), a change in basement slopes >1° (Smit et al., 2003), and translation above an incipient basement normal fault (Faisal and Dixon 2015). We suggest that the presence and movement of salt, steeper basement slope and a relatively thin stratigraphic wedge are the factors that acted collectively in shaping the simple structural style of the southern Potwar and the Salt Range.

The cross-sections in the Kohat suggest that deformation propagated on two décollements: the flat basal décollement at the sedimentary rock-crystalline boundary and the secondary, weaker décollement in the Eocene evaporites. Deformation on the thrust ramps cut stratigraphic sections towards the foreland. The older thrust ramps are translated and rotated above newly formed ramps, resulted in tectonic thickening and hence uplift of the stratigraphic sections. Box folding and faulting of surface structures in the Kohat suggests buckling above the Eocene décollement prior to faulting above an active roof thrust in the Eocene evaporites (Fig. 3.9). Our interpretation of the southern Kohat is similar to the interpretation of deformation on double décollements by Abbasi and McElroy (1991); however, due to change of facies from evaporites to shale in the northern Kohat and the lack of seismic data, the model remains to be tested with a double décollement structural style in the northern Kohat. Due to the broader extent and the 3D compatibility of structures between the Kohat and the Potwar in our model, it differs from the one by Abbasi and McElroy (1991) in four main aspects. 1) The structural geometries of the surface structures and the duplexes in our sections are laterally well constrained through closely spaced parallel cross-sections. Duplexes in our model are transported and rotated above younger ramps forming toward the foreland and laterally continue toward Potwar as blind thrusts (compare figures 3.2b, 6 and 11). 2). Our sections suggest that the surface structures in the Kohat evolved above an active roof sequence (Bonini, 2007; Couzens-Schultz et al., 2003), contrary to the interpretation of a passive roof model (Banks and Warburton, 1986). The southward vergence of surface structures towards the foreland above north dipping duplexes in the Kohat is the opposite of the passive roof duplex models in which roof sequence vergence is opposite to the vergence of underlying horses in duplexes. 3) We have interpreted out-of-sequence thrusting on the ramp of the duplex beneath the Banda Lakhoni thrust (Fig. 3.6). 4) The Banda Lakhoni thrust in our cross-sections is well constrained and modeled to have originated from a secondary décollement under the Eocene strata instead of developing from the basal décollement (Fig.

3.6). The balance cross-section of McDougall and Hussain (1991) shows extensive movement of thrust sheets, translating out-of-sequence on top of younger ramps and forming duplexes and fault bend folds. Our section shows the same shape of the duplex; however, it doesn't agree with models that show a passive roof thrust in the molasse. The molasse strata in their sections are not restored and exempted based on the assumption of excessive erosion. In our section, we have modeled the complete molasse stratigraphic sequence for consistency in structural geometries and calculation of overall shortening. The sections of Pivnik and Sercombe (1993) does not cover the southern Kohat, so we didn't compare our results to their sections.

The total minimum shortening in the Kohat is reported 55 ± 5 km by Abbasi and McElroy (1991) and 84 km by McDougall and Hussain (1991) from the MBT to the Surghar Range. The difference in shortening is a result of a 1 km difference in depth to basement between the sections, an overestimation of shortening below the molasse in McDougall and Hussain (1991), and the absence of out-of-sequence movement on the ramps. Our shortening estimate for central and southern Kohat is 38 ± 4 km, which is comparable to the parallel section in the Kohat and Potwar. The remaining shortening is accommodated by the structures in the northern Kohat. The overall shortening obtained from our cross-sections are almost the same: ~40 km at both ends of the model (Fig. 3.11).

The Salt Range is ENE-WSW oriented in most of the eastern and central part (Figs. 3.1) (Gee, 1980). The orientation of the Salt Range changes to NW-SE between the villages of Sakesar and Kalabagh (Figs. 3.1, 3.3). The area is known as Kalabagh Fault zone (McDougall and Hussain, 1991). It is interpreted as a 120 km long tear fault (McDougall and Hussain, 1991) linking the Salt and Surghar ranges and the lateral ramp for the Potwar (Butler et al, 1987). Farah et al. (1984) propose a basement step of 2 km under the Kalabagh Fault Zone. The structure style of the Salt Range in this area changes from a fault bend fold to a simple anticline above the SRT (Butler, 1987), except near the Daud Khail, where it forms the Ghundi lobe (Figs. 3.3, 3.8). The trend of folds and faults have an en-echelon pattern in the Ghundi lobe. In our model, the Kalabagh Fault Zone is interpreted as a complex fault zone. The structural evolution of the zone is associated with thrusting overprinted by salt tectonics and associated normal faulting. Salt diapirs in the footwall of the KF1 and a salt dome beneath Kalabagh are associated with the expulsion of salt beneath the hanging walls of normal faults towards the footwall (Fig. 3.10a). The expulsion of salt from some parts and the accumulation in other parts triggered normal faulting in the Kalabagh Fault Zone and the Salt

Range, and out-of-sequence thrusting in the Kohat. Movement of salt and associated normal faulting is reported from areas having salt involved in deformation (Alsop et al., 2015). The Visor fault and the Banda Lakhoni thrust in Kohat joins the KF1 of the Kalabagh Fault Zone (Fig. 3.3). The reverse slip movement of the Visor fault is linked to the dextral normal slip movement of KF1 in the Kalabagh Fault Zone. We interpret the Kalabagh Fault Zone to be a rotational fault comprised of dextral normal slip faults in the Kalabagh fault zone and out-of-sequence reverse fault in the Kohat. The strike-slip displacement in the KF1 is~7 km and dip slip displacement is~1.5 km. The strike slip movement along KF2 and KF3 is 2-3 km.

There are problems in all of the previous work that require clarification. How is the translation of 20-30 km in the Salt Range accommodated in the western Potwar and Kalabagh Fault Zone? What are the causes for the formation of the Ghundi Lobe in the western Salt Range? The amount of displacement restored on the frontal thrust is 20-30 km in the Eastern and Central Salt Range. This magnitude of displacement is absent in the area between the Sakesar and Kalabagh, where the Potwar thrust sheet is displaced for less than 5 km across the lateral ramp, except in the Ghundi Lobe, where it shows~15 km of displacement across the lateral ramp (Figs 3.6, 3.8). Displacement of 15 km requires rotation in the western Potwar; however, paleomagnetic data does not show rotation in the western Salt Range compared to the eastern Salt Range (Opdyke et al., 1982; Burbank and Beck, 1989). The solution proposed in this research for this problem is that the translation of 20-30 km in the Salt Range is accommodated by out-of-section motion along the lateral ramp perpendicular to the plane of cross-section GG' (Fig. 3.12). The 10 km additional displacement in the Ghundi Lobe is a direct result of 7 km of strike-slip displacement on fault KF1 and late stage movement of salt from the Kalabagh to the Salt Range. This produced the Ghundi Lobe structure in the south and the change in strike of the Hukni thrust from EW to NS in the Kohat (Fig. 12). An alternate interpretation is that a thick accumulation of salt beneath the lobe formed this feature. In both solutions, the total displacement in the Kalabagh Fault zone from the KF1 to the tip of the Ghundi lobe is not more than~10 -12 km.

The two possible explanations for the formation of Kalabagh Reentrant, the deflection in the range front at the southern boundary of the KP-FTB, and changes in the trends of the structures near Shakardarra (Fig. 3.13). 1) The deflection is directly linked to the change in mechanical strength of the basal décollement. Deformation propagated faster towards the south on the salt in the Potwar compared to the Kohat, as proposed by Cotton and Koyi (2000). The deflection in the trend of the structures in the north followed the same

mechanism as at the range front (Fig. 3.13a). The Kalabagh Fault Zone formed at the transition zone where the basal décollement changed from salt beneath the southern Potwar to a less ductile décollement on flat basement beneath the Kohat. 2) The deflection of the range front is controlled by a preexisting basement normal fault, which provided a frontal and lateral ramp for thrust sheets to form the deflected range front of the KP-FTB. The presence of the basement normal fault itself is a dominant factor that nullifies the role of the basal décollement in the deflection of range front; however, in our opinion, if salt is present beneath the KP-FTB, a basement normal fault would be necessary beneath the entire range front (Fig. 3.13b). In the absence of such a normal fault, it is unlikely that the KP-FTB deformed above a similar basal décollement to form a reentrant and deflected range front.

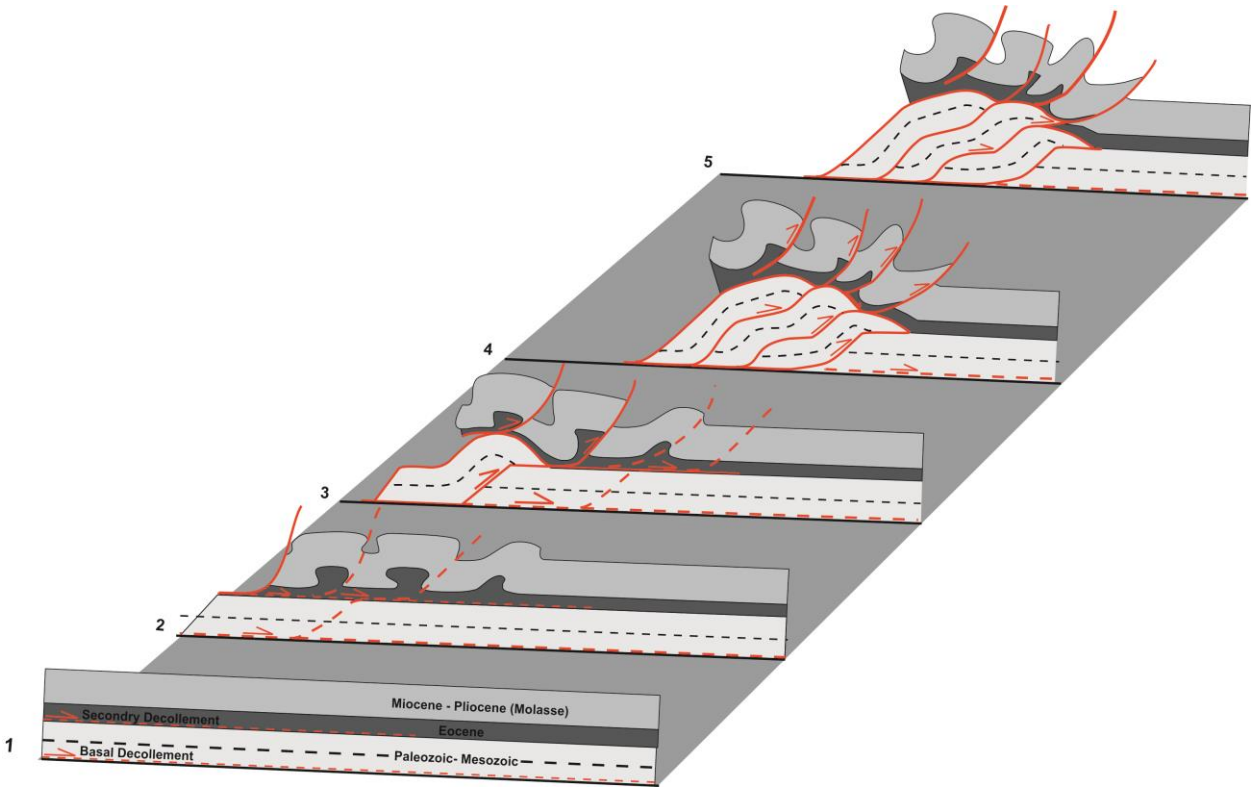

Figure 3.9. Proposed sequential structural evolution within the Kohat. 1) Undeformed sequence and position of décollements. 2) Folding on secondary décollement prior to faulting. 3) Movement on floor and active roof thrust toward foreland 4) Formation of duplex between floor and roof thrust. Note the different geometry of folds and faults above the roof thrust and in the duplexes below. 5) Out-of-sequence movement on ramp of breached duplex.

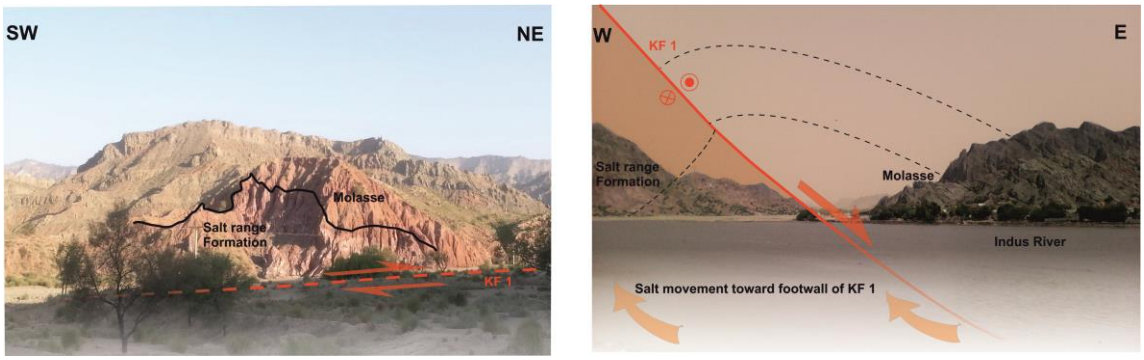

a) *b)*

Figure. 3.10. Field photographs of the Kalabagh Fault Zone. a) Salt diapir in the molasse sequence. b) KF1 fault shows dextral shear and normal slip movement. The SRF is in the footwall and molasse is in the hanging wall.

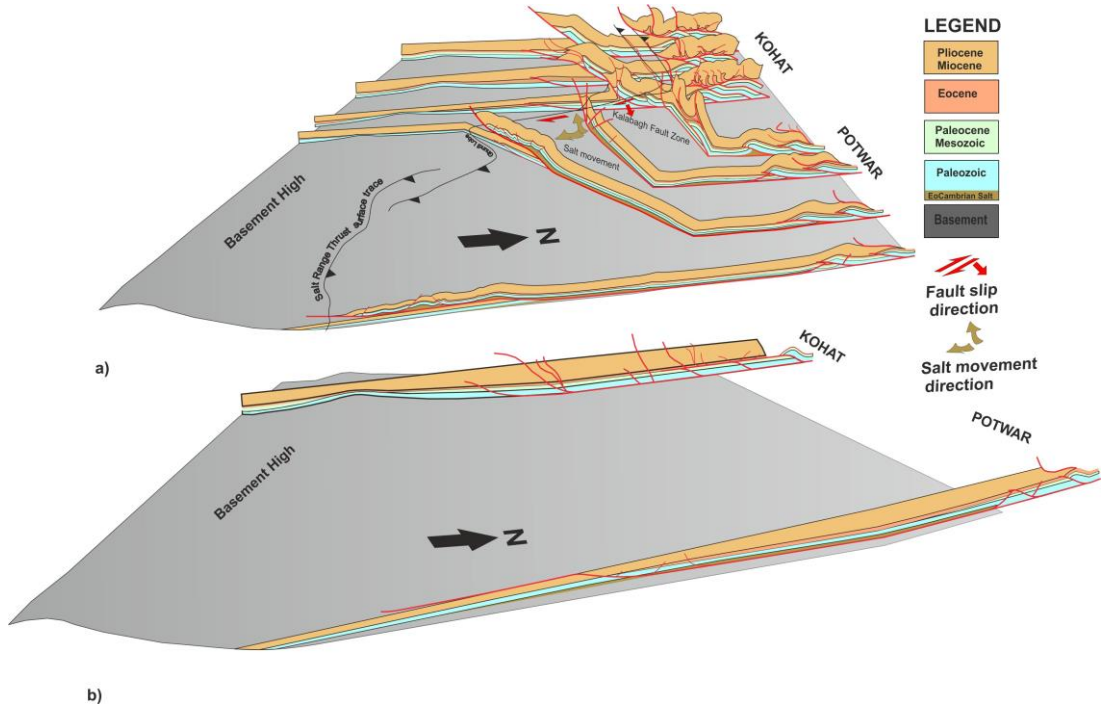

Figure 3.11. Deformed and restored model of the KP-FTB. a) Structural model shows deformation style in the study area. Note the continuation of structures in the northern part from Kohat to Potwar. Ramps in the duplexes of Kohat continue into Potwar as blind thrusts. The secondary detachment in the Eocene steps up into the molasse in the boundary zone. We hypothesize that the movement of salt from the Kalabagh Fault Zone towards the Salt Range formed the Ghundi lobe structure. The footwall of the Salt Range thrust is faulted and can be correlated with the blind thrust in the footwall under the Ghundi lobe and the Surghar thrust. b) The restored structural model shows that restored fault planes can be correlated from Kohat to Potwar and almost same magnitude of shortening at the eastern and western end of the model.

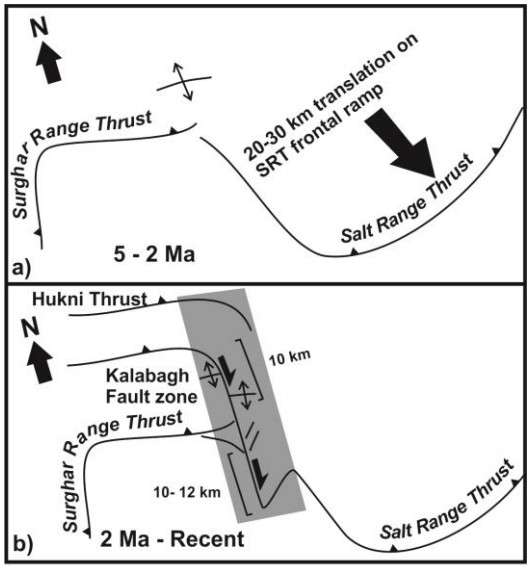

Figure 3.12. Sketch to show the sequence of thrusting that shaped the Kohat and Potwar range front. a) The formation of Surghar and Salt Ranges through translation on range front thrusts until 2 Ma. b) Late-stage strike-slip and normal-slip movement in the Kalabagh fault zone of 10 – 12 km forms 13 km Ghundi lobe and changing strike for some part of Hukni thrust in the north. The shaded area is only effected by strike-slip movement and accommodated all the shortening related to it, thus plane strain for the balanced cross-sections AA', BB' and GG' is conserved.

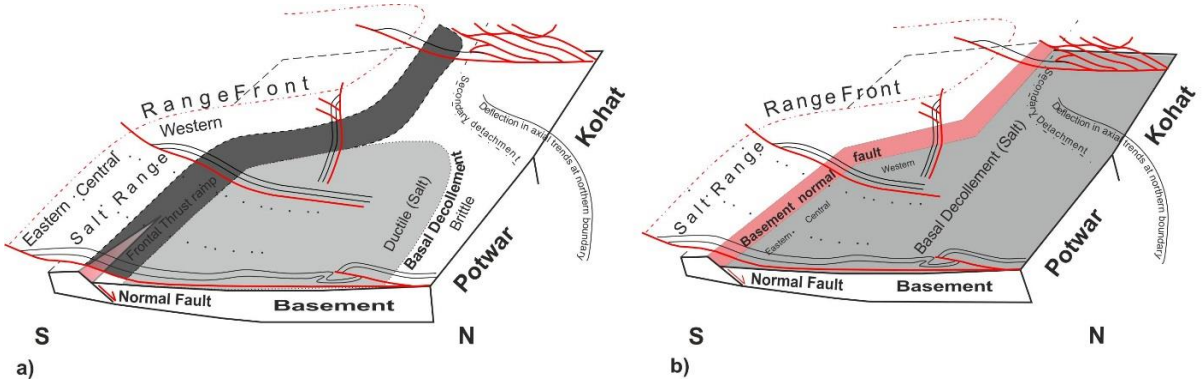

Figure 3.13. 3-D diagram of the KP-FTB illustrating two possible geometries for the basal décollement and the basement normal fault and how these could influence the deflection of the range front. a) A ductile décollement is present in the southern Potwar and a brittle décollement is present beneath the Kohat and northern Potwar. A basement normal fault is present in the eastern and central Salt Range. The deflection in range front is caused by faster propagation of deformation in the Potwar above salt. b) A preexisting basement normal fault controls the surface expression of range front despite having the same basal detachment (salt) beneath entire KP-FTB.

3.6 Conclusions

The structures at the surface in the Kohat evolved as an active roof sequence above the Eocene décollement. The subsurface section in Kohat is tectonically thickened by north-dipping duplexes formed of Cambrian to Paleocene strata between the basal and secondary décollements. In contrast, due to the absence of a secondary décollement in the Potwar, a thick molasse sequence is preserved there. The ramps forming duplexes in Kohat continue as thrusts in the core of fault propagation folds in Potwar. In the southern part of the Potwar, a 2-3° basement slope and the presence of salt carried the range front farther to the south. Movement of salt has triggered late stage normal faulting in the Kalabagh Fault Zone, out-of-sequence thrusting in Kohat, and resulted in the formation of the Ghundi lobe structures in the western Salt Range.

The Kalabagh Fault Zone at the boundary of Kohat and Potwar is characterized by dextral rotational faulting. The reverse slip movement of faults in Kohat is linked to the dextral normal slip movement of faults in the Kalabagh Fault Zone. The deformed and restored model of the KP-FTB show ~ 40 km of shortening in the southern Kohat, Surghar Range, western Potwar and Salt Range. The consistent amount of shortening provides a very important constraint, showing that deformation propagated synchronously south of the MBT after 10 Ma into the Kohat and Potwar wedge. The presence of a double décollement in Kohat compared to single ductile décollement in the Potwar, a greater cross sectional wedge taper in the southern Potwar and a smaller stratigraphic thickness resulted in the dramatic structural variations of the KP-FTB.

Acknowledgments

Andrew Meigs and Delores Robinson are gratefully acknowledged for their technical reviews of the balanced cross-sections and suggestions for improving the manuscript. We thank the German Academic Exchange Service (DAAD) for providing financial assistance to complete this research and to Midland Valley for providing the Move program through their Academic Support Initiative Programme. We thank the Directorate General of Petroleum Concessions (DGPC) Pakistan for providing seismic data and faculty members and students of Bahria and Peshawar Universities for their assistance during field work.

Chapter 4. Paleozoic to Pliocene tectonic evolution of the Salt Range constrained by low temperature thermochronology

Abstract

The Salt Range in Pakistan contains the oldest exposed stratigraphy at the range front along the entire Himalayan Arc. To better understand the long term tectonic evolution of the Salt Range, we have conducted low-temperature thermochronologic analysis using apatite (U-Th-Sm)/He and fission track dating. In our new modeling approach, we combine different age samples with different detrital histories to predict a robust thermal history that shows two major events in the geological history of the Salt Range. The first exhumation event shows that Late Paleozoic rifting, reported widely in the Lesser Himalaya, extended southward to the Salt Range. The second exhumation event occurred as a result of motion on the Main Frontal Thrust (MFT) at 4 Ma. Structural reconstructions confirm that the MFT maintained a constant shortening rate between 5 - 6 mm/yr after 4 Ma and a maximum exhumation rate of ~3 mm/yr on the MFT ramp. The results suggest that higher cooling and exhumation rates on the ramp are related to ~3 km erosion of molasse. Erosion rates reduced drastically when carbonate rocks were exposed to the erosion surface, the carbonate rocks less erodibility resulted in their preservation, eventually resulted in preservation of Precambrian to Eocene strata. The interplay between the exhumation pattern and the role of carbonates is responsible for the formation of fault bend fold in the Salt Range.

4.1 Introduction

Detrital low temperature thermochronologic data, especially when coupled to structural geology, can provide important information about the structural style, exhumation pattern and long term history of 2-4 km deep parts of sedimentary basins. Thermochronologic studies of the Himalayan foreland have examined the Cenozoic history (e.g., Burbank and Beck, 1989; van der Beek et al., 2006; Gavillot et al., 2018). However, details about the Paleozoic - Mesozoic basin depositional and deformational history have yet to be explored. Precambrian - Paleozoic strata exposed in the Salt Range in Pakistan (Fig. 4.1) have, due to only shallow burial (2-3 km) beneath the molasse, the potential to retain the “memory” of older thermal events that occurred in the basin and therefore can provide a complete Paleozoic-Cenozoic history of the basin.

We present here a thermal history of the long-term thermo-tectonic evolution of both the Salt Range and the Paleozoic source areas. We will demonstrate that if structural and stratigraphic characteristic for samples are taken into account, different aged detrital samples can be combined within a single thermal model using a new version of the QTQt program (5.7.0) (Gallagher, 2012). The model output predicts robust thermal paths respecting the different detrital histories of the samples. The results of this study 1) illustrate the influence of older normal faults on localizing Cenozoic deformation, 2) provide new temporal and exhumation constraints for the Main Frontal Thrust (MFT) by coupling age data to a balanced cross-section, 3) highlight the importance of carbonate rocks on topographic relief development and structural style variations along the Himalayan range front and 4) show the influence of molasse deposition in erasing the older basin thermal history.

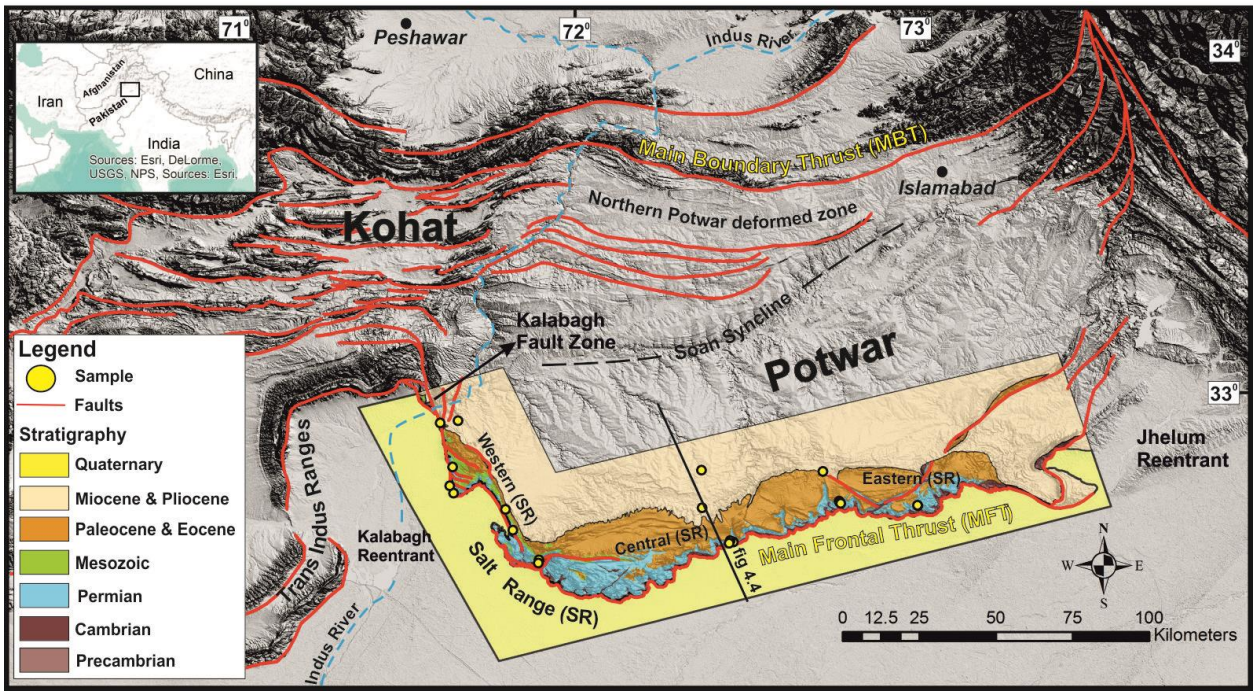

Figure 4.1. Structural map of Salt Range and surrounding regions. The inset shows Pakistan and neighboring countries (modified after Gee, (1980); Ghani et al., (2018)).

4.2 Tectonic framework and stratigraphy

The ca. 250 km wide Kohat and Potwar regions represent the external zone of the Himalayan fold and thrust belt in Pakistan (Fig. 4.1). The northern and western border of Kohat and Potwar is marked by the Main Boundary Thrust (MBT), which formed around ~10 Ma (Meigs et al., 1995). The Salt Range, a major ENE-WSW trending structural and topographic feature with ca. 800 m of relief, marks the southern border of Potwar. In the Salt

Range, Precambrian to Pliocene strata are thrust above Quaternary sediments along the emergent MFT, forming a fault bend fold (Baker et al., 1988; Ghani et al., 2018). The stratigraphic sequence in the Salt Range can be subdivided into three major units: 1) the Precambrian Salt Range Formation (SRF), 2) the Cambrian to Eocene siliciclastic and carbonate sequences of the Tethyan and Indian passive margin, and 3) the Miocene to Pliocene molasse sedimentary sequence derived from erosion of the Himalayan orogen (Gee, 1980, Burbank et al., 1996) (Fig. 4.2, Appendix 1, section SM 4.1). The overall stratigraphic wedge thickness reduces southward from 5 km in the northern Potwar to 2 – 2.5 km in the Eastern and Central Salt Range.

4.3 Thermochronologic data

We systematically sampled Cambrian to Miocene age clastic strata from different stratigraphic sections exposed in the Salt Range (Fig. 4.2). Out of 28 samples, only 20 yielded apatite suitable for apatite (U-Th-Sm)/He (AHe) dating; 15 were used for apatite Fission Track (AFT) dating, 11 of which yielded confined track lengths (Appendix 1, Section SM 4.2, Tables SM 4.1, 4.2). The 80 AHe cooling ages are dispersed between 0.8 ± 0.1 and 135 ± 7 Ma; however, the majority of the AHe cooling ages are less than 10 Ma (Fig. 4.2). The AFT ages span from 3.7 ± 0.7 to 355 ± 16 Ma. Thirteen Cambrian and Permian samples yield AFT ages that fail the chi squared test (see Appendix 1, Table. SM 4.2). This test examines whether the ages represent a single population. The dispersion in our AFT data is primarily related to different mineral kinetics, expressed by Dpar values between 1.1 – 3.5 μm; however, different source histories have also influenced the age distributions (see Appendix 1, section SM 4.2 for details). Only two Permian age AFT samples passed the chi squared test: TgKr, 355 ± 15 Ma, and TbDk, 3.7 ± 0.7 Ma. TgKr is a granite clast sampled from the basal conglomerate bed and TbDk was the deepest buried sample beneath molasse, located at the western end of the Salt Range (Fig. 4.2). The 11 track length distributions range from 9 to 12.5 μm; track lengths decrease from the Eastern towards the Western Salt Range. The Dpar of grain populations that pass the chi-squared test are similar to the Dpar of the grains used for length measurements, so we assume that they represent the same populations. These modeled population ages are presented in figure 4.2.

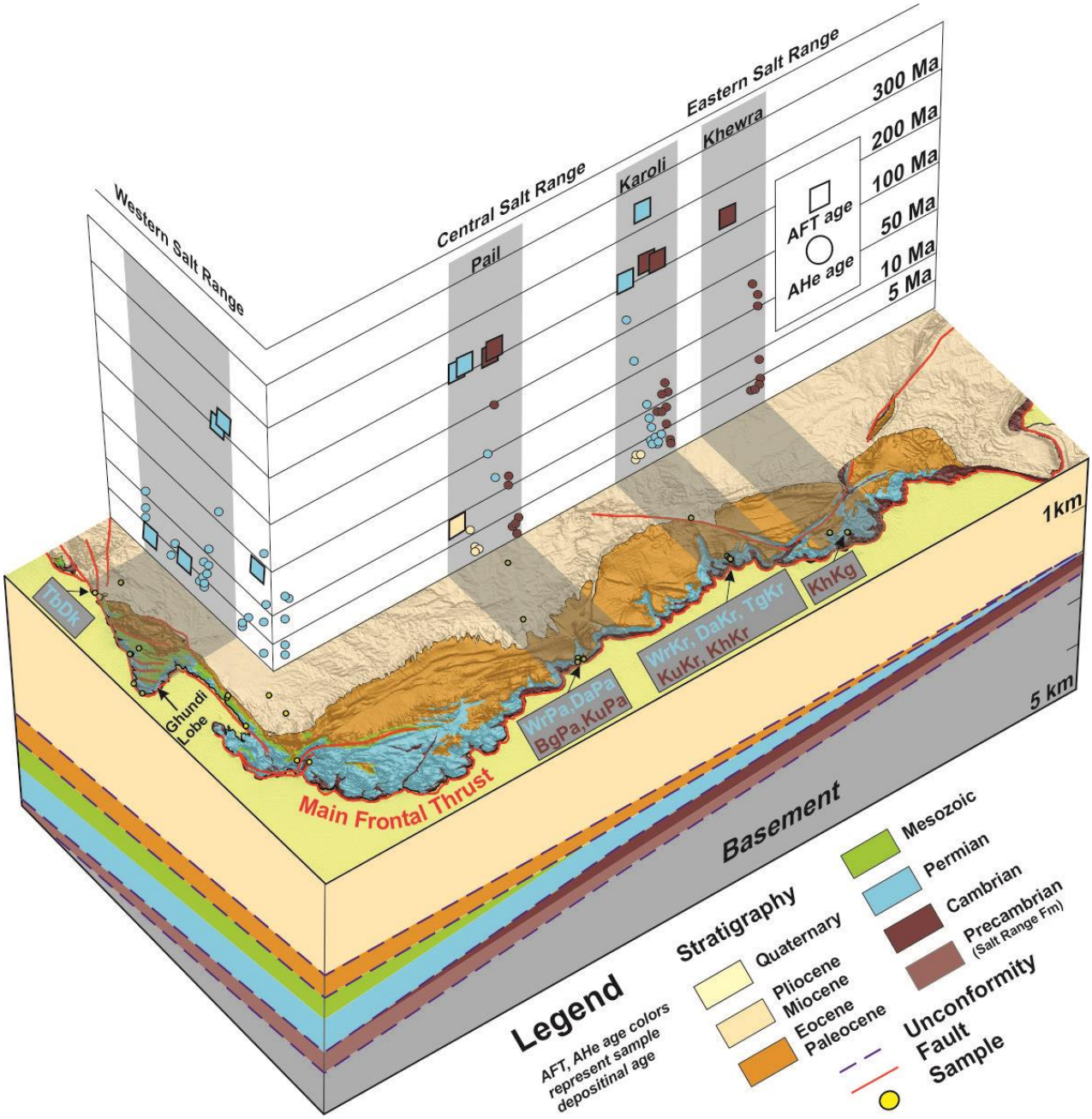

Figure 4.2. Geological block diagram showing geometry of the stratigraphic wedge in the Salt Range. The AFT and AHe age distributions vary along strike in the Salt Range. Please note the difference in age scale. The Cambrian and Permian age samples from the Khewra, Karoli and Pail sections (labeled here) are used in the combined thermal model presented in the Figure 4.3. Individual sample details and models from all sections are provided in the Appendix 1(section SM 4.3).

4.4 Thermal modelling

Modelling of low-temperature thermochronologic data is usually performed either on individual samples or on a suite of samples from a vertical or stratigraphic section that share the same thermal history. The new version of the QTQt program (v. 5.7.0; Gallagher, 2012) is

used to model a suite of samples which retain different provenance histories. We used two different modeling approaches. First, we ran thermal models on individual samples from the Khewra and Western Salt Range sections and then we combined different age samples with different detrital histories into a single thermal model for the Karoli and Pail sections. The results of individual and multi sample models predicted a similar thermal history (Appendix 1, section SM 4.3). Second, to reconcile the individual models, we combined all Cambrian and Permian age samples from the Khewra, Karoli and Pail sections into a single thermal model (Fig. 4.3). We hypothesize that all these samples experienced the same thermal history based on compelling stratigraphic and structural arguments that these samples are 1) structurally located on the edge of same fault bend fold, 2) experienced similar burial temperatures, 3) reproducible AHe and AFT partial reset ages 4) absence of major faults between sampled sections (Appendix 1, section SM 4.3). We jointly modeled four parameters to decipher the detailed thermal history: AFT populations that pass the chi-squared test, AHe ages, C-axis projected track-lengths, and Dpar. Modeling parameters, constraints and model predictions are described in Appendix 1, section SM 4.3.

The thermal model results suggest that Cambrian samples were reheated up to 80 ± 5 °C between 450 to 350 Ma, partially resetting the AFT ages (Fig. 4.3). Exhumation commenced in the Devonian and persisted until the Permian. The samples remained within 1 km of the surface from Permian to Miocene time. The final subsidence event is marked by rapid burial up to 90 ± 10°C beneath molasse, totally resetting the majority of AHe ages, partially resetting all AFT ages, and moderately annealing track lengths. The final exhumation began at 4 Ma.

The modeling results are presented in Figure 4.3 as a) the path with the highest likelihood (max likelihood) and b) the average of the best model paths (expected). The 2 thermal histories are similar except that the max likelihood path is ~ 10 °C hotter in the Late Paleozoic and stays colder from Permian to Miocene time. The max likelihood model predicts the observed distribution of all track lengths, Dpar, younger less than 10 Ma AHe ages and AFT ages; however, the expected model despite being similar predicted older ages for Cambrian samples.

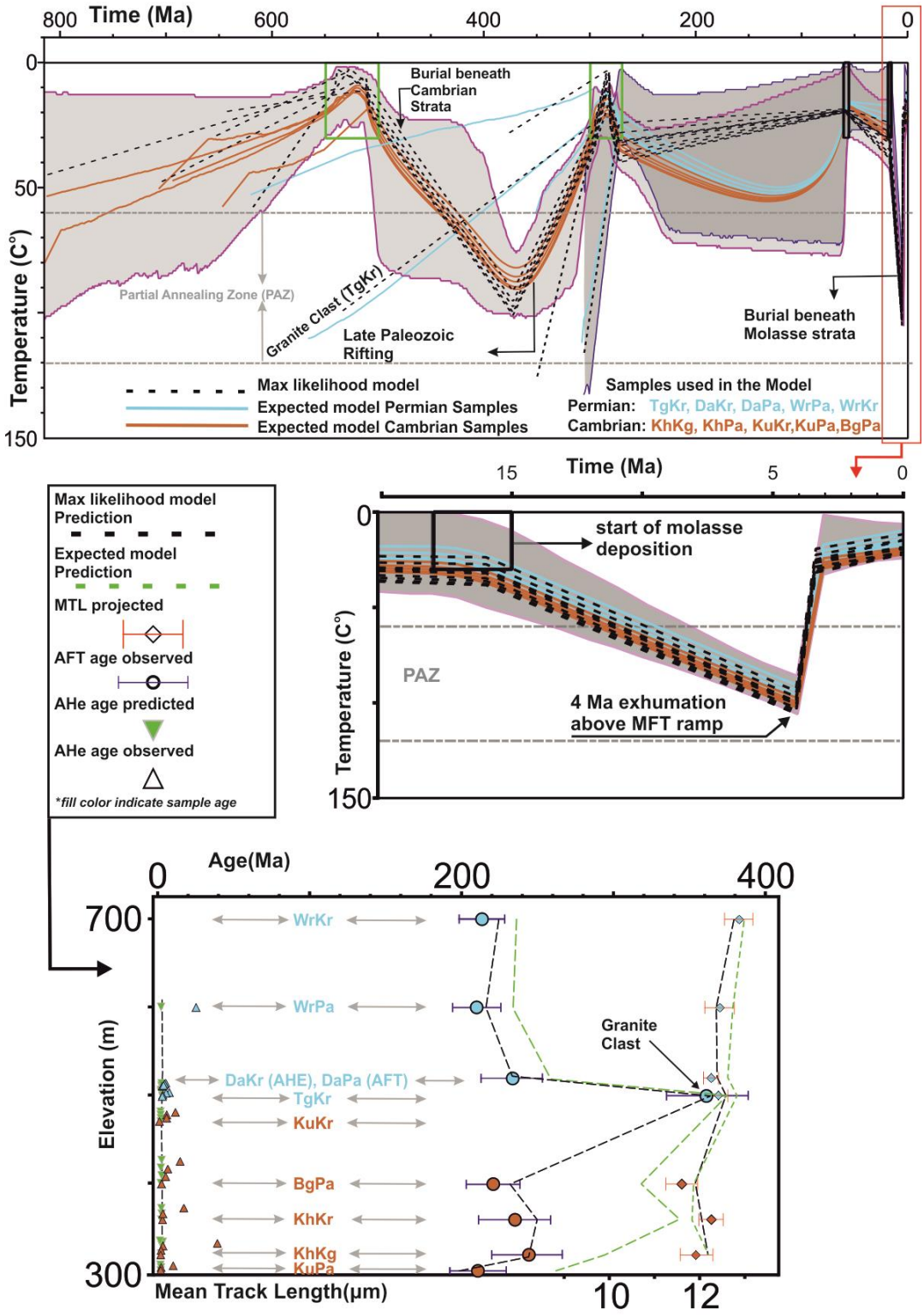

Figure 4.3. QTQt thermal model and age - elevation profile for ten Cambrian and Permian samples combined into a single thermal model. Shaded area represents path probability, thick lines represent expected model and dashed lines represent max likelihood model. Block at the bottom show observed versus model predictions. Track length distribution and model parameters are provided in the Appendix 1.

4.5 Discussion and conclusions

4.5.1 Pre-Himalayan basin history

Clastic sediments were deposited on top of Precambrian Salt in a shallow epicontinental sea during the early Cambrian (Hughes et al., 2019 and references therein). The Cambrian strata in the Salt Range was buried beneath 2 to 2.5 km of Ordovician to Carboniferous strata, partially resetting the AFT ages of Cambrian samples such that they were similar to the AFT ages of the Permian samples (Figs. 4.2-4.3). Therefore, we propose that the depositional area of the Cambrian to Carboniferous Peshawar and Hazara Basins (Pogue et al., 1992a) extended to the Salt Range (Figs 2.1, 4.1). The major unconformity spanning 200 Ma between Cambrian and Permian strata in the Salt Range was previously considered to be a depositional hiatus (Gee, 1980; Pogue et al., 1992a). Our model suggests that this major unconformity represent a carboniferous cooling/exhumation event that is related to a major Late Paleozoic rifting phase reported in the Peshawar Basin of Pakistan, and Kashmir and Zanskar in India, caused by the opening of the Neo-Tethys and the formation of the Indian passive margin in northern Gondwana (Pogue et al., 1992b; Garzanti et al., 1996). The area affected by this major rifting phase resulted in the formation of half graben structures through ENE-WSW trending and northward dipping normal faulting. The stratigraphic relationship also suggests that in the Eastern and Central Salt Range, Permian strata lies on top of Cambrian strata, forming a very gently (< 2°) dipping angular unconformity; however, in the western Salt Range, Cambrian strata is completely eroded and Permian strata lies on top of the Precambrian Salt Range Formation (Fig. 4.2). Lower to middle Paleozoic strata was presumably eroded in the western, uplifted part of the half graben and the lower Paleozoic succession was preserved in the deeper, eastern part. We propose that north dipping normal faults observed in Potwar and the Salt Range formed in the Late Paleozoic rather than in the Pliocene; evolution of these faults was previously attributed to a flexural bulge formed by stacking of thrust sheets in the Hinterland toward north (Baker et al., 1988).

Mesozoic strata are absent in the Central and Eastern Salt Range; however, in the Western Salt Range, up to 500 m are exposed (Fig. 4.2). Although the thermal model shows slight reheating in the Mesozoic, we do not interpret this interval because the amount of reheating is close to the resolution of the model. Paleocene to Eocene shale and carbonate rocks blanket the underlying stratigraphic succession in the Central and Western Salt Range.

4.5.2 Development of the Salt Range

Beginning at 18 Ma, the Precambrian – Eocene strata in the Salt Range was rapidly buried beneath 2 to 3.5 km of molasse (Johnson et al., 1985; Najman et al., 2003). The northward decrease of AFT ages and track lengths in the Western Salt Range is caused by stronger annealing due to the northward thickening molasse strata (Fig. 4.2). The youngest AFT sample (3.7 ± 0.7 Ma), collected from Permian strata at the western end of the Salt Range, was buried beneath ~ 4 km of molasse and thick Permian to Eocene strata, causing total resetting. This sample delineates a boundary in the Salt Range. To the north, low temperature thermochronologic systems are reset by thick molasse deposition in the Potwar and the pre-Cenozoic low temperature thermal history is erased from the Paleozoic – Mesozoic strata. This is one among other reasons why most detrital and in-situ low temperature thermochronologic studies in India, Nepal and Pakistan only constrain the Cenozoic deformation history of the Himalaya.

Seven individual thermal models show that the final exhumation commenced between 4 - 9 Ma (Appendix 1, section SM 4.3). However, the more robust multi-sample thermal model combining ten Cambrian and Permian samples better constrains the onset of the final exhumation as 4 Ma (Fig. 4.3). The restored structural section (Fig. 4.4) illustrates that the Cambrian-Permian AFT samples, prior to the onset of horizontal movement along the MFT footwall flat, were located near the ramp at ~4 Ma. The exhumation pattern in the Salt Range, as inferred from our data, is consistent with the fault bend fold exhumation model proposed by Lock and Willet (2008), where samples cool when they are uplifted across the ramp; the maximum exhumation rates are pinning to the ramp. In our structural and thermal model, the maximum exhumation rates of ~3 mm/yr are calculated for cooling of samples below ~90 ^{0}C assuming thermal gradient of 25 ^{0}C between 3 to 4 Ma when samples started uplifting from a depth of~ 3 km above MFT ramp. The molasse sequence erosion rate was almost in balance with the uplift rate above the MFT ramp. However, where samples were moving horizontally along the lower and upper flat of the MFT, the exhumation rates were lower than above the ramp. The average shortening rate calculated in our structural model is 5 – 6 mm/yr for 22 ± 2 km for the last 4 Ma, similar to the ~5 mm/yr, geodetically-determined rate in the Central Salt Range (Jouanne et al., 2014). Based on the shortening rates and exhumation pattern in the Salt Range, we propose that the range developed by a continuous process above the MFT in the Himalayan foreland since~4 Ma.

The structural style of the Salt Range is different from the range front along strike of the MFT exposed to the east in the Central and Western Himalaya. The range front is a fault bend fold in the Central and part of the Eastern Salt Range. This changes towards the east into a series of fault propagation and fault bend folds exposed in the easternmost part of the Salt Range and the Subhimalaya of India and Nepal. The variation in structural style is considered a consequence of the salt present at the base of the section in the Potwar and Central Salt Range; however, this idea fails to explain structural variations in the easternmost part of the Salt Range, which is very similar to the structural style of the range front in India and Nepal.

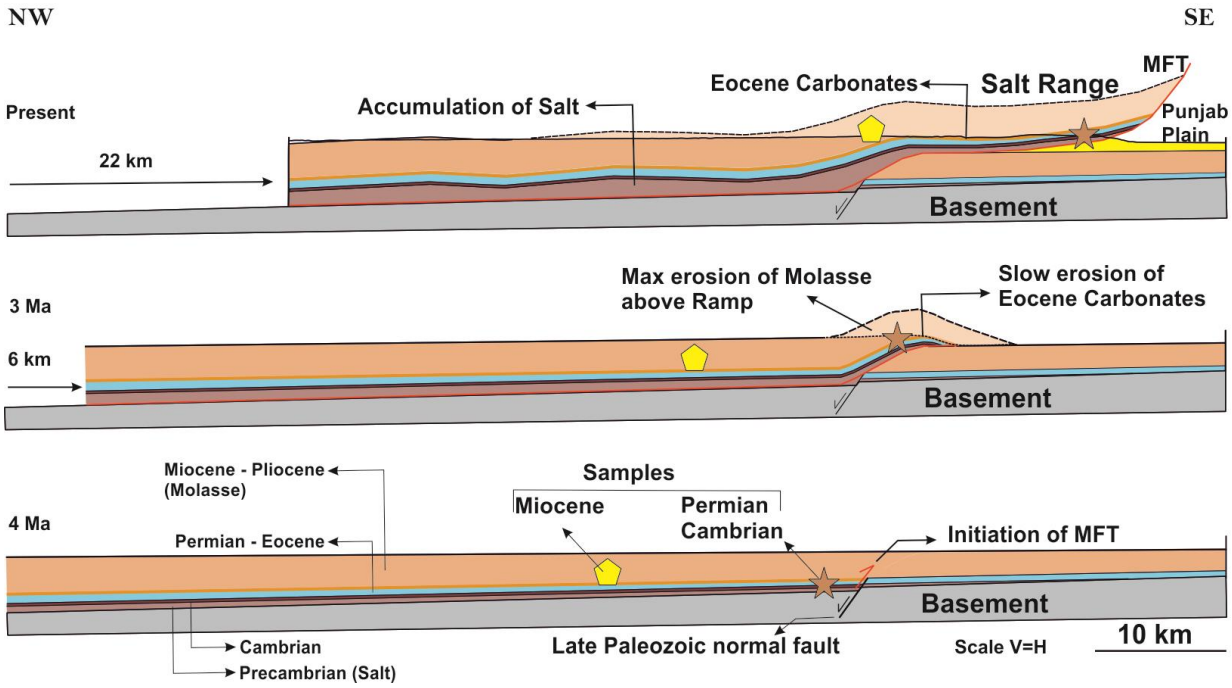

Figure 4.4. Development of the Salt Range based on MOVE modeling (Ghani et al., 2018) and our new thermochronologic results.

We propose that both salt and the inherited basement normal fault were responsible for forming and localizing movement on the MFT ramp; however, the shape of the range front is strongly influenced by the Eocene carbonate rocks. The clastic molasse strata was quickly stripped off over the ramp in the semiarid climatic conditions prevalent for atleast last 5 Ma at the Salt Range; the erosion processes became less efficient when carbonate rocks was exposed (Fig. 4.4). The resilience of only 200 m of carbonate rocks protected the older strata and formed the fault bend fold shape of the range front. Rather than forming higher relief, the thrust sheet exploited the weaker molasse strata in the footwall and started horizontal

translation above the MFT upper flat. The Eocene carbonate rocks were apparently not deposited in the easternmost part of the Salt Range and farther east. That and the shift of the basal detachment into molasse in the Western Himalaya are the major reasons for structural style variations along the Himalayan range front.

Acknowledgments

We thank the German Academic Exchange Service (DAAD) and DFG (StRATEGy program) for financial assistance. We thank K. Gallagher and Petex for providing the QTQt and Move programs for academic use. We thank faculty members and students of Bahria and Peshawar Universities for their assistance during field work.

- ***Appendix 1 (Chapter 4)*** *contain details on sample location, mineral separation, AHe and AFT dating and thermal modeling. Figure SM 4.1 (Sample location map and generalized stratigraphic table), Figure SM 4.2 (AHe age versus effective U content), Figure SM 4.3 (AFT radial plots and Age versus Dpar), Figure SM 4.4-4.7 (Thermal models and model predictions of Khewra, Karoli, Pail, Western Salt Range sections).*

Chapter 5. Structural evolution of the Kohat fold and thrust belt, Pakistan

Abstract

To better understand the spatio-temporal structural evolution of the Kohat fold and thrust belt, we have combined balanced cross-sections with apatite (U-Th-Sm)/He (AHe) and apatite fission track (AFT) dating. The AHe and AFT ages appear to be totally reset, allowing us to date exhumation above structural ramps. The results suggest that deformation propagated earlier on the Surghar Thrust at 15±2 Ma, earlier than the development of the Main Boundary Thrust at 12±2 Ma. Deformation propagated southward from the Main Boundary Thrust after 11 Ma on a double décollement, resulting in a disharmonic structural style. The surface folds and faults formed above an active roof thrust that connected to a lower décollement through subsurface ramps in the pre-Eocene stratigraphic sequence. Southward transport along the ramps formed duplexes that facilitated tectonic thickening of the wedge and erosion of the Miocene to Pliocene molasse strata. The spatial distribution of AHe and AFT ages in combination with the structural forward model suggest that, within the Kohat fold and thrust belt, construction of the orogenic wedge taper occurred first by accretion of undeformed foreland and then by out-of-sequence deformation.

5.1 Introduction

Low temperature thermochronometery used in combination with balanced cross-sections can help to decipher important details about the sequential structural evolution of fold and thrust belts. This combination has been used in studies that provide important information about shortening and exhumation rates, and the timing and sequence of fold and thrusts that carry deformation towards the foreland and form the overall structural style of the fold and thrust belt (e.g., Lock and Willet, 2008; Castelluccio et al., 2015; McQuarrie and Ehlers, 2015; Mora et al., 2015; Gavillot et al., 2018).

The collision of India with Asia resulted in the development of the Himalayan fold and thrust belt. The Kohat and Potwar fold and thrust belts (herein called Kohat and Potwar) represent the external sedimentary zone, or Subhimalaya, of the Himalayan fold and thrust belt in Pakistan (Fig. 5.1). The Kohat and Potwar are bordered to the north by the Main

Boundary Thrust (MBT), which forms the major geologic terrain boundary between the Subhimalaya and the Lesser Himalaya along the length of the entire fold and thrust belt. The structural style in the Kohat is controlled by double décollements that resulted in formation of box folds and imbricates above upper décollement and formation of duplex between two décollements. It is very different from the structural style of the rest of the Subhimalaya and especially Potwar, located to the east (Ghani et al., 2018). Detailed thermochronologic, morphotectonic and structural studies in the Subhimalayan regions of India and Nepal have documented the Miocene to Holocene subsidence and deformation history (e.g., Van der Beek et al., 2006; Dey et al., 2017; Gavillot et al., 2018). In Pakistan, detailed paleomagnetic studies of Neogene molasse deposits and stratigraphic relationships have been used to constrain the structural evolution of Potwar and the Salt Range over the past 10 Ma (Burbank et al., 1996 and references therein; Grelaud et al 2002). The same chronologic scheme has been adopted for the ages of the Neogene strata and structures in the Kohat and Trans Indus Ranges (McDougall and Hussain, 1991; Pivnik and Khan, 1996; Pivnik and Wells, 1996); however, significant concerns remain about the timing and sequence of the structural evolution and exhumation in the Kohat and Potwar. For example, there are no age constraints for the development of major thrusts in the Kohat. It is unclear if the MFT and Surghar Thrust (SGT) are actually segments of a single structure which developed contemporaneously (Fig. 5.1). Existing data do not explain why the Neogene molasse in Kohat has been effectively removed while the > 4 km-thick sequence is preserved in the subsurface of the Potwar. In summary, there is no structural models for this area present that can explain the pattern, timing, and propagation of deformation south of the MBT.

In this paper, we present the first low temperature thermochronologic data from the Kohat. We then present our new structural forward model for the sequential structural evolution of Kohat. The thermochronologic data is coupled to a balanced cross-section to elucidate the fold and thrust kinematics from the MBT to the SGT. Detailed information about shortening and exhumation rates, and the timing of structural activations provides new insight into the role of décollements in shaping the structural style, exhumation and sequence of deformation in this portion of the Subhimalayan fold and thrust belt.

5.2 Tectonic framework and stratigraphy

Kohat is a ~100 km wide and 70 km long geological terrain bounded by the Kohat and Surghar Ranges (Fig. 5.2). The Kohat Range is comprised of intensely folded Mesozoic

to Paleocene strata that started developing above the MBT hanging wall at ~11 Ma (Meigs et al., 1995). The Kohat Range forms the topographic barrier between Kohat and the Peshawar Basin, to the north. The range front of Kohat is known as the Surghar Range; this formed by translation of thrust sheet above the Surghar Thrust (SGT) (McDougall and Hussain, 1991; Ghani et al, 2018). The surface geology in the Kohat is comprised of overturned and box-shaped folds cut by steeply dipping fore-thrusts and back-thrusts that expose Eocene strata throughout the Kohat.

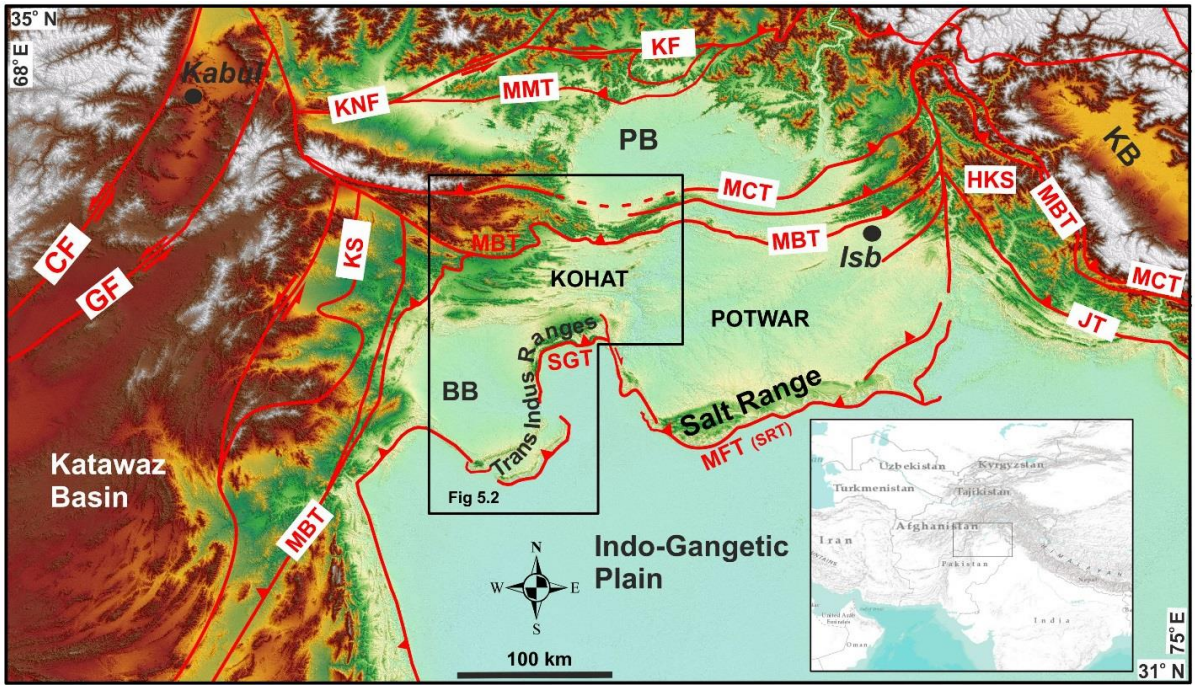

Figure 5.1. Regional tectonic map of northwestern Pakistan and eastern Afghanistan. Inset map in the lower right shows map location. The inset box shows the location of Kohat and surrounding areas map presented in the figure 2. CF: Chamman Fault; GF: Gardez Fault; HKS: Hazara Kashmir Syntaxis; JT: Jawalamukhi Kotli Thrust; KF: Kohistan Fault; KNF: Kunar Fault; KS: Khost Suture; MBT: Main Boundary Thrust; MBZ: Main Boundary Zone; MCT: Main Central Thrust; MMT: Main Mantle Thrust; NPS: Nanga Parbat Syntaxis. Modified after Beck et al (1995), Badshah et al (2000) and DiPietro and Pogue (2004).

In contrast, in Potwar, Eocene strata are buried beneath thick younger Neogene molasse strata. The Marwat and Khisor Ranges and the western segment of the Surghar Range jointly form the Range front of the Bannu Basin. Taken together, these ranges are known as the Trans Indus Ranges (Figs. 5.1-5.2). The Kohat was created by deformation along a double décollement that formed duplexes in the subsurface and disharmonic folds exposed at the surface (Abbasi and McElroy, 1991; Ghani et al., 2018). In contrast to Kohat,

the Potwar has a simpler structural style with less internal deformation; it was translated as a single thrust sheet above the Main Frontal Thrust (MFT) (called the Salt Range Thrust (SRT) in Pakistan) ramp, forming a topographically-pronounced range front known as the Salt Range (Baker et al., 1988; Ghani et al., 2018). The area between the range fronts is the strike slip Kalabagh Fault Zone (KFZ) (Fig. 5.1) (McDougall and Khan, 1990; Ghani et al., 2018).

The oldest exposed strata in the Kohat and Surghar Ranges are of Mesozoic age; however, the presence of Paleozoic strata in the Salt Range, Peshawar and Hazara Basins, seismic data interpretation and well bore data implies that similar units are present at depth in the Kohat. The Mesozoic succession is comprised of both clastic and carbonate lithologies in the Surghar Range; the succession changes to dominantly carbonate in the Kohat Range (Denlichik and Shah, 1968; Meisnner et al., 1974). The Paleocene succession exposed in the Kohat and Surghar Ranges is also comprised of clastic and carbonate rocks. The Eocene stratigraphy in the Kohat, including carbonate and evaporites, represent a restricted marine environment (Meissner et al., 1974; Pivnik and Wells, 1996).

The molasse strata in the Kohat are comprised of Miocene to Pliocene clastic deposits, subdivided into the Early to Middle Miocene Rawalpindi Group and the Middle Miocene to Pliocene Siwalik Group (Johnson et al., 1985). The Rawalpindi Group is comprised of the Murree and Kamlial Formations, which were deposited in the Potwar from ≥ 22 to 14 Ma (Johnson et al., 1985; Najman et al., 2003). The Murree Formation is ~4 km thick and widely exposed in the northern part of the Kohat and the southern part of the Peshawar Basin; however, it has a reduced thickness of ~500 m in the central part and is absent in the Surghar Range (Burbank and Beck, 1996). The Kamlial Formation is ~1 km thick exposed south of the MBT in the Kohat; the thickness gradually decreases to ~700 m to the south and it is absent in the Surghar Range. The Siwalik Group is comprised of the Chingi, Nagri and Dhok Pathan Formations, dated between 14 to 5 Ma in the Salt and Trans Indus Ranges (Johnson et al., 1985; Pivnik et al., 1996). The Siwalik Group is not present in the northern part of Kohat and Potwar; however, it is up to 4 km thick in the southern part of Kohat and the Surghar Range (Fig. 5.2). In the east-west oriented part of the Surghar Range, the Chingi Formation overlies the Eocene strata with a gentle angular unconformity. However, the Chingi Formation pinches out towards the southwestern part of the Surghar Range. A conglomeratic bed containing clasts of pre-molasse strata is exposed on top of Eocene strata in the westernmost part of the Surghar Range; this 150 m thick bed is called the Mitha Khattak Formation (Denlichik and Shah, 1968; Blisnuik et al., 1998).

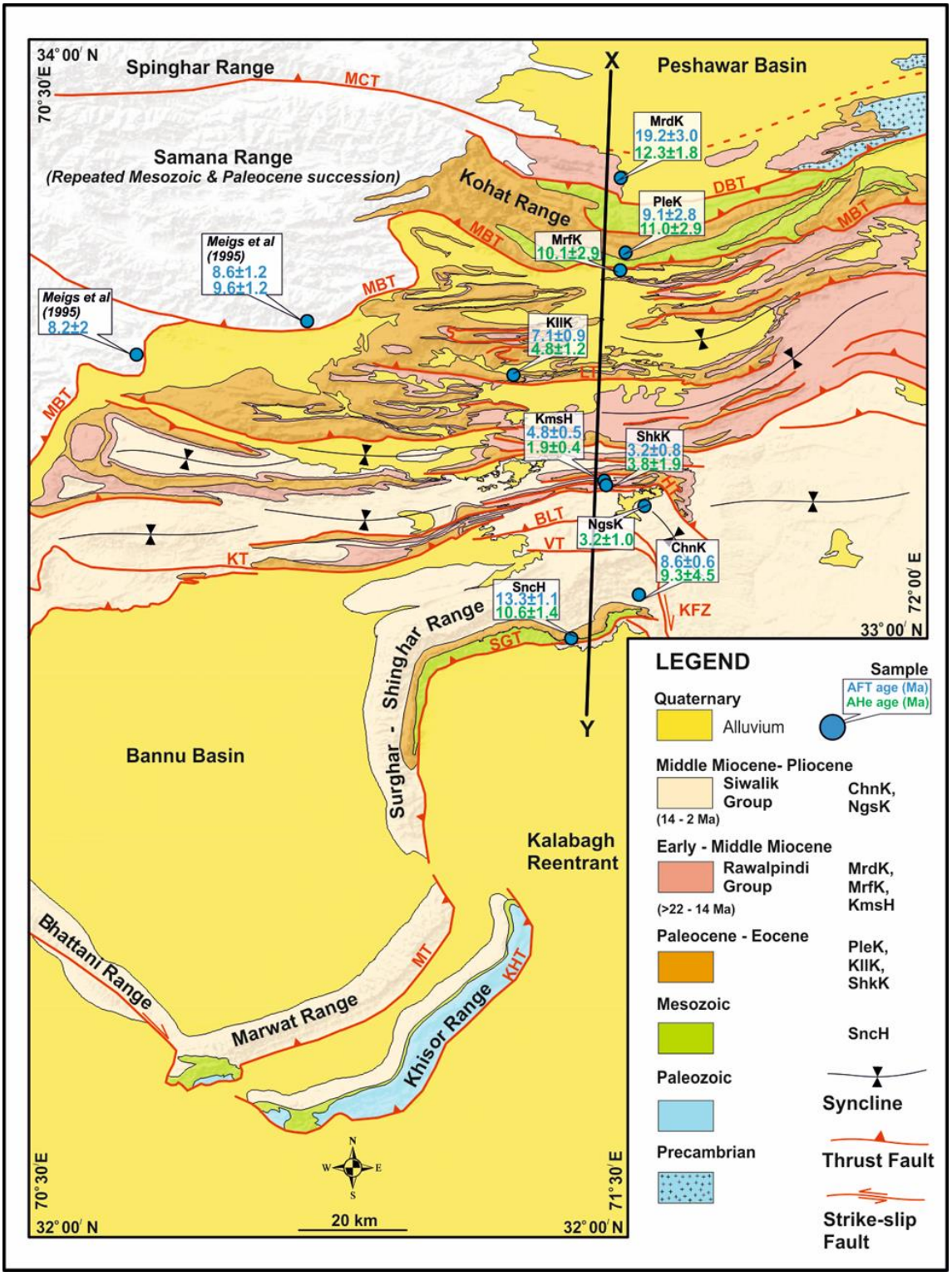

Figure 5.2. Geological map of the Kohat and Trans Indus Ranges (modified after Meissner et al. (1974), Blisniuk et al. (1998), and Pivnik and Wells (1996)). Dark blue circles represent sample locations with callout labels showing name and respective AFT pooled age and AHe mean ages. BLT: Banda Lakhoni Thrust; DBT: Darra Back-thrust; HT: Hukni Thrust; KFZ: Kalabagh Fault Zone; KHT: Khisor Thrust; KT: Karak Thrust; LT: Lachi Thrust; MBT: Main Boundry Thrust; MBZ: Main Boundary Zone; MT: Marwat Thrust; VT: Visor Thrust. See figure 5.4 for cross-section XY.

A similar conglomeratic bed is reported below the Siwalik Group in the Khishor Range (Blisnuik et al., 1998).

The Nagri and Dhok Pathan Formations of the Siwalik Group unconformably overly Cambrian to Eocene strata in the western part of the Surghar and Khisor Ranges. The deposition of the Siwalik Group in the Trans Indus Ranges was diachronous, starting in the Surghar Range at 12 Ma and younging southward to the Marwat and Khisor Ranges at 4 Ma (Khan et al., 1988; Burbank and Beck, 1996).

5.3 Apatite low temperature thermochronology

5.3.1 Sampling and mineral separation

Thirteen sandstone samples were collected from the hanging wall and footwall units of major thrusts in the Kohat to constrain thrust kinematics and related exhumation (Fig. 5.2). The samples were collected from sandstone in Jurassic, Cretaceous, Eocene and Miocene strata. The Mesozoic succession in the Salt, Surghar and Kohat Ranges contain thick limestone and white quartz arenite beds that did not yield apatite; this adversely affected the number of usable samples. Therefore, only nine samples could be used for thermochronologic analysis. Apatites were separated from the sandstone samples at the University of Potsdam using standard magnetic and heavy liquid separation techniques.

5.3.2 Analytical methods

5.3.2.1 U-Th-Sm/He dating (AHe)

Alpha decay from ^{235}U, ^{238}U, ^{232}Th and ^{147}Sm produces radiogenic ^{4}He that can completely diffuse out of apatite crystals at temperatures above 80-90°C. The ^{4}He is partially retained within the crystal between 40-80°C; this temperature interval is known as the apatite partial retention zone (APRZ) (Farley 2000; Farley 2002). The AHe age is based on quantifying the parent (U-Th-Sm) and daughter (He) isotopes as a measure of time since the crystal passed through the APRZ closure isotherm (Farley 2000).

The method involves selection and measurement of three to eight inclusion- and crack-free apatite crystals with a diameter > 60 μm using a binocular microscope. The ^{4}He is extracted by laser heating of platinum tubes containing single crystals of apatite. ^{4}He abundance is measured with an Alphachron equipped with a quadrupole mass spectrometer at the thermochronology lab at the University of Potsdam. Next, apatites are dissolved in dilute

nitric acid and spiked with ^{235}U, ^{230}Th and ^{149}Sm to measure the concentrations of U, Th and Sm using inductively coupled plasma mass spectrometry (ICP-MS) at the German Research Centre for Geoscience (GFZ) Potsdam. The calculated single grain ages are corrected using the alpha ejection (FT) correction (Farley et al 1996). Additional methodological details are in Zhou et al. (2017).

5.3.2.2 Apatite Fission Track dating (AFT)

The spontaneous fission of ^{238}U damages the crystal lattice of apatite. These damage structure are known as natural or spontaneous fission tracks. These tracks accumulate in apatite as a direct function of the uranium concentration in the crystal and time. The AFT method is based on quantifying the parent (uranium concentration represented by induced tracks) and daughter (spontaneous tracks) products to calculate the time since the crystals passed through ~120°C closure temperature isotherm. The initially formed tracks reduce their length at temperatures between 60 and ~120°C, known as the Apatite Partial Annealing Zone (APAZ) (e.g., Wagner et al., 1989, Gallagher et al., 1998).

Spontaneous fission tracks on internal surfaces of apatite were revealed by etching the fission track mounts in 5.5 M HNO_3 solution for 20 seconds at 21°C. Mica sheets were attached to the fission track mounts, which were then irradiated at the FRMII reactor at Garching (Munich, Germany). During irradiation with thermal neutrons, induced tracks are produced by fission of ^{235}U; some of these tracks penetrate the micas. After irradiation, induced tracks are revealed by etching the mica sheets in 40% HF at 21°C for 45 minutes. Additional details of the analytical process are described in Sobel and Strecker (2003). AFT ages are calculated using the external detector method (Hurford and Green, 1982) with a zeta value of 353±7 (HG). The samples did not yield any confined track lengths.

5.3.3 Results

We obtained single grain AHe ages from nine samples (Appendix 2, Table. SM 5.2.1). Fifty-four ages represent consistent, replicable analysis. Only six AHe ages were discarded on the basis of analytical inconsistency in the laboratory measurements. Aliquots SncH-1, KmsH-2 and MrdK-1 were discarded due to either very low or very high concentration of U, Th or Sm, which suggests that the mineral analyzed was not apatite. Aliquots KmsH-1 and MrfK-2 were discarded due to presence of inclusions in the crystal, detected in the re-extract analysis. Aliquot PleK-8 was discarded because of possible

contamination with another sample, confirmed by consulting the lab notebook. Mean AHe ages were calculated from the remaining aliquots of each sample and reported with uncertainties as a standard error of the mean. The mean AHe ages of all samples range from 1.9 ± 0.3 Ma to 12.2 ± 1.8 Ma (Fig. 5.2, Table SM 5.2.1).

The AFT ages pass the chi squared test p(χ^2) and thus are reported as pooled ages with ± 1σ error (Galbraith and Laslett, 1996) (Appendix 2, Table. 5.2.2). Passing this test usually shows that either all of the dated apatite crystals in a sample were derived from a source with a single age or that the ages were fully reset *in-situ*. We discuss two exceptions to this interpretation below.

The three northernmost samples, MrdK, PleK and MrfK, were collected from the hanging wall and footwall of MBT (Fig. 5.2). Samples MrdK and MrfK were collected from the Miocene Murree Formation (depositional age ≥22-18 Ma) part of the Rawalpindi Group and sample Plek was collected from the Paleocene age Patala Formation. Samples MrdK and PleK from the hanging wall of the MBT yield AHe mean age of 12.2±1.8 and 11.0±2.8 Ma and AFT ages of 19.2±3.0 and 9.1±2.8 Ma, respectively. Sample MrfK yielded a very small amount of apatite that was only used for AHe analysis; 2 crystals yielded a mean age of 10.0±2.9 Ma. The AHe ages are younger than the depositional ages; burial beneath the thick stratigraphic sequence of the Rawalpindi Group have fully reset the ages. The AFT age of PleK is younger than the depositional age, and map relationship and cross-sections show that the sample came from a deeply buried section, therefore, we interpret the AFT and AHe ages to be fully reset. In contrast, the AFT age of sample MrdK is very close to the depositional age. It was collected from the upper part of the stratigraphic section, which was not buried deep under as thick a pile of sediments as sample PleK. Therefore, we interpret the AFT age of MrdK to be partially reset.

Sample KllK, collected from the Eocene Kuldana Formation in the hanging wall of the Lachi Thrust (LT) in the central part of Kohat, yields an AFT age of 7.1±0.9 and an AHe age of 4.8±1.1 Ma. Samples KmsH and ShkK were collected from the Kamlial Formation, part of the Rawalpindi Group, and the Kuldana Formation; both are from the hanging wall of the Hukni Thrust (HT). Sample KmsH yields an AFT - AHe age pair of 4.8±0.5 and 1.9±0.3 Ma and sample ShkK has an AFT - AHe age pair of 3.2±0.8 and 3.7±1.9 Ma, respectively. Sample NgsK, from the Nagri Formation of the Siwalik Group yielded an AHe age of 3.1±0.9 Ma. The AFT and AHe ages are interpreted to be reset ages because the cooling ages are

younger than the corresponding depositional ages of the sample, and the samples were buried below thick (3-4 km) Rawalpindi and Siwalik Group strata.

Sample SncH was collected from the Jurassic age Shinawri Formation in the Surghar Range. The sample is located in the hanging wall of the SGT. The sample yield an AFT - AHe age pair of 13.3±1.1 and 10.6±1.4 Ma, respectively. We interpret the AFT and AHe ages to represent reset ages because the cooling ages are younger than the depositional age of the sample. Although a thick Siwalik Group succession of ~4 km was deposited in the hanging wall of the SGT between 12 and 2 Ma (Pivnik and Khan, 1996), this apparently does not influence the age of this sample. We further discuss the burial and exhumation of this sample in section 5.2.1.

Sample ChnK was collected from the top of 700 m thick Chingi Formation (depositional age 12-10 Ma), located at the eastern end of the Surghar Range. The sample has AFT and AHe ages of 8.6±0.6 and 9.2±4.4 Ma, respectively. AFT age is very close to the depositional age of the sample and the individual AHe aliquot ages are highly dispersed, therefore, the ages are probably partial reset due to shallow stratigraphic burial. Overall, AFT and AHe ages are older (13-19 Ma) in the Kohat and Surghar Ranges and younger (<8 Ma) within the Kohat (Fig. 5.2, Appendix 2, Table SM 5.2.1-5.2.2).

5.4 Thermal modelling

Forward and inverse thermal modelling are important tools to examine possible thermal histories that are compatible with the observed thermochronologic data (e.g., Ketcham, 2005; Gallagher, 2012). We performed inverse thermal modelling using the QTQt software, v. 5.7.0 (Gallagher, 2012). The software uses a trans-dimensional Bayesian Monte Carlo Markov Chain (MCMC) statistical approach to find the best possible time – temperature path for the data. We used the Flowers et al. (2009) radiation damage model for He diffusion and the Ketcham et al. (2007) AFT annealing model.

In order to better understand the kinematics and exhumation related to the MBT and SGT, we used AFT and AHe data from Jurassic and Paleocene samples SncH and PleK for inversion. The PleK thermal model examines whether exhumation on the MBT lasted for 2-3 Ma with faster rates or if the fault remained activate at a slow rate for 10-12 Ma. The SncH thermal model will be used to test the possibilities 1) ages are fully reset and show cooling

due to early thrusting along the SGT, 2) ages are partial reset and reflect late stage development of the Surghar Range at 1 Ma (Pivnik and Khan, 1996).

The models were set to a time - temperature space of 200 ± 200 Ma and 100 ± 100 °C for sample SncH and 50 ± 50 Ma and 75 ± 75 °C for sample PleK to allow the programme to search freely for acceptable solutions. The only imposed low temperature constraints in the model, 15 ± 15°C, are used for the depositional age of the samples and the present day surface temperature.

The expected thermal history path of the sample is a product of 200,000 iterations after 50,000 initial burn-in iterations. The modeling results are presented as an expected path, which is the average of model predicted paths within a 95% confidence interval (Fig. 5.3). The thermal model results for sample PleK suggests that the sample was reheated to 115±25 °C until ~15-13 Ma. The model predicted path shows that an episode of rapid cooling started at 12±2 Ma; the sample remained close to surface temperatures after 8±1 Ma. The thermal model results for sample SncH suggest maximum reheating of the samples to 135 ± 45 °C until ~17 Ma followed by cooling from 15± 2 Ma (Fig. 5.3). The expected model prediction shows monotonic cooling through the PAZ from ~17 Ma to the present. Unfortunately, the models are not well constrained in the APAZ, which could have provided more detailed information about the onset of cooling. The reason for a broad spread in possible cooling paths is because no additional constraints are forced on the model to limit the maximum onset of cooling for the model. In particular, the depositional constraints based on the Rawalpindi Group (~22-14 Ma), which is responsible for reheating and therefore resetting ages in both samples, was not forced in the model.

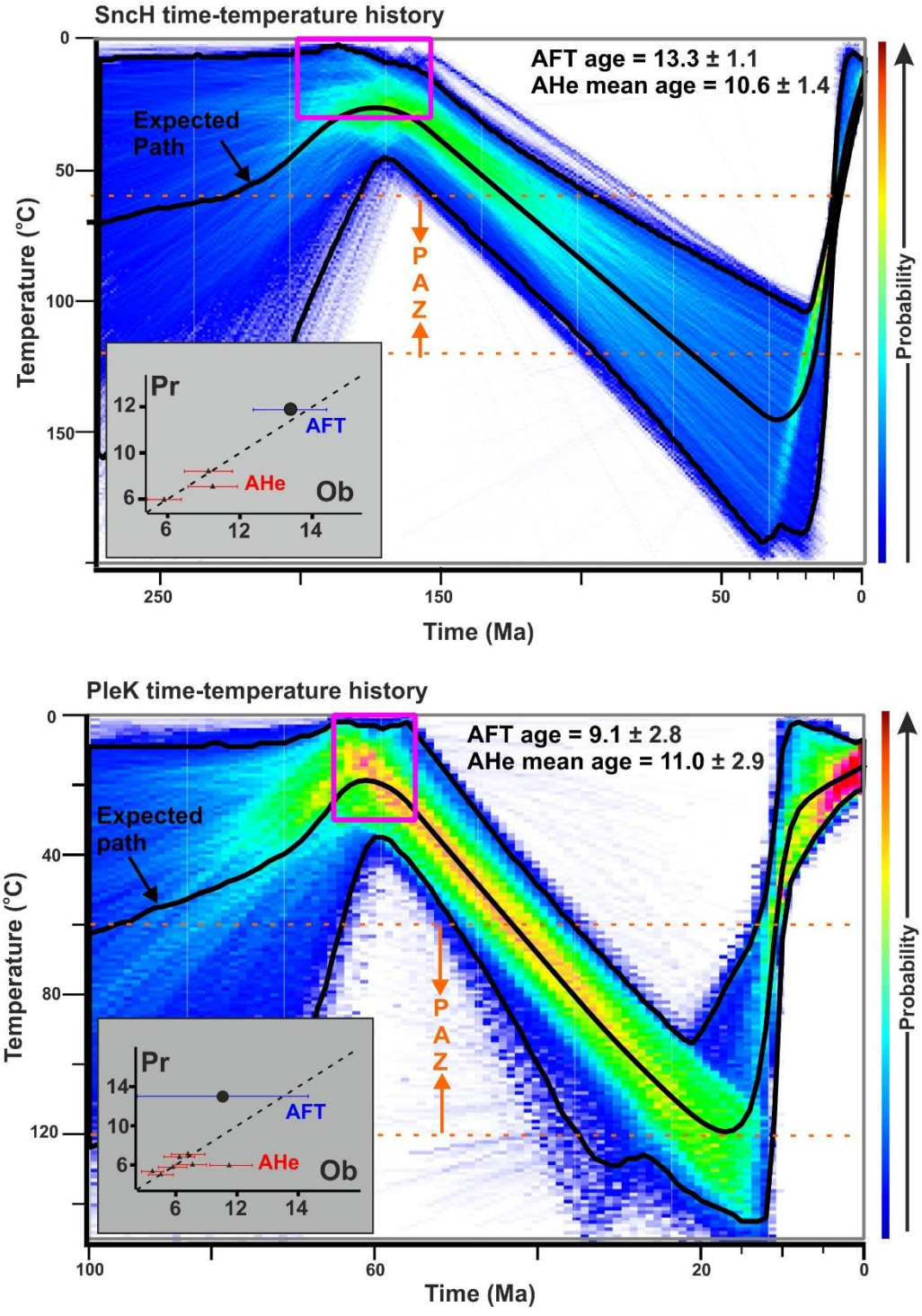

Figure 5.3. *Thermal models for samples SncH and Plek located in the hanging wall of SGT and MBT. See Table SM 5.2.1 and 5.2.2 for the data used in the models and Table 5.2.3 for model parameters. Ob, Observed age, Pr, Predicted age*

5.5 Balanced cross-section

The balanced cross-section is a regional cross-section presented in Ghani et al. (2018) where details about the orientation data, seismic and well data, the cross-section construction procedures and depth to basement calculation can be found. The 120 km long, north-south oriented cross-section XY is constructed from the southern part of the Peshawar Basin to the Kalabagh Reentrant (Figs. 5.2, 5.4). The first prominent topography at the north end of the profile is the Kohat Range, a major structure formed on the hanging wall of the MBT. The strata are translated above the MBT ramp from a present depth of 10 km, where the MBT ramp joins the basal décollement. The hanging wall is comprised of tightly folded structures in Mesozoic and Paleocene strata that were thrust above Rawalpindi Group rocks in the footwall. Fore and back-thrusts cut the hanging wall of the MBT, leading to the repetition of the stratigraphic section. The Darra back-thrust (DBT) places Mesozoic strata northward on top of the Rawalpindi Group. The fore- and back-thrusts join the main fault ramp of the MBT in the Kohat Range. Structural geometries above Eocene units are a complex assemblage of box and overturned folds cut by steeply-dipping thrust faults. The Rawalpindi and Siwalik Groups are eroded above Eocene strata in the hanging walls of thrusts. The Paleozoic to Paleocene stratigraphic section is duplicated between the lower and upper décollements, forming north-dipping duplexes that thicken the tectonic wedge (denoted as B, C, D and E in Figure 5.4). The double décollement structural style is present from the MBT to the Visor Thrust (VT) in the northern and central part of Kohat. In the Surghar Range, Eocene facies change from evaporate to carbonate rocks; this is correlated with the elimination of the upper décollement.

In the southern part of Kohat, the Rawalpindi Group thickness is reduced and pinches out south of the Banda Lakhoni thrust (BLT). A ~4 km Siwalik Group section is present on top of the Paleozoic to Eocene strata between the BLT and the Surghar Range. A duplex ramp linked to the BLT cuts the upper roof thrust that places pre-Eocene strata on top of the Siwalik Group in the subsurface. The SGT ramps up from a basal décollement, translating the Paleozoic to Pleistocene strata upward on the ramp, forming the Surghar Range. Two thrusts splay out from the SGT hanging wall: Mesozoic strata is thrust on top of Eocene strata and the Eocene strata is thrust above the Siwalik Group.

The cross-section is restored using fault parallel flow and line length restoration techniques. The present 120 km-long deformed section is restored to a length of ~220 km.

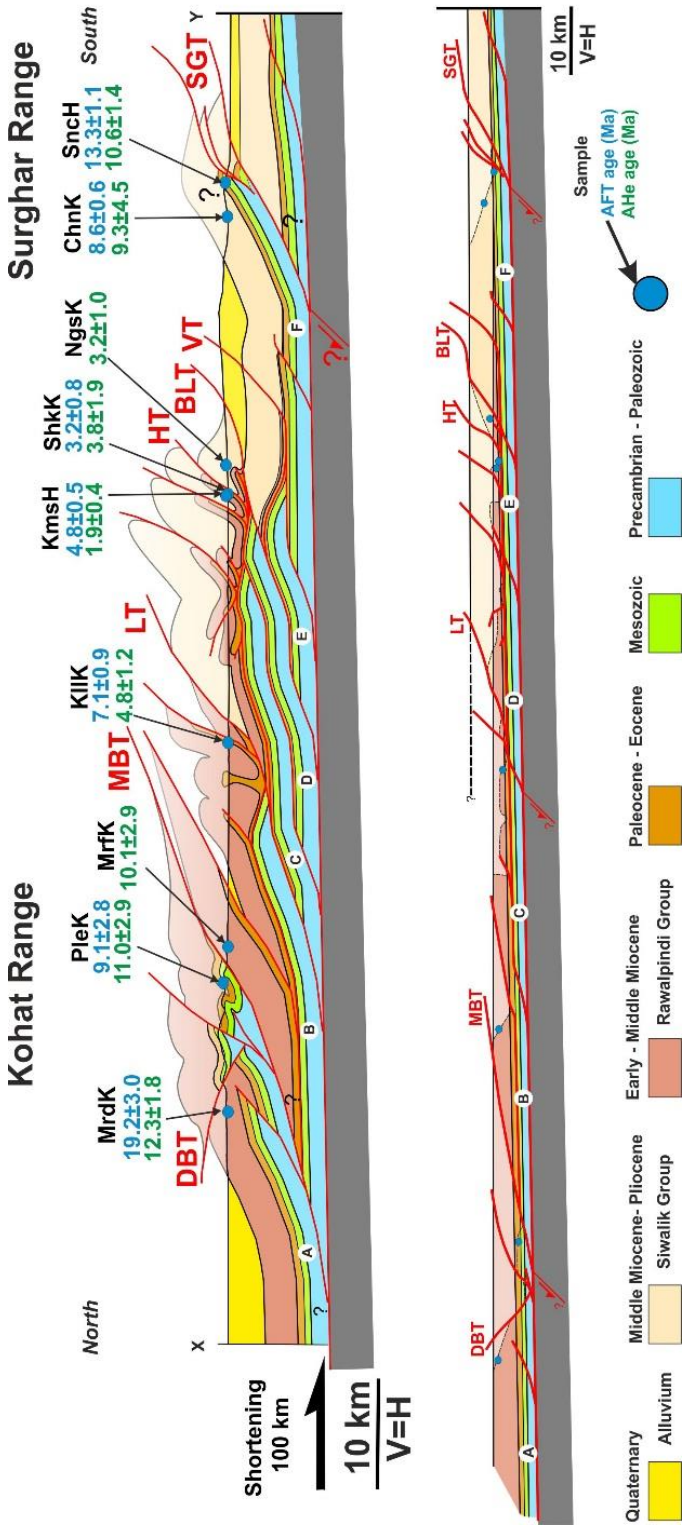

Figure 5.4. Regional deformed and restored cross-section XY from the Peshawar Basin to the Kalabagh Reentrant. Abbreviations and symbols for faults, stratigraphy and samples are the same as in figure 5.2. The restored section is used for the retro-deformable section in figure 5.6a. Note change in scale between deformed and restored section.

A total of 100 ± 10 km of shortening between the southern Peshawar Basin and the Surghar Range is calculated in our restored section. We estimate 75 ± 5 km of shortening for the Kohat, south of the MBT to the Surghar Range, noting the uncertainty in the depth to basement calculation, eroded and subsurface cutoff angles, additional shortening in the MBT footwall and for areas with a weak Eocene décollement. The amount of shortening 25 ± 5 km is calculated for the MBT above a thin-skinned décollement. The errors on calculated shortening cover the uncertainty for the eroded and subsurface cut-off angle of the MBT, internal shortening of intensely folded Mesozoic and Paleocene strata, and 2-3 km of slip along a basement normal fault lying beneath the restored location of the MBT (Fig. 5.4). The restored section shows ~7 km less shortening in the Rawalpindi Group compared to Eocene and older strata. The difference in shortening is mainly because the section above the Eocene strata is eroded and restored lengths are not well constrained for this interval.

5.6 Discussion

5.6.1 Sequential structural evolution of Kohat from the MBT to the SGT

We constructed a retro-deformable forward model based on our deformed section in order to explain the sequential structural evolution of the Kohat (Fig. 5.5). We have simplified the displacement between the two décollements by connecting upper and lower thrust ramps. Consequently, the displacement on the upper ramp is considered equal to the combined slip on all thrusts above the upper décollement. The geometry of the thrusts is designed to simulate an active roof thrust kinematic model (Couzens-Schultz et al., 2003) that we find is responsible for the structural evolution of the Kohat (Ghani et al., 2018). The shape of the undeformed wedge, the position of ramps and the amount of slip on the ramps is adopted from the restored section (Fig. 5.4).

The AFT and AHe cooling ages from the Surghar Range indicate that deformation propagated earlier at the southern end of Kohat. Sample SncH from the Surghar Range yields AHe and AFT cooling ages of ~11-13 Ma. Thermal modeling of data from this sample suggests that cooling was underway at 15±2 Ma (Fig. 5.3). Our thermal model shows burial of a Mesozoic age sample to a temperature near to or above AFT closure isotherm of ~120 °C. The burial is most probably caused by Rawalpindi Group deposits, which were thick enough to reset AHe and AFT ages. This thick section (3-5 km) is present today in the northern part of Potwar; it is dated in the Potwar and Salt Range as between ≥ 22 and 14 Ma (Johnson et al., 1985; Najman 2003). Rapid cooling started due to the erosion of the

Rawalpindi Group when the underlying stratigraphic section was uplifted due to translation over the SGT ramp. The movement on the SGT at the range front is most likely localized by pre-existing normal faults in the basement that helped to accrete the foreland to the deforming wedge. The ≥2 km slip on the SGT and consequent exhumation and basin-wide erosion of the Rawalpindi Group has uplifted this sample through the AFT and AHe closure isotherms. The 15±2 Ma cooling age can be used to constraint the exhumation rate related to uplift on the SGT. In the Kohat, a portion of the Rawalpindi Group was removed by erosion; in the Surghar Range, this group was completely removed until ~12 Ma, when the Siwalik Group started accumulating to the north of the Surghar Range (Fig 5 b-c). We have calculated fast exhumation rate of 3.1±1.5 mm/yr for the 15±2 Ma until ~12 Ma activation of SGT. We assume a thermal gradient of 23 ± 2°C based on published thermal gradient from different boreholes in the Kohat FTB and Potwar FTB and published thermal gradients in the Subhimalaya (Khan & Raza, 1986; Kadri, 1995; van der Beek, 2006).

The thermal model for the sample PleK suggest that significant rapid cooling started around 12±2 Ma and persisted until 8±1 Ma. Our active roof thrust kinematic model suggests that the lower ramp at the base of the décollement is connected to the ramp in the upper décollement. In this case, any movement on the lower ramp is transferred to the upper ramp. Assuming this kinematic model, the displacement propagated along the MBT ramp transferred displacement to the upper ramp at the same time. For example, the 10 km shortening on the basal ramp uplifted the PleK sample through the AFT closure isotherm and Mrdk and MrfK samples through the AHe isotherm; all these samples have similar AHe ages. The initial displacement on the MBT ramp and upper flat is followed by 20 km slip on the major MBT ramp, resulting in the development of the Kohat Range (Fig. 5.5c). An exhumation rate of 1.5±0.6 mm/yr and shortening rate of 11±4 mm/yr is calculated by assuming a 23±2°C geothermal gradient and ~15°C surface temperature for the ~30 km slip on the MBT between12±2 Ma and 8±1 Ma. During this time span, the Siwalik Group (Chingi and Nagri Formations age: 14-8 Ma) was deposited in the basin south of the MBT (Figs. 5.5 d-e). This basin infill was syn-tectonically deposited to the north and south of the active SGT, resulting in a gentle 3-4° angular unconformity above the older Eocene strata (Fig. 5.5e). The thickness of the Siwalik Group was sufficient to reheat the foreland samples (KllK, KmsH, ShkK, NgsK) south of the MBT, resetting the AFT and AHe ages in the Kohat.

The AFT and AHe ages show a southward-younging trend in cooling ages from ~7 to 3 Ma to the south of the MBT in the central and southern part of Kohat. Activity on the B, C, D and E duplex ramps propagated south of the MBT between ~8-3 Ma (Fig. 5.5 f-i). The model for Kohat suggests that development of duplexes between two décollements is balanced by shortening above the roof thrust. The thrust faults exposed at the surface in Kohat, such as the LT and HT (Fig. 5.4), originate from the upper décollement. The samples in this region have been exhumed due the formation of duplexes that tectonically thickened the section up to 5 km in the central Kohat that caused rock uplift and erosion. Cooling due to this thickening is more significant than that caused by motion along surface-breaking thrusts. The thrusting on the younger ramps passively rotated the older ramps and transported them to the south. We have not calculated shortening and exhumation rate for individual thrusts; rather, we prefer to calculate it for the region because the same deformation mechanism controlled the rates. We calculate a rate of ~10 mm/yr for the 53 km shortening accommodated by double décollements during the formation of duplexes and shortening above the roof thrust. We have calculated exhumation rate of ~ 0.9 mm/yr with a thermal gradient of 23±2 °C and surface temperature of ~15 °C assuming uplift due to formation of duplexes and assuming steady state exhumation between 8 and 3 Ma.

The Dhok Pathan Formation of the Siwalik Group was deposited in a newly developed piggyback basin in the southern part of Kohat, between the Surghar Range and Central Kohat, between 8 and 5 Ma. After 3 Ma, locally-derived conglomerates containing Eocene limestone clasts were shed to the south from the roof sequence uplifted above the duplexes. Since 3 Ma, the displacement was concentrated on the SGT, thus contributing to the folding of younger deposits in the piggyback basin to the north of the Surghar Range (Fig. 5.5j). The activity on the SGT resulted in the synkinematic deposition of thick sediment to the the north. As sample ChnK has partial reset AFT and AHe ages, the amount of burial prior to final exhumation was likely less than 3 km. The SGT is modeled to be active over the last 15±2 Ma with an average shortening rate of 0.9±0.1 mm/yr for 13 km slip.

Some ramps are active today in the Kohat (Fig. 5.5k) because of salt migration and strike-slip transfer movement in the Kalabagh Fault Zone and the Salt Range. The out-of-sequence thrusting in the interior of the belt contributes to the internal deformation of the wedge. This suggests that the wedge is building taper; therefore, deformation is not propagating into the undeformed foreland. Internal shortening within Kohat balances

shortening in the Potwar and Salt Range (~5 mm/yr) , preventing formation of a major salient in the trace of the MBT, which borders Kohat and Potwar to the north.

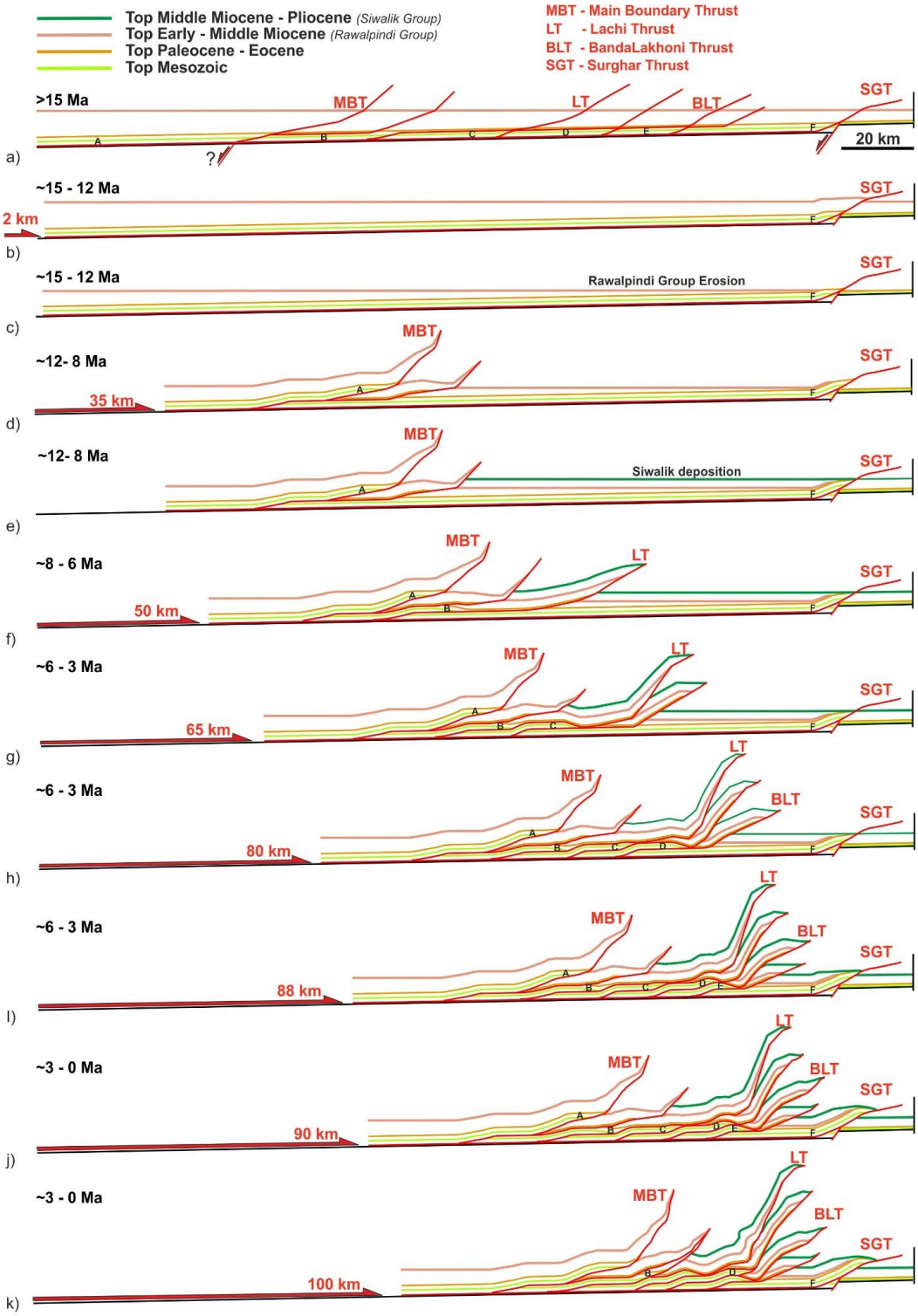

Figure 5.5. Retro deformable forward model based on restored cross-section in figure 5.4 to show sequential structural evolution of Kohat. Please note the horizontal and vertical scale is same, colors used for Siwalik is different than the map.

5.6.2 Early accretion of the foreland: implications for the Trans Indus Ranges

5.6.2.1 Burial and exhumation mechanisms in the Surghar Range

The development of the Surghar Range started at the southern end of the Kohat, constrained by the 13 ± 1 Ma AFT age of Jurassic sample SncH. However, this AFT age is not consistent with magnetostratigraphic age constraints that show that deposition of the Siwalik Group above Eocene strata in the Surghar Range started at 12 Ma (Pivnik and Khan, 1996). The location of the dated section is ~1 km north of sample SncH. So far, it is unclear which mechanism is responsible for the burial or reheating of the Jurassic sample. We present three different solutions that could explain this burial, exhumation and the unconformity between Eocene and Siwalik strata (Fig. 5.6).

The first possibility is that the Siwalik succession in this area is older than 15 Ma and the sample was reset as a direct consequence of burial beneath thick Siwalik strata, similar to the situation in the Salt Range (Fig. 5.6a).

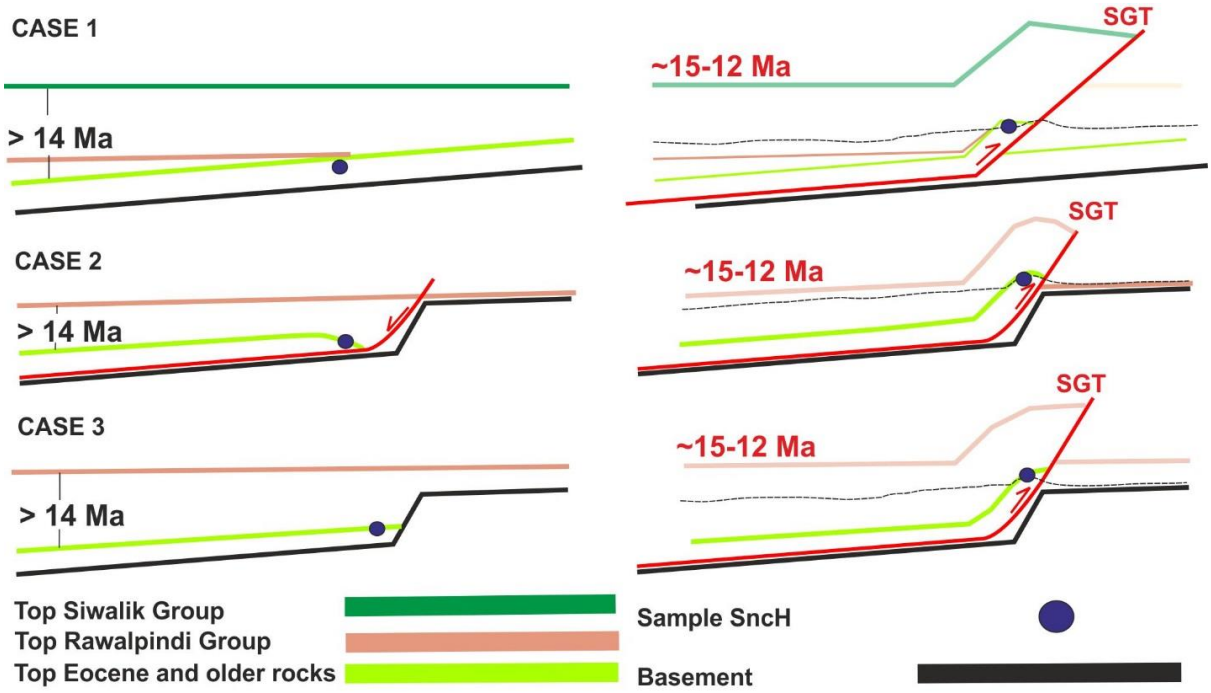

Figure 5.6. Sketches showing three possibilities for the development of the Surghar Range. Abbreviation's. CE: Cambrian to Eocene; RG: Rawalpindi Group SW: Siwalik Group

The second possibility is that localized thickening of the Rawalpindi Group above a listric normal fault adjacent to the Surghar Range has reheated the Jurassic strata (Fig. 5.6b).

The third possibility is that burial of the sample beneath a thick Rawalpindi Group led to a fully reset AFT age. In this case, the exhumation and subsequent erosion of the complete Rawalpindi Group in the Surghar Range and partial removal from the Kohat occurred before the development of the MBT (Fig. 5.6c). We prefer this solution, because it explains the formation of the angular unconformity between the Siwalik and Eocene strata, the absence of the Rawalpindi Group along the unconformity and Siwalik deposition in the Trans Indus Ranges. Clearly, better stratigraphic age control is required to definitively resolve this question.

5.6.2.2 Development of the Surghar and Khisor Ranges

Paleomagnetic and stratigraphic studies have proposed several possible times for the development of the Trans Indus Ranges. The development of the Surghar Range was proposed to have begun at 1 Ma (Pivnik and Khan, 1996) based on paleomagnetic dating of the youngest deposits involved in the deformation. The earlier development of the Khisor Range at 4 Ma (Blisniuk et al., 1998) was proposed by assuming that it formed at the same time as the Salt Range. This assumption was based on the observation of conglomerate beds at the base of the Siwalik Group that contain clasts from older stratigraphic sequences. The presence of conglomerates is used as a proxy to infer that earlier uplift in the region must have occurred prior to deposition of the Siwalik Group.

Assuming that the Trans Indus Ranges were developed in a very short interval requires a reinterpretation of three geological observations. 1) The Rawalpindi Group, exposed just 60 km south in the Salt Range, is absent in the Surghar and other Trans Indus Ranges. 2) The deposition of the Siwalik Group started in the Surghar Range at 12 Ma, significantly earlier than in the other Trans Indus Ranges (4 Ma; Burbank et al., 1996). 3) The angular unconformity between Eocene and Siwalik strata in the southwestern part of the Surghar and Trans Indus Ranges, marked by the 150-m-thick conglomeratic bed (Mitha Khattak Formation) which bears intra-basin clasts of Permian and Triassic strata, has an unclear origin.

Paleomagnetic studies suggest that the Trans Indus Ranges formed a topographic high during the Early to Middle Miocene, preventing the deposition of Rawalpindi Group sediments (Pivnik and Khan, 1996). The magnetostratigraphic ages of the Siwalik Group suggest that deposition started at 12 Ma in the Surghar Range and then gradually filled the basin southward, reaching the Marwat and Khisor Ranges where the strata was first deposited

at 4 Ma (Fig. 5.2). The proposed model for the development of the Surghar Range at 1 Ma (Pivnik and Khan, 1996) does not explain how an angular unconformity and conglomerate beds containing clasts of Permian and Triassic strata clasts developed at the base of the Siwalik Group. The source region of these conglomerate clasts is the pre-molasse stratigraphy, exposed today in the Salt and Trans Indus Ranges. Furthermore, provenance and paleocurrent studies for the Rawalpindi Group suggest that the source was located in the northern Himalaya; transport directions pointed to the south to southeast (Burbank et al., 1996; Najman et al., 2003). Considering the paleoflow directions, the provenance and the synchronous sedimentation in the surrounding areas such as the Salt Range, Bannu Basin and Western Axial fold and thrust belt, it is unlikely that the Rawalpindi Group was not deposited in the region that later became the Trans Indus Ranges; deposition followed by erosion seems more probable.

The presence of the conglomerate at the base of the Siwalik Group in the Khisor Range could be related to an earlier uplift event caused by normal faulting at or before 4 Ma, as suggested by Blisniuk et al. (1998). This uplift event brought Paleozoic and Mesozoic strata to the surface along a significant topographic step created by the normal fault. The conglomerates, sourced from the uplifted footwall, were then deposited on top of the hanging wall. The onset of Siwalik deposition in the location of the present Khisor Range at 4 Ma covered the conglomerate and pre-molasse strata; these were subsequently uplifted in the hanging wall of the Khisor Thrust at 2 Ma. Although this hypothesis of earlier normal faulting (Blisniuk et al., 1998) is feasible, we suggest that earlier thrusting could also explain the formation of the angular unconformity, the missing Rawalpindi Group and the preservation of conglomerates more convincingly in terms of the overall structural evolution of the Trans Indus Ranges.

In order to understand the evolution of the Trans Indus Ranges, we examine the similar case for the development of the Salt Range at 4 Ma. We suggested two major episodes of exhumation in the Salt Range based on detailed thermochronologic studies. Late Paleozoic rifting created normal faults in the region of the Salt Range that later acted as ramps for the MFT to localize deformation at 4 Ma, forming the modern range (Fig. 5.1). Motion along ramps in the Salt Range focused the maximum amount of exhumation above the ramps, leading in the rapid removal of molasse and pre-molasse strata which were shed as intra-basinal conglomerate towards the north and east (Burbank and Beck, 1989). We suggest that the Khisor Range developed earlier, at 13 Ma, similar to the Surghar Range. The

Rawalpindi Group formerly covered the area that was subsequently uplifted and eroded, thus exposing older rocks. The Siwalik strata in the Surghar Range has been deformed syn-kinematically since 12 Ma above the hanging wall of the SGT, which had a slow shortening rate. If we assume the development of the Khisor Range initiated at 13 Ma, then there would be a significant amount of time available to erode the Rawalpindi Group and to expose older strata for erosion and deposition to the north of range, before it was eventually covered by Siwalik sediments at 4 Ma. In order to better constrain the depositional and deformational processes active in the Trans Indus Ranges from the Miocene to present, more low temperature thermochronology analysis of Cambrian to Permian rocks will be required.

5.6.3 Thick vs. thin skinned structures

Fold and thrust belts display three types of structural styles. Thin-skinned deformation of a cover sequence above basement can accommodate a larger amount of horizontal shortening. Thick-skinned deformation involves basement and contributes to crustal thickening. Thin-skinned basement-involved deformation describes a system where basement structures influence the deformation of the cover sequence (e.g., Pfiffner, 2006; Pfiffner, 2016). Large-scale Late Paleozoic rifting in the Western Himalaya (Garzanti et al., 1996; Pogue et al., 1992) created normal faults in Northern Gondwana. The structural style of the Salt and Trans Indus Ranges was controlled by thrust faults that utilized these normal faults as ramps to propagate deformation. We modeled the development of the Surghar Range with and without basement normal faulting (Ghani et al., 2018). Our new thermochronologic data and structural model suggest that the long-term development of the Surghar Range was geographically fixed at the same position, most probably due to localization of the ramp above a pre-existing basement normal fault. The presence of normal faults and subsurface basement ridges were also proposed in earlier studies of the Surghar Range (Farah et al., 1987; McDougall and Hussain, 1991).

Restored balanced sections in the Kohat and Potwar document 65 to 80 km of total shortening (Baker et al., 1988; McDougall and Hussain, 1991; Abbasi and McElroy, 1991; Ghani et al., 2018). This restored length of section coincides geographically with the northern margin of the Peshawar Basin, where Permian igneous rocks are exposed today. A possibility of major basement steps present at the northern margin of the Peshawar Basin (Figs. 5.4, 5.5) could have resulted in the formation of the MBT ramp, similar to the mid-crustal ramp reported in the Nepalese Central Himalaya (Lavé & Avouac, 2001; DeCelles et al., 2001).

We suggest that thin-skinned structures in the Kohat and Potwar were influenced by preexisting basement structures that provided weak zones for the generation of major fault ramps.

5.7 Conclusions

Constraining the spatio-temporal sequence of deformation for the Kohat fold and thrust belt illustrates the role of structural style in localizing exhumation. Deformation propagated to the range front of the Kohat at 15±2 Ma, earlier than the development of the MBT in Pakistan. The range front remained active from 15±2 Ma to the present with a shortening rate significantly lower than in the interior of Kohat. The development of the MBT at 12±2 Ma is constrained in the Kohat. Deformation propagated southward resulting in tectonic thickening by stacking of thrust sheets. The process of duplex formation is spatially correlated with exhumation due to erosion of molasse strata. Rapid cooling occurred in the early phases of SGT that reduced after ~12 Ma. The average exhumation rates, remained less than ~1.5 mm/yr for the last ~12 Ma, associated with exhumation caused by major thrusts and duplexes in the Kohat. Approximately, 100 km of shortening is accommodated in the last 15±2 Ma between the Peshawar Basin and Kalabagh Reentrant. The presence of an angular unconformity between Eocene strata and the Siwalik Group and the presence of basal conglomerate beds above the basal contact suggest early development of the Surghar Range. The early accretion of the foreland into the Kohat deforming wedge has contributed to the internal deformation on the double décollements; this has built up the taper of the wedge, allowing younger out-of-sequence deformation within Kohat.

Acknowledgments

We thank the German Academic Exchange Service (DAAD) for providing financial assistance to complete this research and to PETEX for providing the Move program through their Academic Support Initiative Programme. We thank faculty members and students of Bahria and Peshawar Universities for their assistance during field work.

Chapter 6. Synthesis and conclusions

The research presented in this thesis aims to present the spatiotemporal structural evolution of the Kohat and Potwar fold and thrust belts (herein called as Kohat and Potwar) in Pakistan. This study analyzed in detail the structural style by constructing balanced cross-sections and then coupling them with low temperature thermochronologic data to decipher the timing of the structural development in this region. The important deformational events in the long term history of the region from the Cambrian to the Recent are deciphered by inverse thermal modeling of detrital apatite low temperature thermochronologic data. The findings of this study provide information about the shortening and exhumation rates related to major structures in the region.

The sedimentary succession of the Kohat, Potwar, Salt and Trans Indus Ranges can be subdivided into three major units: 1) the Precambrian Salt Range Formation (SRF), 2) the Cambrian to Eocene siliciclastic, carbonate and evaporite platform sequence and 3) the Miocene to Pliocene Himalayan molasse sequence. Systematic sampling was conducted along strike from different sections in the Salt Range and across strike from the stratigraphic succession in the Kohat for apatite U-Th-Sm/He (AHe) and apatite fission track (AFT) dating.

6.1 Pre-Himalayan history of the Salt Range and the adjoining areas

The Salt Range is the only location in the hanging wall of Main Frontal Thrust (MFT) that exposes an almost complete stratigraphic sequence from Precambrian to Pliocene (Figs. 4.1-4.2). The Precambrian Salt Range Formation is the oldest stratigraphic unit, comprised of evaporites deposited in a shallow epicontinental sea from EoCambrian until the early Cambrian (Gee, 1980). The Cambrian to Devonian clastic succession was sourced from the Indian craton and deposited on the northern part of Gondwana (Brookfield, 1993; Deb et al., 2001; McKenzie et al., 2011; Qasim et al., 2017; Hughes et al., 2019). The geochronologic data obtained from the Cambrian to Carboniferous stratigraphic succession exposed in the Salt Range, Peshawar and Hazara basins (Pogue et al., 1992a; Qasim et al., 2017; Hughes et al., 2019) show that the region was receiving sediments from an Indian craton source rocks that are exposed in the southern part of India. The major unconformity between Cambrian and Permian strata (Gee, 1980; Pogue et al., 1992a; Ghazi and Moutney, 2011) was

previously considered to represent a depositional hiatus in the Salt Range. Inverse thermal modeling of partially reset AHe and AFT detrital samples shows a cooling event in the Carboniferous (Fig. 4.3). We suggest that this cooling is related to exhumation during a regional Late Paleozoic rifting phase reported in the Peshawar Basin of Pakistan and Kashmir- Zanskar areas in India. The Late Paleozoic rifting resulted in the opening of the Neo-Tethys and formation of the Indian passive margin (Pouge et al 1992b, Grazanti 1996, Dipetro et al 2001). Rifting in the basin created the normal faults that were reactivated as ramps during the Late Cenozoic. Permian strata in the rift basin is overlapped by thick carbonate-bearing Mesozoic sedimentary sequences deposited on the Indian passive margin exposed today in the Western Salt Range, Lesser Himalaya and Western Axial fold and thrust belt in Pakistan. The Early Eocene collision of India with Asia resulted in the influx of Asian detritus to the basin (e.g., Beck et al., 1995; Ding et al., 2016) and establishing a restricted marine environment in the Kohat (Pivnik and Wells, 1996). The evaporite succession deposited in this basin later played an important role as a secondary décollement during the structural development of the Kohat (Abbasi and McElroy 1991; Ghani et al 2018) (Figs. 3.2-3.5). Large-scale Himalayan shortening after collision, particularly and thrust sheets stacking in the northern part during the Oligocene-Miocene, has transformed the Kohat and Potwar area into the Himalayan foreland basin that started to accumulate molasse sediments eroded from Himalayan Orogen (Pivnik and Wells, 1996; Burbank and Beck 1996; Najman et al., 2003).

6.2 Development of the Main Boundary Thrust (MBT)

The MBT forms the major geologic terrain boundary between the Subhimalaya and the Lesser Himalaya along the Himalayan fold and thrust belt. The regional development of the MBT at 11 Ma has been temporally constrained in the Central and Western Himalaya by Meigs et al (1995) and in the Hazara Syntaxis by Turab et al (2017). Structure and thermochronologic studies in the Central and Northwestern Himalaya in India and Nepal show that the MBT was active until 5 Ma (DeCelles et al., 2011; Gavillot et al., 2018) or may even remain active today after development at 10 Ma due to removal of material from the hanging wall of the MBT by climatically-enhanced erosional processes (Deekan et al., 2011; Theide et al., 2018). Previous studies in the eastern part of Kohat Range of Pakistan (Figs. 5.1-5.2) suggested that Pliocene – Pleistocene motion along the MBT has accommodated 40 km of shortening (McDougall et al., 1993). However, these balanced cross-sections have not taken shortening in the Rawalpindi and Siwalik Groups into account, resulting in an

overestimate of the amount of shortening accommodated by the MBT and other structures in the region (McDougall and Hussain 1991; McDougall et al 1993). In our cross-sections we have balanced shortening along all stratigraphic horizons from the Paleozoic to the Pliocene in order to constrain the minimum amount of shortening along major thrusts in the Kohat from the MBT to the Surghar Thrust (SGT).

In this study, I have used the combination of balanced sections and AFT and AHe data to demonstrate that the MBT became active to the north of the present day Peshawar Basin at 12±2 Ma; since that time, it has accommodated 25 ± 5 km of shortening (Figs. 5.2-5.5). The similar AFT and AHe ages (~10 Ma) suggest that samples cooled rapidly through PAZ and PRZ closure isotherms and imply cooling rates of 1.5±0.6 mm/yr in the hanging wall of MBT. I suggest that translation up the MBT ramp localized rock uplift, causing exhumation and cooling between 12±2 and 8±1 Ma when deformation propagated towards the south with a shortening rate of 11±4 mm/yr. Turab et al. (2017) suggested a second episode of exhumation at 3 Ma on the MBT in the Hazara Syntaxis, that is related to fluvial erosion. In the Kohat and Potwar, the fault trace of the MBT cuts across the Early to Middle Miocene Rawalpindi Group; no evidence of Siwalik or younger strata truncated by the MBT has been mapped or reported so far. Therefore, we suggest that MBT activity formed a major physiographic barrier to the north of Kohat and Potwar, blocking the deposition of Siwalik strata downstream. After ~ 8 Ma, the MBT was passively transported southward by younger thrusts in the Kohat and Potwar (Fig. 5.5). There is no evidence for reactivation of the MBT in the Kohat and Potwar, likely for two reasons. First, because deformation propagated towards the south very efficiently on décollements in the Precambrian Salt Range Formation and Eocene evaporite rocks in the wider Subhimalayan terrain of Pakistan. Secondly, the semi-arid climate was likely present since ~10 Ma in this region (Burbank et al., 1996) and the absence of significant monsoonal precipitation in the area prevented efficient climatically-enhanced erosion that might have reactivated the MBT in this region in the same manner as occurred in the Indian Central Himalaya (Deekan et al., 2011).

6.3 Temporal evolution of the structural style and exhumation in the Kohat and Potwar

Deformation propagated to Kohat and Potwar after major deformation on the MBT ramp and its footwall stopped at 8 Ma (Fig. 5.5). Deformation in the Kohat is localized on two décollements while in the Potwar only one décollement is active; therefore, the shortening style is quite different in these two regions (Figs. 3.11, 5.5). We suggest that the

structural evolution in the Kohat is controlled by active roof thrusting. In the Kohat, the lower flat and ramp in the basal décollement are connected to the upper flat and ramp in the Eocene and younger strata. This mechanism of displacement on ramps results in tectonic thickening of the section in the subsurface by the formation of duplexes between the upper and lower décollements, and removal/erosion of Rawalpindi and Siwalik strata above the upper décollement. Thrusting in the Kohat propagated out-of-sequence towards the foreland from ~8-3 Ma on the younger ramps with a shortening rate of ~10 mm/yr. The exhumation rate of ~0.9 mm/yr above the roof thrust is caused by formation of duplexes in the subsurface.

The ramps forming duplexes in the Kohat continue as tip lines of fault propagation folds in the Potwar, so we consider that there was a similar timing for structural development in the northern part of Potwar. In the Potwar, the absence of an upper décollement results in the preservation of a thick sequence of Rawalpindi and Siwalik Groups (Ghani et al., 2018). Compared to the Kohat, the cooling rate in the northern part of Potwar is negligible, illustrating the influence of structural style on exhumation. In the southern part of the Potwar, a simple structural style in the area south of the Soan syncline is due to a steeper cross sectional taper of wedge ($\geq 3^0$) and the presence of salt at the base (Fig. 3.8). These factors contributed to evolution of gentle folds and translation of thrust sheet towards the south with very little internal deformation.

6.4 Spatiotemporal development of the Kohat and Potwar range fronts

The Salt and Surghar Ranges are the range fronts of the Kohat and Potwar, respectively, and are connected by the Kalabagh Fault Zone (Fig. 3.1-3.3). Previous paleomagnetic studies of Neogene deposits and stratigraphic relationships suggest the development of Salt Range occurred during different time intervals, ranging between 10 Ma to 2 Ma (Burbank and Beck, 1989; Yeats et al., 1987; Grelaud et al 2002). The inverse thermal modeling of AHe and AFT data presented in this study suggests that the development of the Salt Range started at 4 Ma (Figs. 4.3-4.4). The combination of age data with structural reconstruction presented in this study also highlights the pattern of exhumation above the MFT in the Salt Range. We have proposed that maximum rate of exhumation (2 - 2.5 mm/yr) was fixed on the MFT ramp, leading to the extensive erosion of a thick sequence of molasse strata. The mechanical strength of thin Eocene carbonate rocks when exposed to surface were not as efficiently removed by erosional processes compared to removal of soft relatively unconsolidated molasse. The relative stronger nature of carbonate rocks, and translation of a

thrust sheet above salt resulted in the preservation of Precambrian to Paleocene strata and structural style variation along the Himalayan range front. The study also suggests that the MFT remained active after 4 Ma with an average shortening rate of ~5-6 mm/yr.

The development of the Surghar Range was previously proposed to have commenced at 1-2 Ma (Pivnik and Khan 1996; McDougall and Hussain 1991). AFT and AHe data show that the deformation started earlier at the southern end of the Kohat in the Surghar Range at 15±2 Ma (Fig. 5.5). Deformation within the Surghar Range accreted the foreland into the deforming wedge; subsequent deformation in the Kohat took place on a double décollement, building the critical taper. Our structural model (Fig. 3.11) suggests that the early slip on the SGT is responsible for the development of an angular unconformity between Eocene strata and the Late Miocene Siwalik Group and erosion of Early to Middle Miocene Rawalpindi Group in this area. The thermal model suggests rapid exhumation (3.1±1.5 mm/yr) between 15±2 to ~12 Ma, when sample SncH cooled through the APAZ and APRZ closure isotherms (Fig. 5.3). The cooling is due to the removal of the Rawalpindi Group above the SGT ramp. The uplift of the Surghar Range created a piggy back basin towards the north that started to preserve thick syn-deformational Siwalik strata after ~12 Ma (Figs. 5.5).

6.5 Comparative shortening in the Kohat, Potwar and transfer zone kinematics

The amount of minimum shortening in the Kohat and Potwar are comparable: 75 ± 5 and 65 ± 5 km (Figs. 3.11 & 5.4). This shortening is spatially accommodated in a 70 km and 150 km wide area between the MBT and SGT in Kohat and the MBT and MFT in Potwar, respectively. The similar amounts of shortening can explain why there is no significant salient or recess observed along the trace of the MBT west of Hazara Kashmir Syntaxis to the northwestern part of Kohat. The kinematic adjustments between Kohat and Potwar are balanced by internal deformation in the Kohat in response to forward translation on the MFT in the Salt Range and Kalabagh Fault Zone. For example, the 20-30 km of translation on the MFT in the Salt Range is balanced partly by slip on the SGT and translation of thrust sheet on duplex ramps. The 10 – 12 km strike slip transfer movement and salt migration in the Kalabagh Fault Zone during the last 2 Ma is balanced by out-of-sequence slip on duplex ramps that cuts roof strata beneath the Lachi and Banda Lakhoni thrusts and drag structures in the Shakardarra area located north of the Kalabagh Fault Zone (Figs. 3.12). Similarly, the transfer movement and salt migration in the Kalabagh Fault Zone resulted in the developing

of significant curvature of the MFT fault trace in the Western Salt Range directly south of the Kalabagh Fault Zone.

6.6 Conclusions

This study of the Kohat and Potwar fold and thrust belts of Pakistan highlight the inter-relationship between tectonics and exhumation processes active in the fold and thrust belt. The structural style is combined it with thermochronology data to understand the sequence of structural evolution in the Kohat and Potwar. We conclude that the following points are the main finding of this study.

1. The Late Paleozoic Rifting phase created normal faults that resulted in the formation of horst and half graben structures. The erosion of Early Paleozoic strata on the horsts, resulted in the formation of major unconformities in the Salt Range. The normal faults were later exploited by the basal décollement to develop thrust ramps that propagated deformation towards the foreland and formed range fronts.
2. The difference of structural style in the two areas is primarily controlled by deformation along the double décollement in Kohat compared to a single décollement in Potwar. The steeper (≥3°) basement slope and thick (~1 km) salt on the base of stratigraphic wedge has contributed in lesser internal deformation within the southern Potwar.
3. The Kalabagh Fault zone is comprised of strike-slip normal faults that are formed by expulsion of salt from below the hanging wall of the fault towards the footwall. The migration/flow of salt toward the foreland and fault displacement in the Kalabagh Fault zone has resulted in the formation of the Ghundi Lobe in the Western Salt Range and a change in the orientation of structures from east-west to north-south in the Shakardarra area of Kohat.
4. Deformation on the SGT started at 15 ± 2 Ma, developing the Surghar Range, the range front of the Kohat and Bannu Basin. The early displacement on the SGT accreted undeformed foreland to the Kohat deforming wedge. The earlier displacement on SGT is responsible for the development of an angular unconformity between Eocene and Siwalik strata in the Surghar Range.
5. The development of the MBT in the Kohat area started at 12±2 Ma. Our new data confirm that the MBT developed as a major Himalayan structure at the same time as in the Western Himalaya. Reactivation of the MBT in the Kohat has not been

observed, so we suggest that the MBT was passively transported toward the foreland and rotated above the younger ramps.

6. A new active roof thrust structural model is proposed; this is responsible for the development of the disharmonic structural style in the Kohat. The model effectively explains the fold and thrust kinematics, tectonic thickening in the subsurface and extensive erosion of the cover sequence in the Kohat.
7. The average shortening rate of 11±4 mm/yr and fast exhumation rate of 1.5±0.6 mm/yr are calculated for the ~30 km shortening on the MBT.
8. The average shortening rate of ~5-6 mm/yr and fast exhumation rate of 2 - 2.5 mm/yr on the ramp are calculated for the 22 ± 2 km of shortening on the MFT for the last 4 Ma in the Salt Range.
9. The presence of erosionally-resistant carbonate rocks in the Kohat and Salt Range lead to the development of a different range morphology compared to Potwar, where carbonates are absent or still not exposed to surface.
10. The minimum shortening of 100 ± 10 km in the Kohat and Potwar implies long term rate of 7.5–9 mm/yr. This value is based on significant shortening accommodated through translation on the MBT, and between the MBT and MFT-SGT for the last ~15 Ma.

6.7 Recommendations for future work

The transition of compressional deformation style between the Himalayan fold and thrust belt in to transpressional deformational style in the Himalayan western axial fold and thrust belt in Pakistan provide a new avenue to study the western collisional zone. Extensive geochronologic and thermochronologic analyses of structures exposed between the Naga Parbat syntaxis and the Makran in Pakistan is lacking that is important to understand long term geological history and crucial to constrain the onset of collision along the western suture. Future geochronological research focused on the Western Suture (Fig. 2.1) could also help to test the new hypothesis of a Greater India Basin, that propose the known timing of collision (55-65 Ma) in the north of Himalaya was a collision of portion of India with Asia. A very wide ocean basin called Greater India existed between Tethys Himalaya and Greater Himalaya that is subducted, followed my major collision at 25 Ma (Van Hinsbergen 2012; 2018). Detailed 3D structural modeling integrating surface geology, seismic and petroleum exploration well data, and low temperature thermochronology data from the Himalayan western fold and thrust belt would provide detailed information for the first time about

difference of structural style, fold and thrust kinematics and sequence of deformation propagation into the foreland. The future study in this zone will help us understand the dynamics of continental deformation and its implications on the development of complex structural style displayed by fold and thrust belts along the Himalayan Orogen.

References

Abbasi, I.A., McElroy, R. (1991). Thrust Kinematics in the Kohat Plateau, Trans Indus Range, Pakistan. Journal of Structural Geology, 13 (3), 319–27.

Ahmad Abir, I., Khan, S.D., Ghulam, A., Tariq. S., Shah, M.T. (2015). Active Tectonics of Western Potwar Plateau-Salt Range, Northern Pakistan from InSAR Observations and Seismic Imaging. Remote Sensing of Environment, 168, 265–75.

Alsop, G.I., Weinberger, R., Levi, T., Marco, S. (2015). Deformation within an Exposed Salt Wall: Recumbent Folding and Extrusion of Evaporites in the Dead Sea Basin. Journal of Structural Geology, 70, 95–118.

Badshah, M. S., Gnos, E., Jan, M. Q., & Afridi, M. I. (2000). Stratigraphic and tectonic evolution of the northwestern Indian plate and Kabul Block. Geological Society, London, Special Publications, 170(1), 467-476.

Baker, D.M., Lillie, R.J., Yeats, R.S., Johnson, G. D., Yousuf, M. & Hamid, A. S. (1988). Development of the Himalayan frontal thrust zone: Salt Range, Pakistan. Geology, 16 (1), 3-7.

Banks, C. J., Warburton, J. (1986). Passive-Roof' Duplex Geometry in the Frontal Structures of the Kirthar and Sulaiman Mountain Belts, Pakistan. Journal of Structural Geology, 8 (3–4), 229–37.

Beck, R. A., Burbank, D. W., Sercombe, W. J., Riley, G. W., Barndt, J. K., Berry, J. R., & Cheema, A. (1995). Stratigraphic evidence for an early collision between northwest India and Asia. Nature, 373(6509), 55.

Blisniuk, P.M., Sonder, L.J., Lillie, R.J. (1998). Northwest Himalayan Thrust Front Development. Tectonics ,17 (5), 766–79.

Bollinger, L., Avouac, J. P., Beyssac, O., Catlos, E. J., Harrison, T. M., Grove, M., & Sapkota, S. (2004). Thermal structure and exhumation history of the Lesser Himalaya in central Nepal. Tectonics, 23(5).

Bonini, M. (2007). Deformation Patterns and Structural Vergence in Brittle-Ductile Thrust Wedges: An Additional Analogue Modelling Perspective. Journal of Structural Geology, 29 (1), 141–58.

Borderie, S., Graveleau, F., Witt, C., & Vendeville, B. C. (2018). Impact of an interbedded viscous décollement on the structural and kinematic coupling in fold-and-thrust belts: Insights from analogue modeling. Tectonophysics, 722, 118-137.

Burg, J. P. (2011). The Asia–Kohistan–India collision: review and discussion. In Arc-continent collision, Springer, Berlin, Heidelberg, 279-309.

Burkhard, M., & Sommaruga, A. (1998). Evolution of the western Swiss Molasse basin: structural relations with the Alps and the Jura belt. Geological Society, London, Special Publications, 134(1), 279-298.

Butler, R.W.H. (1982). The Terminology of Structures in Thrust Belts. Journal of Structural Geology, 4 (3), 239–45.

Butler, R.W.H. (1985). Thrust Tectonics: A Personal View. Geological Magazine, 122 (3), 223-32.

Butler, R.W.H., Coward, M.P., Harwood, G.M., Knipe, R.J. (1987). Salt Control on Thrust Geometry, Structural Style and Gravitational Collapse Along the Himalayan Mountain Front in the Salt Range of Northern Pakistan. In: Lerche, I., O'Brien, J.J. (Eds.), Dynamical Geology of Salt and Related Structures. Academic Press Inc. Orlando, 339-418.

Burbank, D. W., Raynolds, R. G. H., and Johnson, G. D. (1986), Late Cenozoic tectonics and sedimentation in the northwestern Himalayan foredeep: II. Eastern limb of the Northwest Syntaxis and regional synthesis, in Allen, P. A., and Homewood, P., eds., Foreland Basins, Volume Special Publication 8, International Association of Sedimentologists, 293-306.

Burbank, D. W., and Raynolds, R. G. H. (1988). Stratigraphic keys to the timing of thrusting in terrestrial foreland basins: Applications to the Northwestern Himalaya, in Kleinspehn, K. L., and Paola, C., eds., New Perspectives in Basin Analysis: New York, Springer-Verlag, 331-351.

Burbank, D. W., and Beck, R. A. (1989). Early Pliocene uplift of the Salt Range: Temporal and constraints on thrust wedge development, in Malinconico, L. L., and Lillie, R. J., eds., Tectonics of the Western Himalaya, Volume Special Paper 232: Boulder. Geological Society of America, 113-128.

Burbank, D. W., and Beck, R. A. (1991). Rapid, long-term rates of denudation. Geology, 19, 1169-1172.

Burbank, D. W., Beck, R. A., and Mulder, T. (1996). The Himalayan foreland basin, in Yin, A., and Harrison, T. M., eds. The tectonic evolution of Asia: Cambridge, Cambridge University Press, 149–188.

Calkins, J. A., Offield, T. W., Abdullah, S. K., & Ali, S. T. (1975). Geology of the southern Himalaya in Hazara, Pakistan, and adjacent areas (No. 716-C). US Geological Survey Professional Papers, 29.

Carlson, W. D., R. A. Donelick, and R. A. Ketcham (1999). Variability of apatite fission-track annealing kinetics: I. Experimental results. American Mineralogist, 84, 213–1223.

Castelluccio, A., Andreucci, B., Zattin, M., Ketcham, R. A., Jankowski, L., Mazzoli, S., & Szaniawski, R. (2015). Coupling sequential restoration of balanced cross sections and low-temperature thermochronometry: The case study of the Western Carpathians. Lithosphere, 7(4), 367-378.

Chapple, W.M. (1978). Mechanics of Thin-Skinned Fold-and-Thrust Belts. Bulletin of the Geological Society of America, 89 (8), 1189–98.

Chen, L.Z., Khan, S.D. (2010). InSAR Observation of the Strike-Slip Faults in the Northwest Himalayan Frontal Thrust System. Geosphere, 6 (5), 731–36.

Costa, E., Vendeville, B.C. (2002). Experimental Insights on the Geometry and Kinematics of Fold-and-Thrust Belts Above Weak, Viscous Evaporitic Decollement. Journal of Structural Geology, 24 (11), 1729–39.

Cotton, J.T., Koyi, H.A. (2000). Modeling of Thrust Fronts Above Ductile and Frictional Decollements: Application to Structures in the Salt Range and Potwar Plateau, Pakistan. Bulletin of the Geological Society of America, 112 (3), 351–63.

Couzens-Schultz, B.A., Vendeville, B.C., Wiltschko, D.V. (2003). Duplex Style and Triangle Zone Formation: Insights from Physical Modeling. Journal of Structural Geology, 25 (10),1623–44.

Dahlen, F.A., Suppe, J., Davis, D. (1984). Mechanics of Fold-and-Thrust Belts and Accretionary Wedges: Cohesive Coulomb Theory. Journal of Geophysical Research, 89 (B12), 10087–10,101.

Dahlen, F.A., & Suppe, J. (1988). Mechanics, growth, and erosion of mountain belts. Geological Society of America Special Paper, 218, 161– 178.

Dahlen, F.A. (1990). Critical Taper Model of Fold-And-Thrust Belts and Accretionary Wedges. Annual Review of Earth and Planetary Sciences, 18 (1), 55–99.

Dahlstrom, C. D. A. (1969). Balanced Cross Sections. Canadian Journal of Earth Sciences, 6 (4), 743–57.

Danilchik, W., & Shah, S. I. (1987). Stratigraphy and coal resources of the Makarwal area, Trans-Indus mountains, Mianwali district, Pakistan. United States Geological Survey, Professional Paper, (USA), 75(1341).

Davis, D. M., Suppe, J., Dahlen, F.A. (1983). Mechanics of Fold-and- Thrust Belts and Accretionary Wedges. Journal of Geophysical Research, 88 (B2), 1153–72.

Davis, D. M., Engelder, T. (1985). The Role of Salt in Fold-and-Thrust Belts. Tectonophysics, 119 (1–4), 67–88.

Deb, M., Thorpe, R.R.I., Krstic, D.M., Corfu, F., and Davis, D.W. (2001). Zircon U–Pb and galena Pb isotope evidence for an approximate 1.0 Ga terrane constituting the western margin of the Aravalli-Delhi orogenic belt, northwestern India. Precambrian Research, 108, 195–213.

DeCelles, P. G., Robinson, D. M., Quade, J., Ojha, T. P., Garzione, C. N., Copeland, P., & Upreti, B. N. (2001). Stratigraphy, structure, and tectonic evolution of the Himalayan fold- thrust belt in western Nepal. Tectonics, 20(4), 487-509.

Dey, S., Thiede, R. C., Schildgen, T. F., Wittmann, H., Bookhagen, B., Scherler, D., & Strecker, M. R. (2016). Holocene internal shortening within the northwest Sub-Himalaya: Out- of- sequence faulting of the Jwalamukhi Thrust, India. Tectonics, 35(11), 2677-2697.

Deeken, A., Thiede, R. C., Sobel, E. R., Hourigan, J. K., & Strecker, M. R. (2011). Exhumational variability within the Himalaya of northwest India. Earth and Planetary Science Letters, 305(1-2), 103-114.

Ding, L., Qasim, M., Jadoon, I. A., Khan, M. A., Xu, Q., Cai, F., …& Yue, Y. (2016). The India–Asia collision in north Pakistan: Insight from the U–Pb detrital zircon provenance of Cenozoic foreland basin. Earth and Planetary Science Letters, 455, 49-61.

DiPietro, J. A., Pogue, K. R., Hussain, A., & Ahmad, I. (1999). Geologic map of the Indus syntaxis and surrounding area, northwest Himalaya, Pakistan. Special Papers-Geological Society of America, 159-178.

DiPietro, J. A., & Isachsen, C. E. (2001). U- Pb zircon ages from the Indian plate in northwest Pakistan and their significance to Himalayan and pre- Himalayan geologic history. Tectonics, 20(4), 510-525.

DiPietro, J. A., & Pogue, K. R. (2004). Tectonostratigraphic subdivisions of the Himalaya: A view from the west. Tectonics, 23(5).

Donelick, R. A. (1991). Crystallographic orientation dependence of mean etchable fission track length in apatite: An empirical model and experimental observations. American Mineralogist, 76, 83–91.

Donelick, R. A., R. A. Ketcham, and W. D. Carlson, (1999). Variability of apatite fission-track annealing kinetics: II. Crystallographic orientation effects. American Mineralogist, 84, 1224 –1234.

Drewis, H. (1995). Tectonics of the Potwar Plateau Region and the Development of Syntaxes, Punjab, Pakistan. U.S Geological Survey Bulletin, 2126, 22.

Dunkl, I. (2002). Track Key: A window program for calculation and graphical presentation of fission track data: Computer and Geosciences, 28, 3-12.

Elliott, D. (1983). The Construction of Balanced Cross-Sections. Journal of Structural Geology, 5(2), 101.

Faisal, S., Dixon, J.M. (2015). Physical Analog (Centrifuge) Model Investigation of Contrasting Structural Styles in the Salt Range and Potwar Plateau, Northern Pakistan. Journal of Structural Geology, 77, 277–92.

Faisal, S., Larson, K. P., Camacho, A., & Coutand, I. (2018). Cooling, exhumation, and deformation in the Hindu Kush, NW Pakistan: New constraints from preliminary $^{40}Ar/^{39}Ar$ and fission track analyses. Journal of Asian Earth Sciences, 158, 415-427.

Farah, A. Abbas, G., De Jong, K.A., Lawrence, R.D. (1984). Evolution of the Lithosphere in Pakistan. Tectonophysics, 105 (1–4), 207–27.

Farley, K. A., Wolf, R. A., & Silver, L. T. (1996). The effects of long alpha-stopping distances on (U-Th)/He ages. Geochimica et Cosmochimica Acta, 60(21), 4223-4229.

Farley, K. A. (2000). Helium diffusion from apatite; general behavior as illustrated by Durango fluorapatite. Journal of Geophysical Research,105, 2903–2914.

Farley, K. A. (2002). (U-Th)/ He dating; techniques, calibrations, and applications, *in* D. Porcelli, C. J. Ballentine, and R. Wieler, eds., Noble gases in geochemistry and cosmochemistry. Reviews in Mineralogy and Cosmochemistry, 47, 819–843.

Galbraith, R.F., and Laslett, G.M. (1996). Statistical modelling of thermal annealing of fission tracks in apatite. Geochim. Cosmochim. Acta, 60, 5117-5131.

Gallagher, K., Brown, R., & Johnson, C. (1998). Fission track analysis and its applications to geological problems. Annual Review of Earth and Planetary Sciences, 26(1), 519-572.

Gallagher, K. (2012). Transdimensional inverse thermal history modeling for quantitative thermochronology. Journal Geophysical Research, Solid Earth, 117 (B2), B02408.

Gansser, A. (1980). The significance of the Himalayan suture zone. Tectonophysics, 62(1-2), 37-52.

Garzanti, E., Angiolini, L., and Sciunnach, D. (1996). The Mid-Carboniferous to Lowermost Permian succession of Spiti (Po Group and Ganmachidam Formation; Tethys Himalaya, Northern India): Gondwana glaciation and rifting of Neo-Tethys. Geodinamica Acta (Paris), 9(2), 78-100.

Gavillot, Y., Meigs, A. J., Sousa, F. J., Stockli, D., Yule, D., & Malik, M. (2018). Late Cenozoic Foreland-to-Hinterland Low-Temperature Exhumation History of the Kashmir Himalaya. Tectonics, 37(9), 3041-3068.

Ghazi, S., and Mountney, N.P. (2011). Petrography and Provenance of the Early Permian Warcha Sandstone, Salt Range, Pakistan. Sedimentary Geology, 233, 88-110.

Ghani, H., Zeilinger, G., Sobel, E.R., Heidarzadeh, G. (2018). Structural variation within the Himalayan fold and thrust belt: A case study from the Kohat-Potwar fold thrust belt of Pakistan: Journal of Structural Geology, 116, 34-46.

Gee, E.R. (1980). Salt Range Series Geological Maps: Directorate of Overseas Surveys, United Kingdom, for Government of Pakistan and Pakistan Geological Survey, 6 Sheets, Scale 1: 50,000.

Grelaud, S., Sassi, W., de Lamotte, D. F., Jaswal, T., & Roure, F. (2002). Kinematics of eastern Salt Range and South Potwar basin (Pakistan): a new scenario. Marine and Petroleum Geology, 19(9), 1127-1139.

Green, P. F., Duddy, I. R., Gleadow, A. J. W., Tingate, P. R., & Laslett, G. M. (1986). Thermal annealing of fission tracks in apatite: 1. A qualitative description. Chemical Geology: Isotope Geoscience Section, 59, 237-253.

Hildebrand, P. R., Searle, M. P., Khan, Z., & Van Heijst, H. J. (2000). Geological evolution of the Hindu Kush, NW Frontier Pakistan: active margin to continent-continent collision zone. Geological Society, London, Special Publications, 170(1), 277-293.

Hodges, K. V. (2000). Tectonics of the Himalaya and southern Tibet from two perspectives. Geological Society of America Bulletin, 112(3), 324-350.

Hughes, N. C., Myrow, P. M., Ghazi, S., McKenzie, N. R., Stockli, D. F., & DiPietro, J. A. (2019). Cambrian geology of the Salt Range of Pakistan: Linking the Himalayan margin to the Indian craton. Geological Society of America Bulletin.

Hurford, A.J., and Green, P.F. (1982). A user's guide to fission track dating calibration: Earth and Planetary Science Letters, 59, 343-354.

Jadoon, I.A.K., Frisch, W. (1997). Hinterland-Vergent Tectonic Wedge below the Riwat Thrust, Himalayan Foreland, Pakistan: Implications for Hydrocarbon Exploration. AAPG Bulletin, 81(3), 438–48.

Jaswal, T. M., Lillie, R.J., Lawrence, R.D. (1997). Structure and Evolution of the Northern Potwar Deformed Zone, Pakistan. AAPG Bulletin, 81 (2), 308–28.

Jaumé, S.C., Lillie, R.J. (1988). Mechanics of the Salt Range-Potwar Plateau, Pakistan: A Fold-and-thrust Belt Underlain by Evaporites. Tectonics, 7 (1), 57–71.

Johnson, N. M., Stix, J., Tauxe, L., Cerveney, P. F., and Tahirkheli, R.A.K. (1985). Paleomagnetic chronology, fluvial processes, and tectonic implications of Siwalik deposits near Chinji village, Pakistan. Journal of Geology, 93, 27-40.

Jouanne, F., Awan, A., Pecher, A., Kausar, A., Mugnier, J.L., Khan, I., Khan, N.A., and Melle, J.V. (2014). Present-day deformation of northern Pakistan from Salt Ranges to Karakoram Ranges. Journal of Geophysical Research: Solid Earth, 119, **https://doi.org/10.1002/2013JB010776**.

Kazmi, A.H., Abbasi, I.A. (2008). Stratigraphy and Historical Geology of Pakistan. National Centre of Excellence in Geology, University of Peshawar, Pakistan.

Ketcham, R. A., R. A. Donelick, and W. D. Carlson. (1999). Variability of apatite fission-track annealing kinetics; III. Extrapolation to geological time scales. American Mineralogist, 84, 1235–1255.

Ketcham, R. A. (2005). Forward and inverse modeling of low-temperature thermochronometry data. Reviews in Mineralogy and Geochemistry, 58(1), 275-314.

Ketcham, R.A., Carter, A., Donelick, R.A., Barbarand, J., and Hurford, A.J. (2007). Improved modeling of fission-track annealing in apatite. American Mineralogist, 92, 799–810.

Ketcham, R. A., Gautheron, C., & Tassan-Got, L. (2011). Accounting for long alpha-particle stopping distances in (U–Th–Sm)/He geochronology: Refinement of the baseline case. Geochimica et Cosmochimica Acta, 75(24), 7779-7791.

Khan, M.A., Ahmed, R., Raza, H.A., Kemal, A. (1986). Geology of Petroleum in Kohat-Potwar Depression, Pakistan. AAPG Bulletin, 70 (4), 396–414.

Khan, M. J., Opdyke, N. D., & Tahirkheli, R. A. K. (1988). Magnetic stratigraphy of the Siwalik group, Bhittani, Marwat and Khasor ranges, northwestern Pakistan and the timing of neocene tectonics of the Trans Indus. Journal of Geophysical Research: Solid Earth, 93(B10), 11773-11790.

Khan, M. A., Jan, M. Q., & Weaver, B. L. (1993). Evolution of the lower arc crust in Kohistan, N. Pakistan: temporal arc magmatism through early, mature and intra-arc rift stages. Geological Society, London, Special Publications, 74(1), 123-138.

Khan, S. D., Walker, D. J., Hall, S. A., Burke, K. C., Shah, M. T., & Stockli, L. (2009). Did the Kohistan-Ladakh island arc collide first with India? Geological Society of America Bulletin, 121(3-4), 366-384.

Khan, S.D., Chen, L., Ahmad, S., Ahmad, I., Ali, F. (2012). Lateral Structural Variation along the Kalabagh Fault Zone, NW Himalayan Foreland Fold-and-Thrust Belt, Pakistan. Journal of Asian Earth Sciences, 50, 79–87.

Laslett, G.M., Gleadow, A., and Duddy, I.R. (1994). The relationship between fission-track length and track density in apatite. Nuclear Tracks, 9, 29-38.

Lave, J. & Avouac, J. P. (2001). Fluvial incision and tectonic uplift across the Himalayas of central Nepal. Journal of Geophysical Research,106, 26561–26591.

Leathers, M. (1987). Balanced structural cross section of the Salt Range and western Potwar Plateau, Pakistan: Deformation near the strike-slip terminus of an over thrust sheet, M.S. thesis, Oregon State Univ, Corvallis, 228.

Lillie, R. J., Johnson, G. D., Yousuf, M., Zamin, A. S. H., Yeats, R. S. (1987). Structural Development within the Himalayan Foreland Fold-and-Thrust Belt of Pakistan. In Beaumont, C., Tankard, A.J. (Eds.), Sedimentary Basins and Basin Forming Mechanisms. Canadian Society of Petroleum Geologists Memoir, 12, 379–92.

Lock, J., and Willett, S. (2008). Low-temperature thermochronometric ages in fold-and-thrust belts. Tectonophysics, 456, 147-162.

McClay, K.R., Whitehouse, P.S., Dooley, T., Richards, M. (2004). 3D Evolution of Fold and Thrust Belts Formed by Oblique Convergence. Marine and Petroleum Geology, 21 (7), 857–77.

McDougall, J.W., Khan, S.H. (1990). Strike-slip Faulting in a Foreland Fold-thrust Belt: The Kalabagh Fault and Western Salt Range, Pakistan. Tectonics, 9 (5),1061–75.

McDougall, J.W., Hussain. A. (1991). Fold and Thrust Propagation in the Western Himalaya Based on a Balanced Cross Section of the Surghar Range and Kohat Plateau, Pakistan. AAPG Bulletin, 75 (3), 463–78.

McDougall, J.W., Hussain, A., Yeats R.S. (1993). The Main Boundary Thrust and Propagation of Deformation into the Foreland Fold-and-Thrust Belt in Northern Pakistan near the Indus River. Geological Society, London, Special Publications, 74 (1), 581–88.

McKenzie, N.R., Hughes, N.C., Myrow, P.M., Xiao, S., and Sharma, M. (2011). Correlation of Precambrian Cambrian sedimentary successions across northern India and the utility of isotopic signatures of Himalayan lithotectonic zones. Earth and Planetary Science Letters, 312, 471–483.

McQuarrie, N., and T. A. Ehlers. (2015). Influence of thrust belt geometry and shortening rate on thermochronometer cooling ages: Insights from Thermokinematic and erosion modeling of the Bhutan Himalaya. Tectonics, 34, 1055–1079.

Meigs, A., Burbank, D.W., Beck, R.A. (1995). Middle-Late Miocene (Pre-10 Ma) Initiation of the Main Boundary Thrust in the Western Himalaya. Geology, 23 (5), 423–26.

Meissner, C.R., Master, J.M., Rashid, M.A., Hussain, M. (1974). Stratigraphy of the Kohat quadrangle, Pakistan: U.S. Geological Survey Professional Paper, 716-D: 30.

Mora, A., Casallas, W., Ketcham, R. A., Gomez, D., Parra, M., Namson, J., ... & Ghorbal, B. (2015). Kinematic restoration of contractional basement structures using thermokinematic models: A key tool for petroleum system modeling. AAPG Bulletin, 99(8), 1575-1598.

Najman, Y., Pringle, M., Godin, L., & Oliver, G. (2001). Dating of the oldest continental sediments from the Himalayan foreland basin. Nature, 410(6825), 194.

Najman, Y., Garzanti, E., Pringle, M., Bickle, M., Stix, J., & Khan, I. (2003). Early-Middle Miocene paleodrainage and tectonics in the Pakistan Himalaya. Geological Society of America Bulletin, 115(10), 1265-1277.

Najman, Y., et al. (2010). Timing of India-Asia collision: Geological, biostratigraphic, and palaeomagnetic constraints. Journal of Geophysical Research, 115: B12416.

Opdyke, N.D., Johnson, N.M., Johnson, G.D., Lindsay, E.H., Tahirkheli, R.A.K. (1982). Paleomagnetism of the middle Siwalik formations of northern Pakistan and rotation of the Salt Range decollement. Paleogeography, Paleoclimatology, Paleoecology, 37, 1-15.

Pennock, E.S., Lillie, R.J., Zaman, A.S.H., Yousaf, M. (1989). Structural Interpretation of Seismic Reflection Data from the Eastern Salt Range and Potwar Plateau. Pakistan. AAPG Bulletin, 73, 841-857.

Pfiffner, O, A. (2006). Thick-Skinned and Thin-Skinned Styles of Continental Contraction, in Mazzoli, S., and Butler, R, W, H., Styles of Continental Contraction. Geological Society of America Special Paper, 414, 153–77.

Pfiffner, O. A. (2016). Basement-involved thin-skinned and thick-skinned tectonics in the Alps. Geological Magazine, 153(5-6), 1085-1109.

Pivnik, D.A., Sercombe, W.J. (1993). Compression-and Transpression-related Deformation in the Kohat Plateau, N W Pakistan. Geological Society, London, Special Publications, 74, 559–80.

Pivnik, D.A., Wells, N.A. (1996). The Transition from Tethys to the Himalaya as Recorded in Northwest Pakistan. Bulletin of the Geological Society of America, 108 (10), 1295–1313.

Pivnik, D. A., & Khan, M. J. (1996). Transition from foreland-to piggyback-basin deposition, Plio-Pleistocene Upper Siwalik Group, Shinghar Range, NW Pakistan. Sedimentology, 43(4), 631-646.

Poblet, J., Lisle, R.J. (2011). Kinematic Evolution and Structural Styles of Fold-and-Thrust Belts. Geological Society, London, Special Publications, 349, 1–24.

Pogue, K.R., Wardlaw, B.R., Harris, A. G., and Hussain, A. (1992a). Paleozoic and Mesozoic stratigraphy of the Peshawar basin, Pakistan: correlations and implications. Geological Society of America Bulletin, 104, 915-927.

Pogue, K.R., DiPietro J.A., Khan, S.R., Hughes, S.S., Dilles, J.H., Lawrence, R.D. (1992b). Late Paleozoic rifting in northern Pakistan. Tectonics, 11, 871-883.

Qasim, M., Ding, L., Khan, M. A., Umar, M., Jadoon, I. A., Haneef, M., ... & Yao, W. (2018). Late Neoproterozoic–Early Palaeozoic stratigraphic succession, Western Himalaya, North Pakistan: Detrital zircon provenance and tectonic implications. Geological Journal, 53(5), 2258-2279.

Qasim, M., Ding, L., Khan, M. A., Jadoon, I. A., Haneef, M., Baral, U., ... & Yue, Y. (2018). Tectonic Implications of Detrital Zircon Ages from Lesser Himalayan Mesozoic-Cenozoic Strata, Pakistan. Geochemistry, Geophysics, Geosystems.

Qayyum, M., Niem, A. R., & Lawrence, R. D. (1996). Newly discovered Paleogene deltaic sequence in Katawaz basin, Pakistan, and its tectonic implications. Geology, 24(9), 835-838.

Qayyum, M., Spratt, D.A., Dixon, J.M., Lawrence, R.D. (2015). Displacement Transfer from Fault-Bend to Fault-Propagation Fold Geometry: An Example from the Himalayan Thrust Front. Journal of Structural Geology, 77, 260–76.

Ramsay, J.G. (1967). Folding and Fracturing of Rocks. P. 568 in Folding and Fracturing of Rocks. McGraw-Hill, New York, 568.

Reiners, P. W., and K. A. Farley (2001), Influence of crystal size on apatite (U-Th)/He thermochronology: an example from the Bighorn Mountains, Wyoming. Earth and Planetary Science Letters, 188, 413–420.

Reiners, P. W., S. N. Thompson, B. J. Tipple, S. L. Peyton, J. M. Rahl, and A. Mulch (2008). Secondary weathering phases and apatite (U-Th)/He ages: Geochimica et Cosmochimica Acta, 72, A784.

Richards, L., King, R.C., Collins, A.S., Sayab, M.K., Haneef, M., Morley, C.K.,Warren, J. (2015). Macrostructures vs Microstructures in Evaporite Decollements: An Example from the Salt Range, Pakistan. Journal of Asian Earth Sciences, 113 (2), 922-934.

Robinson, D. M., DeCelles, P. G., Garzione, C. N., Pearson, O. N., Harrison, T. M., & Catlos, E. J. (2003). Kinematic model for the Main Central thrust in Nepal. Geology, 31(4), 359-362.

Robinson, D.M., and Pearson, O.N. (2006). Exhumation of Greater Himalayan rock along the Main Central thrust, Nepal: Implications for channel flow, in Law, R.D., Searle, M.P., and Godin, L., eds., Channel Flow, Extrusion, and Exhumation in Continental Collision Zones. Geological Society of London Special Publication, 268, 255–268.

Robinson, D. M., McQuarrie, N. (2012). Pulsed deformation and variable slip rates in the Central Himalayan Thrust Belt. Lithosphere, 4, 449-464, DOI: 10.1130/L204.1

Sajid, M., Andersen, J., Rocholl, A., & Wiedenbeck, M. (2018). U-Pb geochronology and petrogenesis of peraluminous granitoids from northern Indian plate in NW Pakistan: Andean type orogenic signatures from the early Paleozoic along the northern Gondwana. Lithos, 318, 340-356.

Satyabala, S.P., Yang, Z., Bilham, R. (2012). Stick–slip Advance of the Kohat Plateau in Pakistan. Nature Geoscience, 5 (2),147–50.

Searle, M.P. (1987). The Closing of Tethys and the Tectonics of the Himalaya. Geological Society of America Bulletin, 98 (6), 678–701.

Searle, M. P., Khan, M. A., Fraser, J. E., Gough, S. J., & Jan, M. Q. (1999). The tectonic evolution of the Kohistan-Karakoram collision belt along the Karakoram Highway transect, north Pakistan. Tectonics, 18(6), 929-949.

Sercombe, W.J. et al. (1998). Wrench Faulting in the Northern Pakistan Foreland. AAPG Bulletin, 82 (11), 2003–30.

Schaltegger, U., Zeilinger, G., Frank, M., & Burg, J. P. (2002). Multiple mantle sources during island arc magmatism: U–Pb and Hf isotopic evidence from the Kohistan arc complex, Pakistan. Terra Nova, 14(6), 461-468.

Shah, S.M. (1977). Stratigraphy of Pakistan. In: Geological Survey of Pakistan Memoir, 12.

Smit, J.H.W., Brun, J.P., Sokoutis, D. (2003). Deformation of Brittle-Ductile Thrust Wedges in Experiments and Nature. Journal of Geophysical. Research, 108 (B10), 2480.

Sobel, E. R., & Strecker, M. R. (2003). Uplift, exhumation and precipitation: tectonic and climatic control of Late Cenozoic landscape evolution in the northern Sierras Pampeanas, Argentina. Basin Research, 15(4), 431-45.

Sobel., E.R. and Seward, D. (2010). Influence of etching conditions on apatite fission-track etch pit diameter: Chemical Geology, 271, 59-69.

Suppe, J., (1983). Geometry and Kinematics of Fault-bend Folding. American Journal of Science, 283, 684- 721, DOI:10.2475/ajs.283.7.684.

Tahirkheli, R. K. (1979). The India-Eurasia suture zone in northern Pakistan: Synthesis and interpretation of recent data at plate scale. Geodynamics of Pakistan, 125-130.

Thiede, R., Robert, X., Stübner, K., Dey, S., & Faruhn, J. (2017). Sustained out-of-sequence shortening along a tectonically active segment of the Main Boundary thrust: The Dhauladhar Range in the northwestern Himalaya. Lithosphere, 9(5), 715-725.

Treloar, P. J., Rex, D. C., Guise, P. G., Coward, M. P., Searle, M. P., Windley, B. F., Luff, I. W. (1989). K-Ar and Ar-Ar geochronology of the Himalayan collision in NW Pakistan: Constraints on the timing of suturing, deformation, metamorphism and uplift. Tectonics, 8(4), 881-909.

Treloar, P. J., Coward, M. P., Williams, M. P., & Khan, M. A. (1989). Basement-cover imbrication south of the Main Mantle Thrust, north Pakistan. Geological Society of America, Special Paper, 232, 137-152.

Treloar, P. J., Rex, D. C., Guise, P. G., Wheeler, J., Hurford, A. J., & Carter, A. (2000). Geochronological constraints on the evolution of the Nanga Parbat syntaxis, Pakistan Himalaya. Geological Society, London, Special Publications, 170(1), 137-162.

Turab, S. A., Stüwe, K., Stuart, F. M., Chew, D. M., & Cogne, N. (2017). Tectonics drives rapid exhumation of the western Himalayan syntaxis: Evidence from low-temperature thermochronometry of the Neelum valley region, Pakistan. Lithosphere, 9(6), 874-888.

Van der Beek, P., Robert, X., Mugnier, J.L., Bernet, M., Huyghe, P., and Labrin, E. (2006). Late Miocene – Recent exhumation of the central Himalaya and recycling in the foreland basin assessed by apatite fission-track thermochronology of Siwalik sediments, Nepal: Basin Research, 18, 413-434.

Van Hinsbergen, D. J., Lippert, P. C., Dupont-Nivet, G., McQuarrie, N., Doubrovine, P. V., Spakman, W., & Torsvik, T. H. (2012). Greater India Basin hypothesis and a two-stage Cenozoic collision between India and Asia. Proceedings of the National Academy of Sciences, 109(20), 7659-7664.

Van Hinsbergen, D. J., Lippert, P. C., Li, S., Huang, W., Advokaat, E. L., & Spakman, W. (2018). Reconstructing greater India: Paleogeographic, kinematic, and geodynamic perspectives. Tectonophysics.

Vermeesch, P., D. Seward, C. Latkoczy, M. Wipf, D. Guenther, and H. Baur. (2007). Alpha-emitting mineral inclusions in apatite, their effect on (U-Th)/He ages, and how to reduce it: Geochimica et Cosmochimica Acta, 71, 1737–1746.

Wagner, G. A., Gleadow, A. J. W., & Fitzgerald, P. G. (1989). The significance of the partial annealing zone in apatite fission-track analysis: Projected track length measurements

and uplift chronology of the Transantarctic Mountains. Chemical Geology: Isotope Geoscience Section, 79(4), 295-305.

Willett, C.D., Fox, M., and Shuster, D.L. (2017). A helium-based model for the effects of radiation damage annealing on helium diffusion kinetics in apatite: Earth and Planetary Science Letters, 477, 195-204.

Wilke, F. D., Sobel, E. R., O'Brien, P. J., & Stockli, D. F. (2012). Apatite fission track and (U–Th)/He ages from the higher Himalayan crystalline, Kaghan Valley, Pakistan: implications for an eocene plateau and oligocene to pliocene exhumation. Journal of Asian Earth Sciences, 59, 14-23.

Wobus, C., Heimsath, A., Whipple, K., & Hodges, K. (2005). Active out-of-sequence thrust faulting in the central Nepalese Himalaya. Nature, 434, 1008–1011.

Yeats, R.S., Khan, S.H., Akhtar, M. (1984). Late Quaternary Deformation of the Salt Range of Pakistan. Geological Society of America Bulletin, 95, 958–66.

Yeats, R.S., Hussain, A. (1987). Timing of Structural Events in the Himalayan Foothills of Northwestern Pakistan. Geological Society of America Bulletin, 99 (2), 161–76.

Yeats, R.S., Thakur, V.C. (2008). Active Faulting South of the Himalayan Front: Establishing a New Plate Boundary. Tectonophysics, 453 (1–4), 63–73.

Yin, A. (2006). Cenozoic tectonic evolution of the Himalayan orogen as constrained by along-strike variation of structural geometry, exhumation history, and foreland sedimentation. Earth-Science Reviews, 76(1-2), 1-131.

Zanchi, A., Poli, S., Fumagalli, P., & Gaetani, M. (2000). Mantle exhumation along the Tirich Mir Fault Zone, NW Pakistan: pre-mid-Cretaceous accretion of the Karakoram terrane to the Asian margin. Geological Society, London, Special Publications, 170(1), 237-252.

Zeilinger, G., Seward, D., & Burg, J. P. (2007). Exhumation across the Indus Suture Zone: a record of back sliding of the hanging wall. Terra Nova, 19(6), 425-431.

Zeitler, P. K. (1985). Cooling history of the NW Himalaya, Pakistan. Tectonics, 4(1), 127-151.

Zeitler, P. K., Koons, P. O., Bishop, M. P., Chamberlain, C. P., Craw, D., Edwards, M. A., Kidd, W. S. (2001). Crustal reworking at Nanga Parbat, Pakistan: Metamorphic consequences of thermal-mechanical coupling facilitated by erosion. Tectonics, 20(5), 712-728.

Zhou, R., Schoennohm, L. M., Sobel, E. R., Davis, D. W., and Glodny, J. 2017. New constraints on orogenic models of the southern Central Andean Plateau: Cenozoic basin evolution and bedrock exhumation: Geological Society of America Bulletin, 129 (1/2), 152–170.

Appendix 1 (chapter 4)

Supplementary material (SM) for Chapter 4: "**Paleozoic to Pliocene tectonic evolution of the Salt Range constrained by low temperature thermochronology"**

1) Section SM 4.1. Sample location and collection strategy

The sedimentary succession of the Salt Range overlies the Precambrian crystalline basement of the Indian craton. It can be subdivided into three major units: 1) the Precambrian Salt Range Formation (SRF), 2) the Cambrian to Eocene siliciclastic, carbonate and evaporite and 3) the Miocene to Pliocene Molasse sequence. Twenty-eight samples were collected from similar stratigraphy in different sections along the strike of the Salt Range (Fig SM 4.1). The systematic sampling was conducted to observe variations in the cooling ages of the samples in different sections and to work out the thermal history of the basin.

The SRF is comprised of salt, gypsum and marl (Gee, 1980; Kazmi and Abbasi, 2008). The Paleozoic succession is comprised of Cambrian and Permian strata separated by

an Ordovician-Carboniferous unconformity (Kazmi and Abbasi, 2008; Gee, 1980; Shah, 1977). These strata are the Cambrian Jhelum group and the Permian Nilawahan and Zaluch groups (Fig. SM 4.1). The Jhelum group is comprised of the Khewra, Kussak, Juttana and Baghanwala formations. The main lithologies in these formations are sandstone interbedded with shale, claystone and dolostone. The group is well exposed in the Eastern Salt Range, pinches out toward the Central Salt Range and is absent in the Western Salt Range. The Tobra, Dandot, Warcha and Sardai formations form the Nilawahan Group. It is comprised entirely of clastic rocks, with a conglomeratic unit at the base overlain by thin to thick bedded sandstone, and siltstone interbedded with shale and clay. It is well exposed in the Eastern and Central Salt Range while in the western Salt Range only the conglomeratic unit (Tobra Formation) and the middle clastic sequence (Warcha Formation) unconformably overlie the SRF. The Upper Permian Zaluch group is a platform carbonate sequence comprised of the Amb, Wargal and Chiddru formations. It is well exposed at the surface in the Western and Central Salt Range; however, it is absent in the Eastern Salt Range (Kazmi and Abbasi, 2008; Gee, 1980; Shah, 1977). The samples were collected from all the formations except the SRF, Dandot, Sardai and Upper Permian formations because these lithologies do not contain detrital apatite.

The Mesozoic succession is comprised of the Mianwali, Tridian, Kingriali, Datta, Shinawri and Samanasuk formations. They contain shale, white sandstone (quartz arenite), dolostone and carbonate. The Mesozoic succession is best exposed in the west, lying unconformably over the Upper Permian strata. The Mesozoic succession thins towards the east and is absent in the Eastern Salt Range and Potwar. Five samples were collected from the Mesozoic sandstone (quartz arenite) exposed in the western Salt Range; unfortunately, no apatite was recovered.

The Paleocene Lockart and Patala formations are comprised of carbonate overlain by shale. In the Salt Range, the Eocene succession is comprised of the Nammal, Sakesar and Chorgali formations. The formations contain carbonates interbedded with shale; both are quite unlikely to yield apatite.

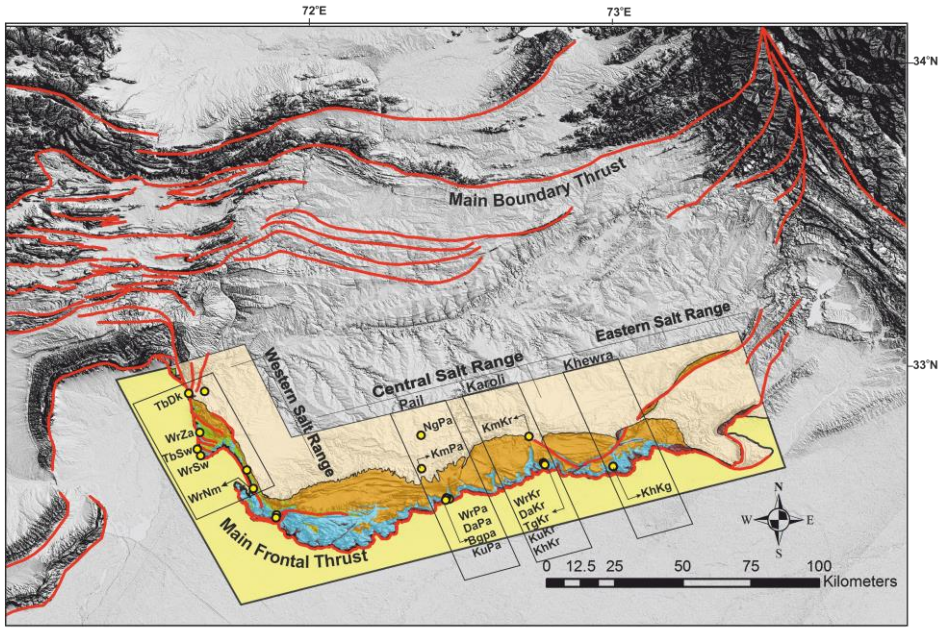

A)

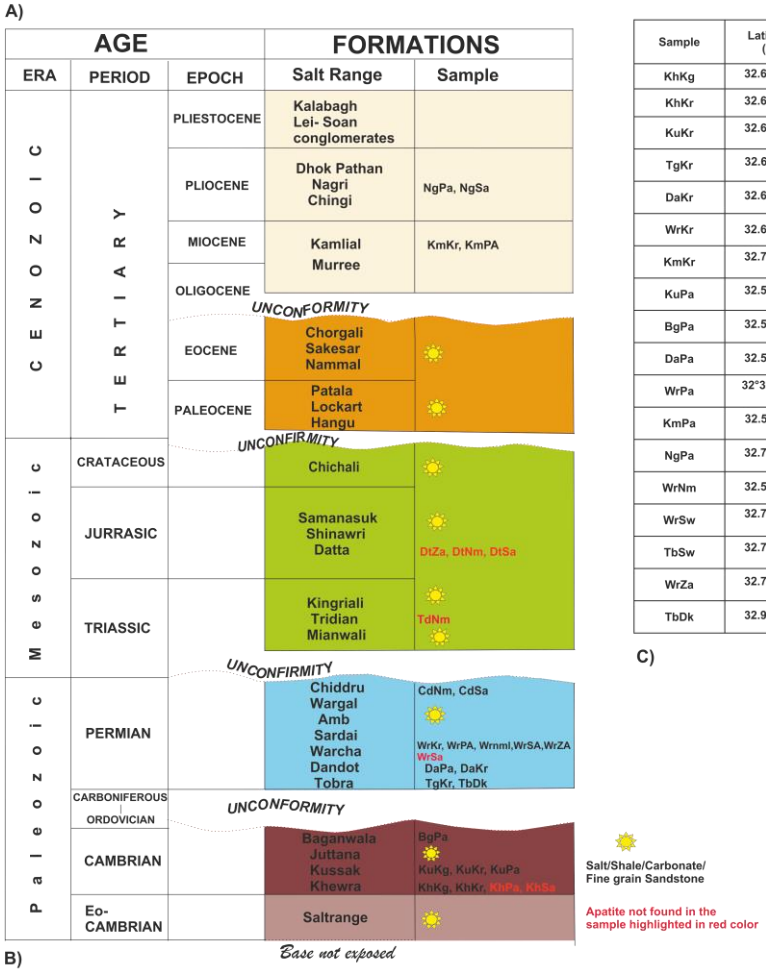

B)

Sample	Latitude (N)	Longitude (E)
KhKg	32.6680°N	73.005°E
KhKr	32.6747°N	72.7783°E
KuKr	32.6766°N	72.7766°E
TgKr	32.6769°E	72.7766°E
DaKr	32.6770°N	72.7766°E
WrKr	32.6808°N	72.7736°E
KmKr	32.7681°N	72.7261°E
KuPa	32.5612°N	72.4642°E
BgPa	32.5578°N	72.4518°E
DaPa	32.5586°N	72.4514°E
WrPa	32°33'54"N	72.4542°E
KmPa	32.565""N	72.3722°E
NgPa	32.7717°N	72.3708°E
WrNm	32.5972°N	71.8167°E
WrSw	32.7042°N	71.6431°E
TbSw	32.7258°N	71.6322°E
WrZa	32.7808°N	71.5406°E
TbDk	32.9097°N	71.6042°E

C)

Figure SM 4.1. *Map and generalised stratigraphic section of the Salt Range. a) Map with sample locations collected from different sections of the Salt Range b) Stratigraphic section of the Salt Range with samples names collected from specific stratigraphic formation. c) Sample location coordinates. Note that only the samples labelled on the map are used in this study; the relevant data is reported.*

The Molasse sequence is comprised of non-marine, syn-orogenic clastic sedimentary rocks. It is divided into two groups: the Miocene Rawalpindi group, comprised of the Murree and Kamlial formations and the Pliocene-Pleistocene Siwalik group, comprised of the Chingi, Nagri and Dhokpathan formations. The samples were collected from Kamlial and Nagri Formation in the Salt Range.

2) Section SM 4.2. Analytical methods

a) Mineral separation

The apatite is obtained from the samples using standard magnetic and heavy liquid separation techniques performed at the mineral separation lab of the University of Potsdam.

b) Apatite (U-Th-Sm)/He (AHe) methods and data analysis

Alpha decay from ^{235}U, ^{238}U, and ^{232}Th produces radiogenic ^{4}He in the apatite. The ^{4}He can completely diffuse out of the crystal at temperatures above 80-90 °C. The ^{4}He is partially retained within the crystal structure between temperatures 40-80 °C, this temperature interval is known as the Apatite partial retention zone (APRZ) (Farley 2000; Farley 2002). The measurement of parent (U-Th-Sm) nuclide and daughter (He) product can be used to calculate the time when the crystal passed through APRZ (Farley 2000).

The samples were analyzed under a binocular microscope to select inclusion and crack free, euhedral shaped apatite crystals, > 60 μm width. The best three to five grains were picked for analysis from the selected grains. The dimensions of the grains are measured under a binocular microscope. Each single grain is packed in a platinum tube for He extraction using an Alphachron at the thermochronology lab of University of Potsdam. The apatite grains are degassed by laser heating of the platinum tubes. Every aliquot is analyzed a second time to test for the presence of parentless He trapped in small inclusions. The ^{4}He abundance is measured with a quadruple mass spectrometer by comparison with ^{3}He spike during the analysis. The platinum tubes containing degassed apatite are dissolved in 5ml dilute nitric acid at 90 °C. The solution is used to measure the concentrations of U, Th and Sm through inductively coupled plasma mass spectrometry (ICP-MS) at German Research Centre for Geoscience (GFZ) Potsdam. The calculated single ages are corrected using alpha ejection (FT) correction (Ketcham et al 2011). The AHe ages are reported in the Table SM 4.1, the 1σ error on single grain ages is the sum of errors in the analytical measurements. Additional methodological details are provided in Zhou et al. (2017).

The AHe ages from the samples have a dispersion between 2 – 110 Ma (Table SM 4.1). The dispersion in AHe ages is widely reported in literature and many factors are invoked to explain this dispersion. The dispersion in AHe ages could be the result of variations in crystal size, which controls the diffusion of He through crystal. The larger size apatite crystals diffuse less He when cooling through APRZ, resulting in older ages for larger crystals compared to smaller crystals from the same sample (Reiners and Farley 2001). The other very important reason is radiation damage caused by the recoil of parent nuclides during alpha ejection, producing damage in the crystal. He is trapped in these sites, resulting in range of AHe ages. The radiation damage is reflected by the amount of effective uranium (eU= [U] + 0.235 [Th]) in the apatite crystal combined with the time since the sample was last exposed to a sufficiently high temperature to anneal the damage (Flowers et al., 2007; Flowers et al., 2009). Additional causes for age dispersion are presence of U- and Th-rich inclusions in apatite crystals (Vermeesch et al., 2007), He implantation by U- and Th-rich neighboring crystal in the host rock (Reiners et al., 2008), and U and Th zonation (Hourigan et al., 2005). The AHe ages for this study are plotted as a function of eU to check for possible positive correlations; however, our data suggest an inverse relationship: older ages to lower eU values and younger ages to higher eU values (Fig. SM 4.2). The older ages with less eU are not related to size but could be the result of a complex thermal history, uranium rich inclusion, He implantation from neighbor crystals, or uranium zoning in the crystal. More detailed analysis is required to explain the factors controlling these ages. The young AHe ages correlated with high (eU) are probably the result of annealing of radiation damage at higher temperature through burial (Flowers et al., 2009; Gautheron et al., 2009; Willett et al., 2017). The comparison of the radiation damage annealing model by Willet et al (2017) has shown that the models do not predict the older ages not positively correlated to eU. We have excluded the older ages with less eU in our models and modeled all of the remaining data.

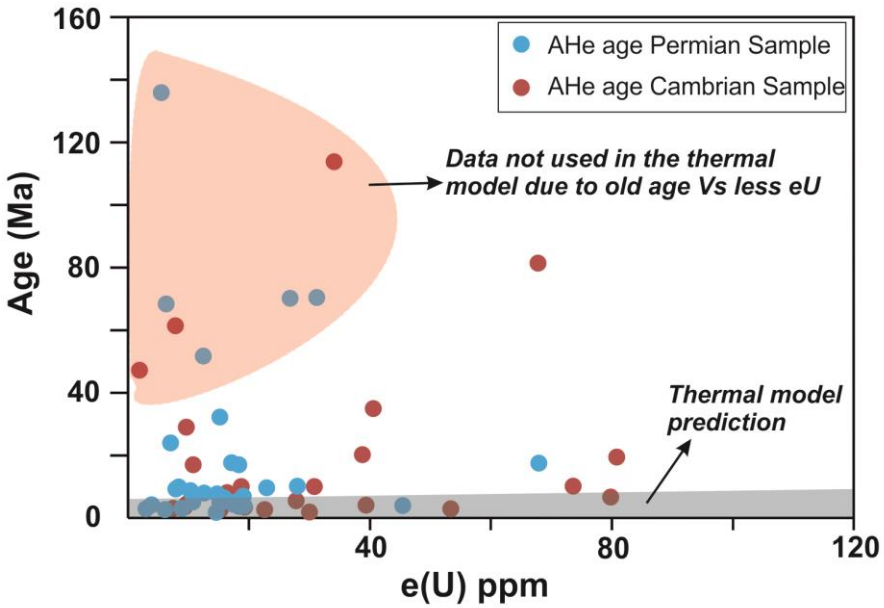

Figure SM 4.2. *AHe individual grain ages of the Cambrian and Permian samples as a function of effective Uranium (eU) content.*

c) AFT dating methods and data analysis

The spontaneous fission of ^{238}U damages the crystal lattice of apatite and zircon. These damage structures are known as fission tracks. The AFT dating method is based on counting these tracks to calculate cooling ages for the apatite. The initially formed tracks reduce their length in the process known as annealing; this occurs at temperatures between 60 to ~120°C known as the Apatite Partial Annealing Zone (APAZ). The track length distribution (TLD) and mean track length (MTL) are used to quantify the amount of annealing (Green et al., 1985). The process of annealing is dependent on temperature, fission tracks orientation relative to the crystallographic c-axis and annealing kinetic parameters (Cl, OH and Dpar). Dpar is the diameter of a fission track etch pit parallel to the c-axis. Dpar is used as a proxy for the annealing kinetics of a crystal; it quantify the resistance to annealing of fission tracks (Carlson et al., 1999; Donelick et al., 1999; Ketcham et al., 1999).

In this study we obtained fission track data from fifteen samples. The apatite grains were glued on glass slides with epoxy and then cut and polished to achieve the desired thickness. The grains were etched by placing slides in 5.5 M HNO_3 solution for 20 seconds at 21°C to reveal spontaneous fission tracks. The slides were covered with mica sheets as an external detector and sent for irradiation to either the Garching (Munich, Germany) or Oregon State University (USA) nuclear reactor for irradiation with thermal neutrons with a

fluence of 9 x 10^{15} neutrons/cm^2). The mica sheets (external detector) were etched by placing them in 40% HF solution at 21 °C for 45 minutes. The zeta value of 353 ± 7 (HG) is calculated by measuring age standards (Durango, Fish Canyon Tuff and Mount Dromadary samples) available in the Fission Track lab of the University of Potsdam. The AFT ages are calculated using the external detector method (Hurford and Green, 1982). AFT ages are reported as central ages with ± 1σ error (Galbraith and Laslett, 1996) for the samples that passed the chi squared test and population ages for the samples that failed the chi squared test (Fig. SM 4.3, Table SM 4.2). The track lengths are measured and recorded by digitizing the track ends using a drawing tube. The track lengths annealing properties are dependent on the orientation of tracks (Donelick, 1991) in the crystal, therefore the orientation of the C-axis is measured in every grain used for length measurements. The orientation of lengths with respect to the C-axis is helpful for track length correction and constraining annealing kinetics for thermal modeling (Ketcham et al., 2007). Four Dpar measurements are recorded on each grain used for age and track length determination; the average value of these measurements is reported in the data and used in thermal models to characterize the kinetic properties (Ketcham et al., 1999) (Fig. SM 4.3, Table SM 4.2). Dpar values were corrected following Sobel and Seward (2010).

The AFT data from fifteen samples show that only two samples passed the chi squared test. The dispersion in age could be representing different detrital source history or different compositional properties convolved with residence in the partial annealing zone. The two samples (TgKr and TbDk) that passed the chi-squared test yielded AFT cooling ages of 355 ± 15 and 3.7 ± 0.7, respectively (Fig. SM 4.3, Table SM 4.2). TgKr is a granite clast sampled from the basal conglomerate bed and TbDk is the structurally-deepest sample, located at the western end of the Salt Range

The age dispersion is a result of both source area history and kinetic characteristics. There are 4 main sources for Cambrian and Permian detrital sedimentary rocks exposed in the Salt Range today (part of northern Gondwana during the Cambrian- Permian). The Aravali-Dehli Orogen, located 500 km to the south-east of the Salt Range, is comprised of PreCambrian Indian shield rocks that supplied Cambrian sediments to northern India (Deb et al., 2001; McKenzie et al., 2011). 2) Diamictites at the base of the Permian were deposited by glacio-fluvial streams sourced from Gondwana glaciers containing sediments from the Indian Craton, located to the south (Ghazi and Moutney 2011, Garzanti 1996). 3) The fine sediments were derived from rift highland to the north (Pogue et al 1992a). 4) Sediment was derived

from an Arabian source area located to the west of India at that time (Stephenson et al., 2013).

The samples have a range of Dpar values between 1.1 to 3.5 μm (Fig. SM 4.3) within and between the samples. There is a positive trend between Dpar and age in all our samples, although there is some exception where small Dpar grains show older ages. The computer program Trackkey (Dunkl, 2002) is used to observe age distributions and decompose the ages into populations that pass the chi squared test (Fig. SM 4.3). The bigger grain population passing Chi squared test correlated with higher Dpar values between 1.8-3.0 μm. The measured track lengths in 11 samples range between 9 to 12.5 μm and the mean track length decreases towards the north of the Western Salt Range. The track lengths and older AFT age population show similar Dpar values in the range of 1.9 – 2.4 μm, showing that the age and lengths most probably represent the same populations (Fig. SM 4.3). The older ages are only reported in the paper and are used in the thermal modeling.

Khewra and Karoli Sections

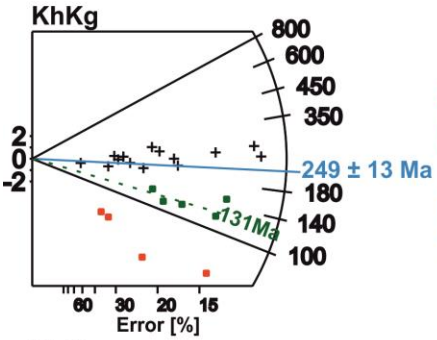

Depositional age
525 ± 25 Ma

AFT age (23 grains)
162 ± 20 Ma
P(χ^2) = 0

AFT age (14 grains)
249 ± 13 Ma
P(χ^2) = 98

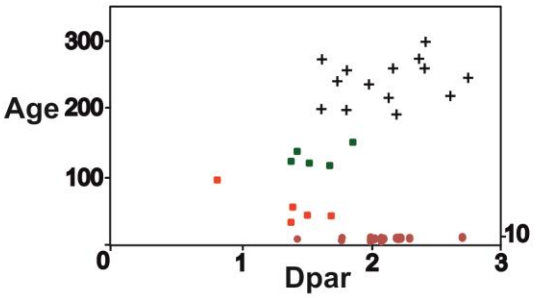

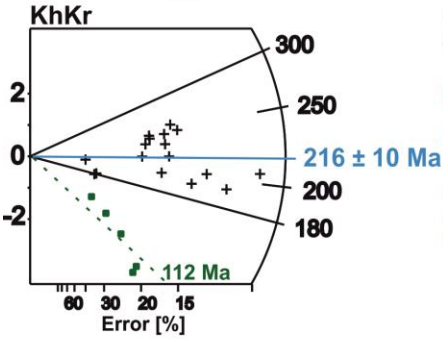

Depositional age
525 ± 25 Ma

AFT age (22 grains)
196 ± 12 Ma
P(χ^2) = 0.6

AFT age (17 grains)
216 ± 10 Ma
P(χ^2) = 98

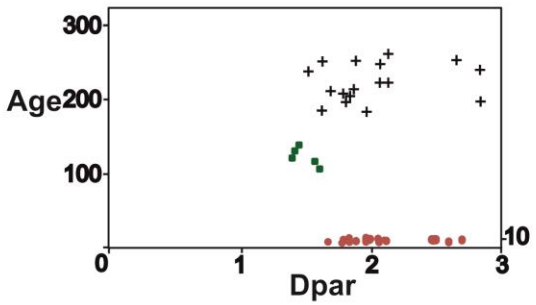

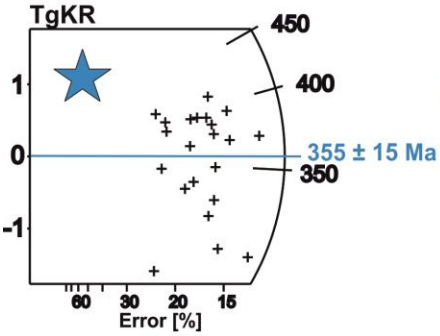

Depositional age
280 ± 12 Ma

AFT age (22 grains)
355 ± 15 Ma
P(χ^2) = 96

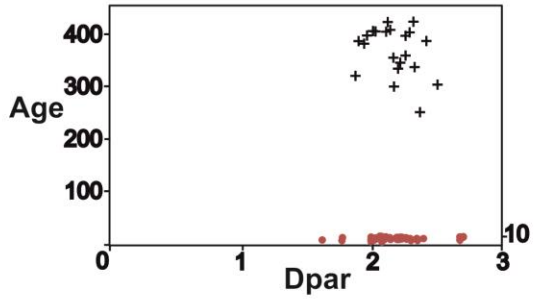

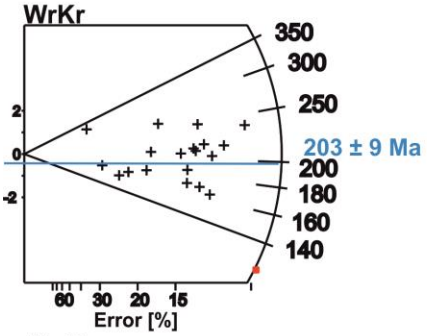

Depositional age
280 ± 20 Ma

AFT age (20 grains)
196 ± 10 Ma
P(χ^2) = 0.09

AFT age (19 grains)
355 ± 15 Ma
P(χ^2) = 42

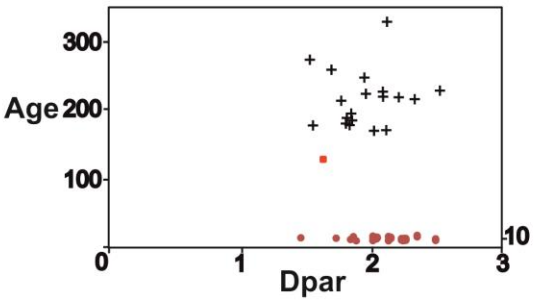

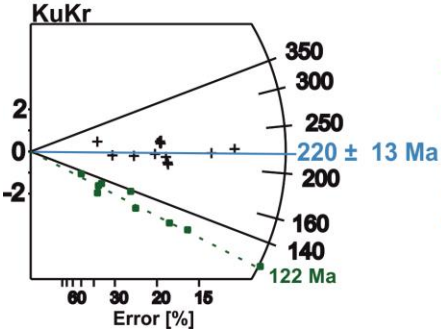

Depositional age
525 ± 25 Ma
AFT age (20 grains)
174± 13 Ma
P(χ^2) = 0.03

AFT age (11 grains)
355 ± 15 Ma
P(χ^2) = 99

+ *major population passing Chi sq test*
■ *minor population passing Chi sq test*
■ *population falling chi sq test*
● *Track Length Vs Dpar*
★ *Granite Clast*
P(χ^2) Probability percentage of Chi Sq value

Pail Section

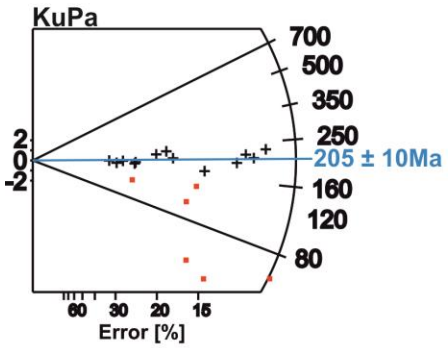

Depositional age
525 ± 25 Ma

AFT age (20 grains)
155 ± 18 Ma
P(χ^2) = 0

AFT age (14 grains)
205± 10 Ma
P(χ^2) = 90

+ *major population passing Chi sq test*
■ *minor population passing Chi sq test*
■ *population falling chi sq test*
● *Track Length Vs Dpar*
P(χ^2) Probability percentage of Chi Sq value

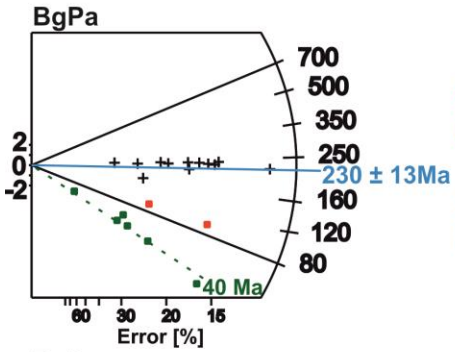

Depositional age
525 ± 25 Ma

AFT age (20 grains)
141± 21 Ma
P(χ^2) = 0

AFT age (12 grains)
230 ± 13 Ma
P(χ^2) = 99

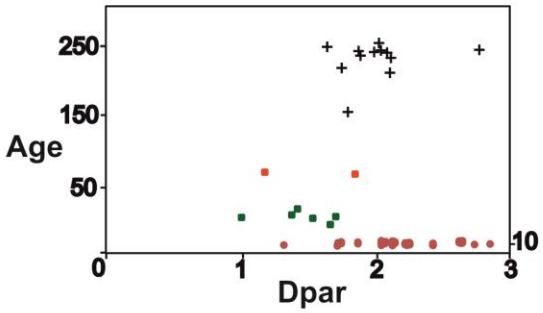

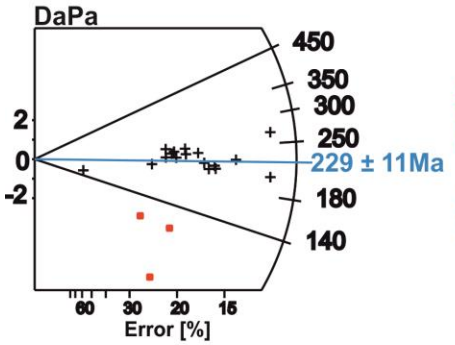

Depositional age
280 ± 20 Ma

AFT age (20 grains)
200 ± 16 Ma
P(χ^2) = 0

AFT age (17 grains)
229 ± 11 Ma
P(χ^2) = 99

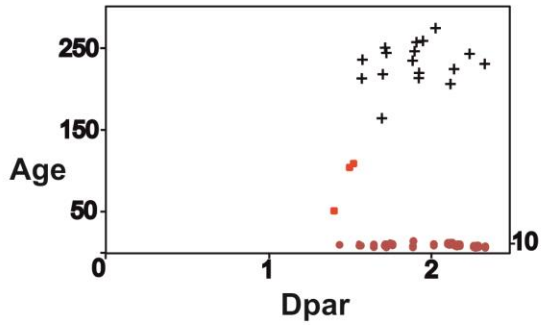

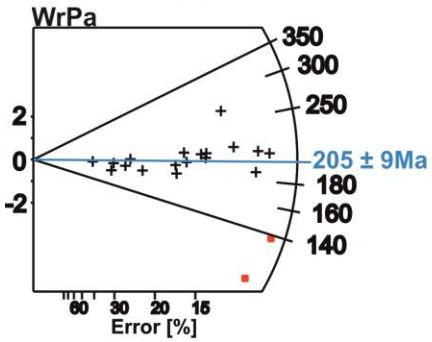

Depositional age
280 ± 20 Ma

AFT age (20 grains)
189 ± 11 Ma
P(χ^2) = 0.02

AFT age (18 grains)
205 ± 9 Ma
P(χ^2) = 98

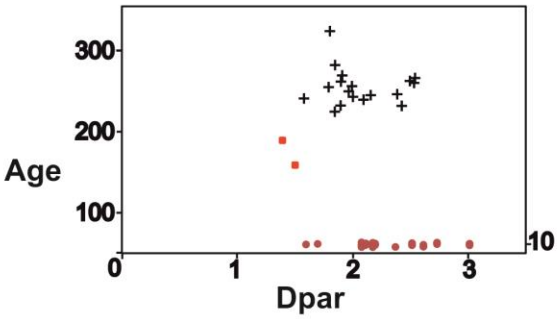

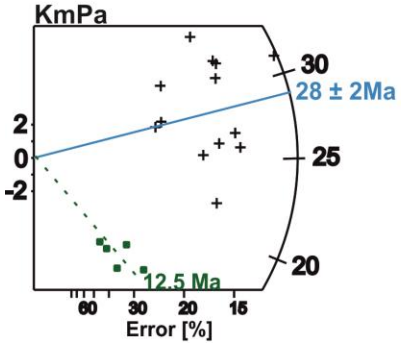

Depositional age
18 ± 2 Ma

AFT age (18 grains)
21 ± 2 Ma
Chi Sq = 0

AFT age (13 grains)
28 ± 2 Ma
P(χ^2) = 70

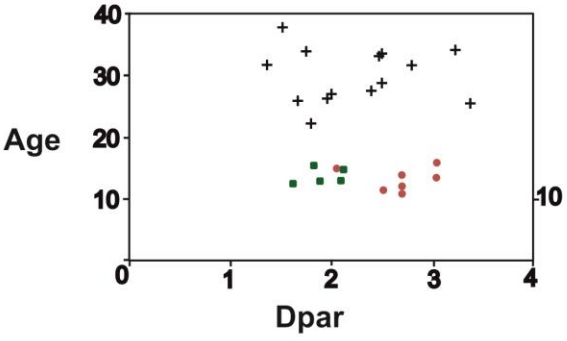

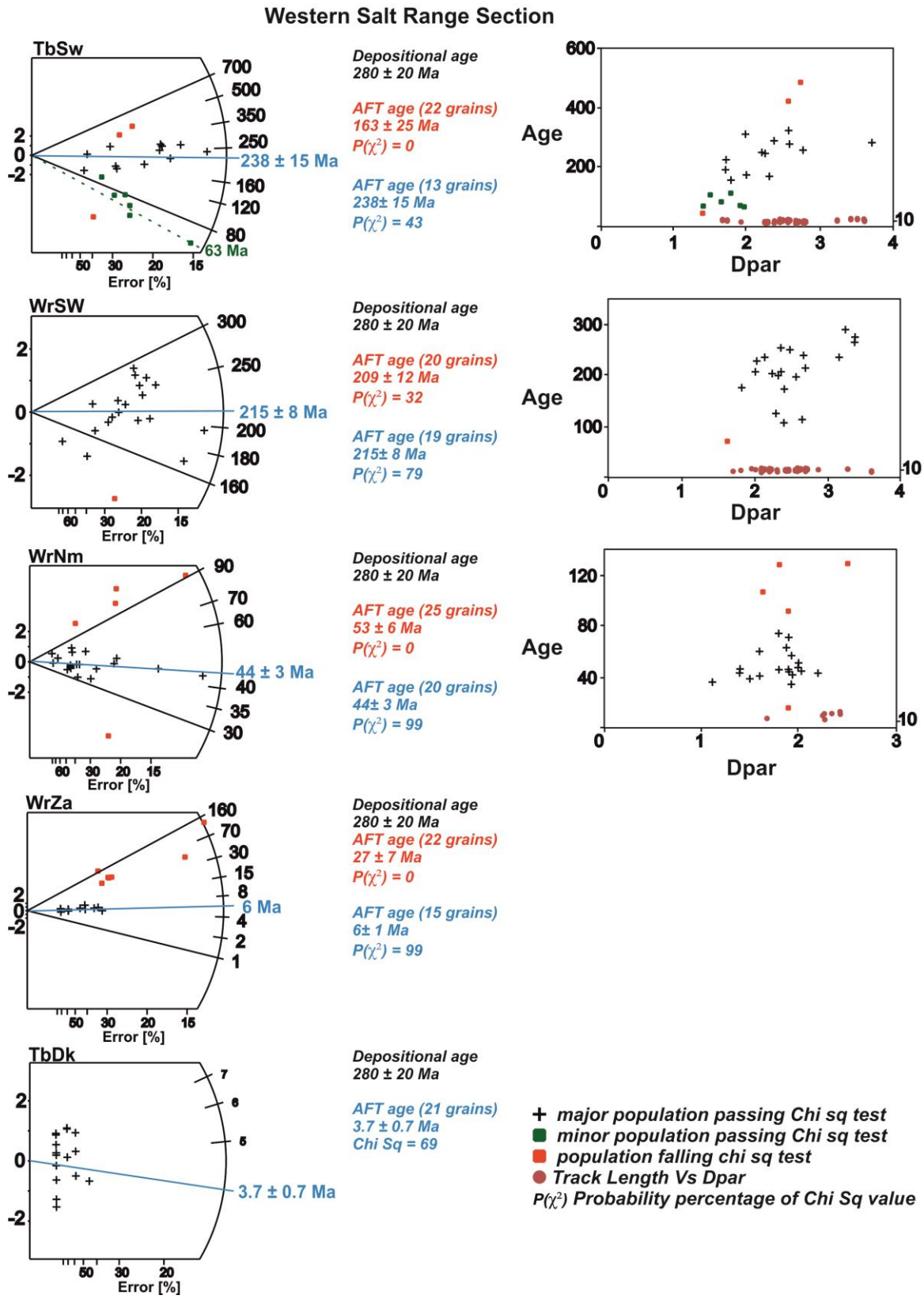

Figure SM 4.3. *AFT age radial plots, age and tracklengths as a function of Dpar plotted for samples. The ages passing chi squared test are labeled blue and green.*

3) Section SM 4.3. Thermal history modeling

Inverse thermal modeling was performed using the QTQt software, v. 5.7.0 (Gallagher, 2012), which uses a trans-dimensional Bayesian Monte Carlo Markov Chain (MCMC) statistical approach to find the best possible time – temperature thermal history path for the data. As an output of the modeling, we present the path with the highest likelihood (Max likelihood) and the averages of the best model (Expected path). The QTQt multiple-sample model allows inverting model large amounts of AFT and AHe data from samples collected in different structural positions, with different depositional ages, and with different detrital signatures. We used the kinetic model of He diffusion proposed by Gautheron et al. (2009) to model radiation damage effects and size controls in the apatite helium system. For AFT data, we used the annealing model of Ketcham et al. (2007).

We used two different modeling approaches. First, we performed individual models for each section; afterwards, we projected the samples into a single structural section (Figs. SM 4.4- 4.7). Single sample models are performed for a Cambrian sample from the Khewra section and for two different Permian samples from the Western Salt Range (Figs. SM 4.4 and 4.7). Single-section multiple sample models were performed for the Karoli and Pail sections, incorporating Cambrian and Permian samples (Figs. SM 4.5-4.6). The model was set to a time - temperature space of 500 ± 500 Ma and 75 ± 75 °C in the Khewra, Karoli and Pail sections. In the western Salt Range, the model was set to time – temperature space of 250 ± 250 Ma and 75 ± 75 °C. The larger space is set to allow different detrital thermal histories for Cambrian and Permian samples.

In the second approach, to reconcile the individual models, we have combined all Cambrian and Permian age samples from the Khewra, Karoli and Pail sections into a single thermal model (Fig. SM 4.8) based on strong stratigraphic and structural reasons to expect that these samples experienced the same thermal history. Our 3D structural model of the Salt Range (Ghani et al., 2018) shows that the strata is translated as a single thrust sheet above the frontal ramp. The Khewra, Karoli and Pail sections can be combined in the Central Salt Range (Figs. SM1) due to their common structural position at the leading edge of the MFT. There are no major faults between the sections, which have similar Cambrian and Permian thickness. We assume similar amount of burial beneath the Molasse (Fig. 4.2), which is justified by the overlapping AHe and AFT ages and track lengths (Tables SM 4.1, SM 4.2).

The geological constraints used in the models are based on the depositional ages and major unconformities in the Salt Range. The constraints include the depositional ages for Cambrian and Permian rocks: 500 – 550 Ma and 270 - 300 Ma respectively, the time when sample were near to the surface (15 ± 15 °C). The Permian depositional constraint is imposed on Cambrian samples by taking into account the 200 m thickness of Cambrian strata and the major unconformity between Cambrian and Permian strata. The major unconformity between the Permian and the Paleocene in the Eastern and Central Salt Range is constrained in the model at 55-60 Ma. The major unconformity between Eocene and Miocene strata formed by the onset of Molasse deposition in the Salt range at 15-18 Ma. It is assumed that samples were near to the surface (15 ± 15 °C) at the time of deposition and formation of unconformities. The Permian depositional constraint is only used in the models of the Western Salt Range (Fig. SM 4.7) because Cambrian strata is missing and Permian strata overlies the Precambrian SRF. The presence of Upper Permian carbonate and Mesozoic strata in the stratigraphic section shows that the Permian samples stayed in the subsurface during the deposition of Paleocene and Molasse strata. The thermal history of each sections is a product of 400,000 iterations after 150,000 initial burn-in iterations. The model likelihood chain, track length distribution and model predictions are provided with every section for detailed review.

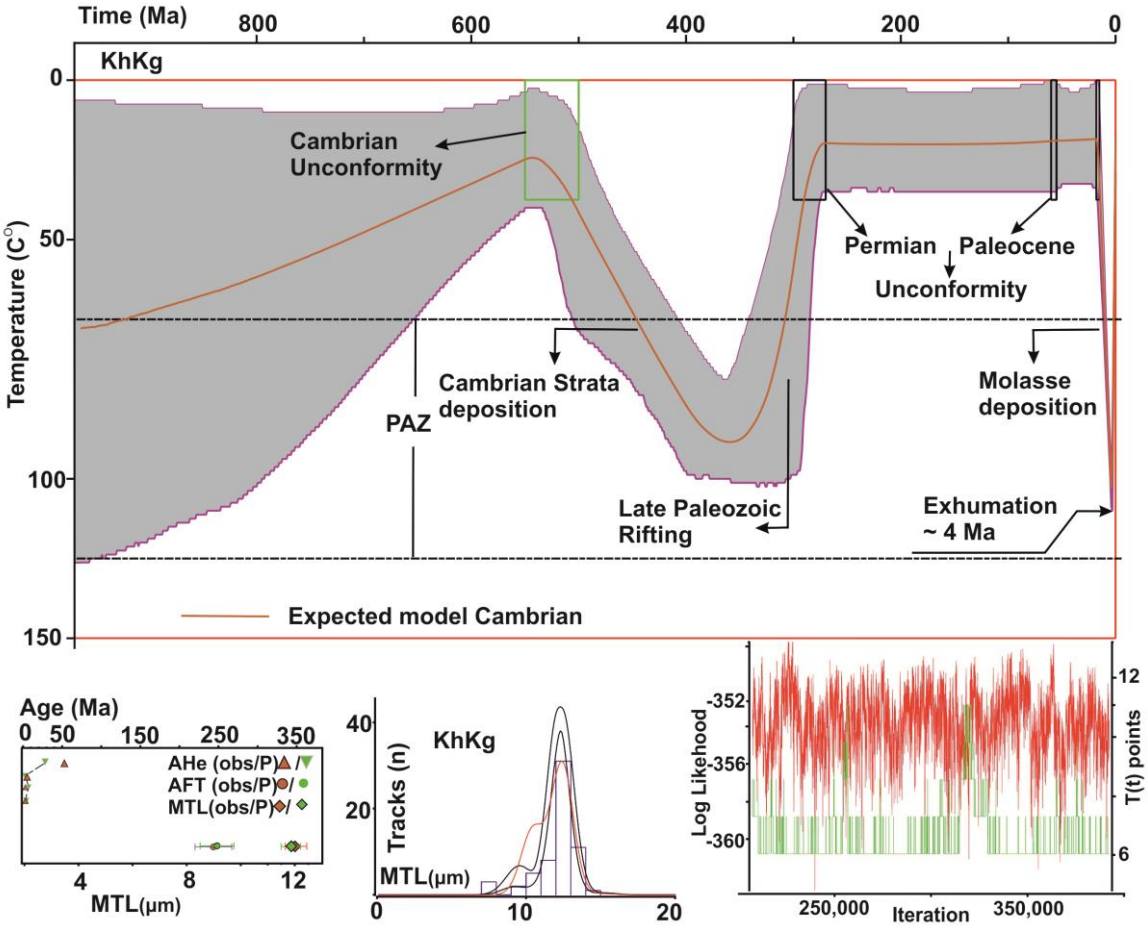

Figure SM 4.4. *Thermal history model of Khewra section sample. The thick brown line shows the expected thermal path of the sample. The green box shows the depositional constraint and black boxes show constraints related to major unconformities. The lower left plot shows the observed vs model predicted AHe, AFT ages and track lengths Lower middel: Track length distribution and model fit. Lower right: the likelihood chain for the model.*

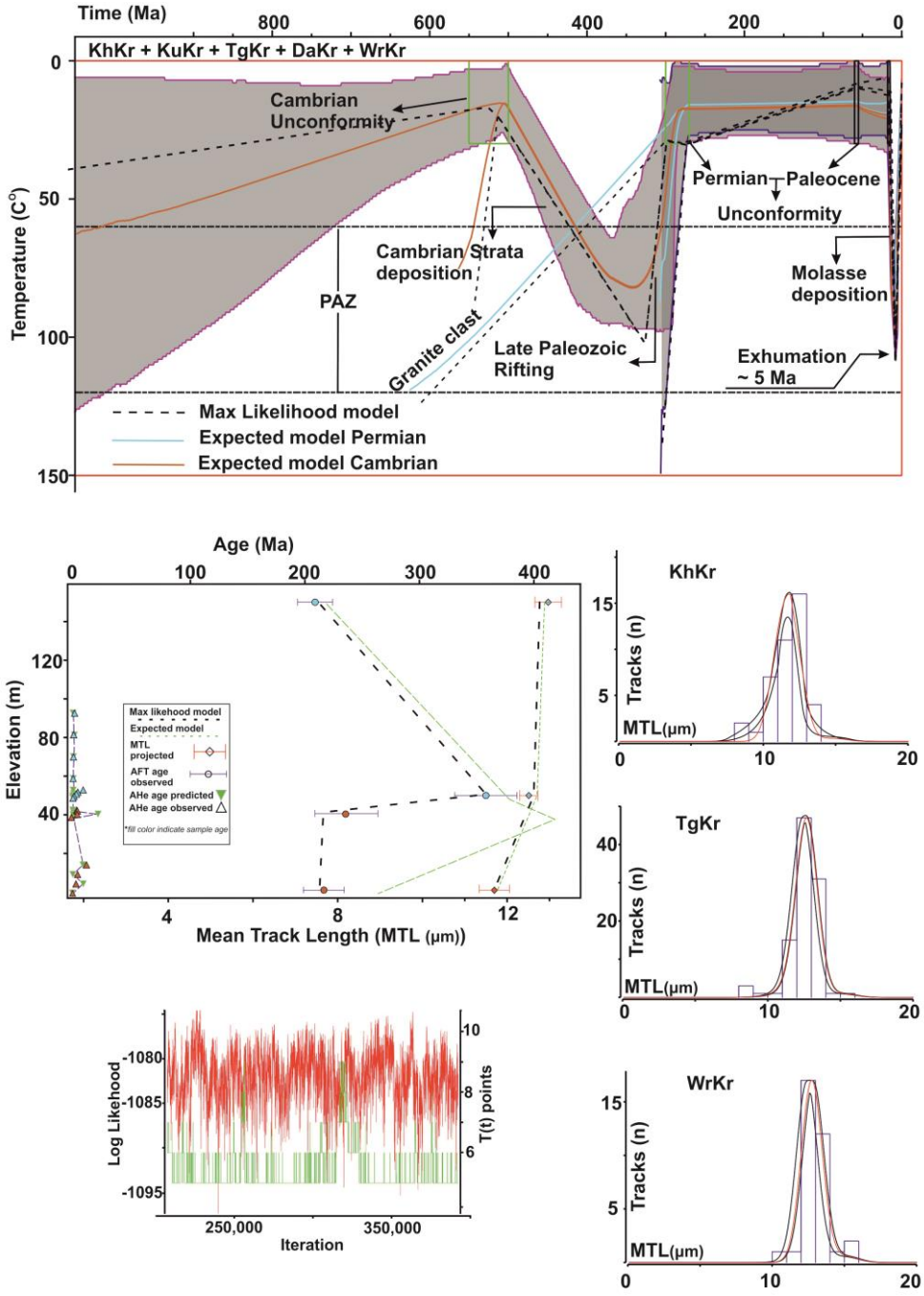

Figure SM 4.5. *Thermal history model and predictions for the Karoli section. Shaded area represents path probability and thick lines represent expected model for two Cambrian (brown lines) and two Permian (blue lines) samples. Thick dashed lines represent max likelihood model of the Cambrian and Permian samples. The green box shows depositional constraints and black boxes show constraints related to major unconformities. The middle left box show observed vs model predicted AHe, AFT ages and track lengths. The expected model predicts older ages for the Cambrian samples but Max likehood predicts the observed ages of Cambrian samples. Expected and max likelihood thermal models are reasonably similar following the deposition of samples. Middle to Lower right: Track length distribution and model fit. Bottom left: The likelihood chain for the model.*

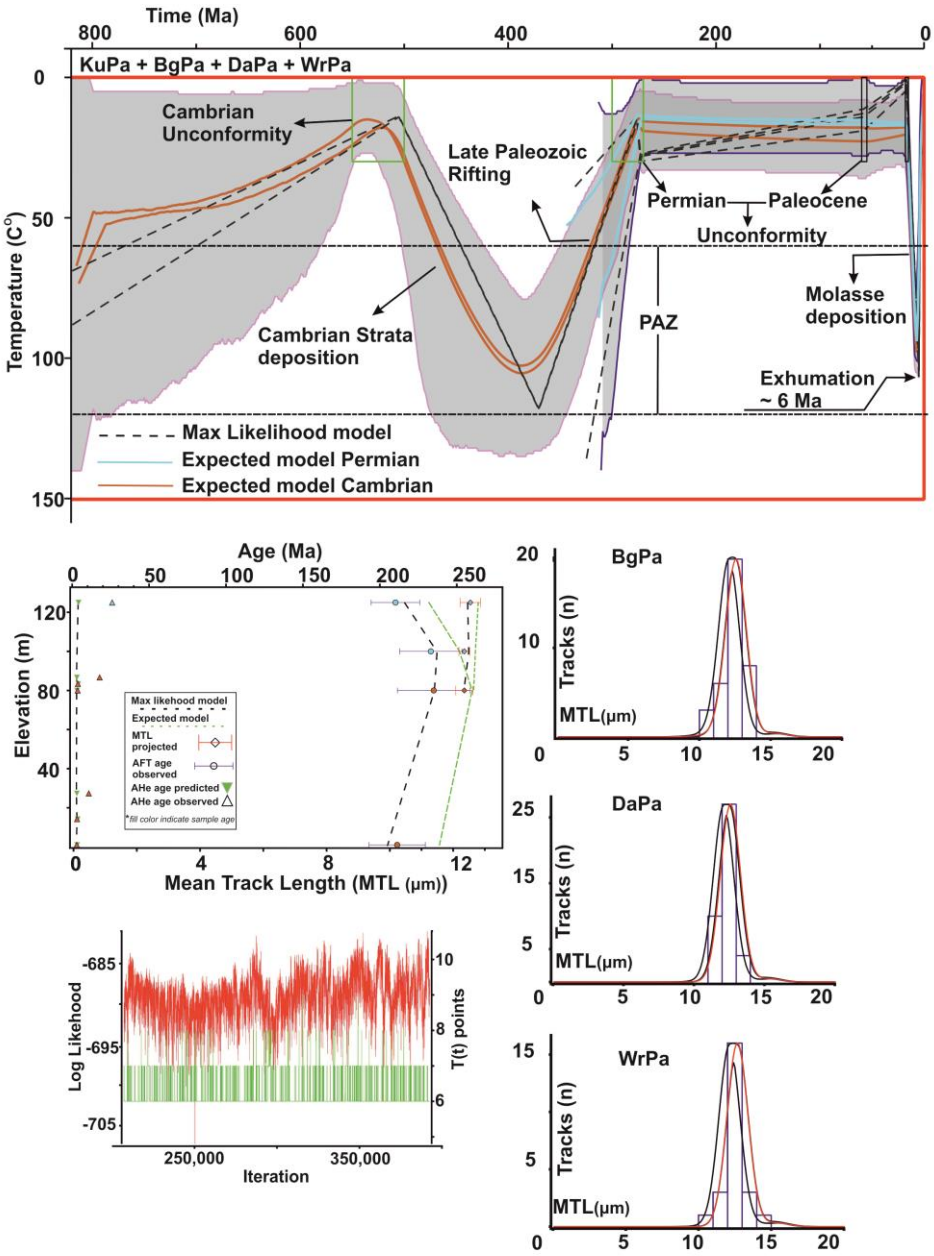

Figure SM 4.6. *Thermal history model and predictions for the Pail section. Shaded area represents path probability and thick lines represent expected model for two Cambrian (brown lines) and two Permian (blue lines) samples. Thick dashed lines represent max likelihood model for the Cambrian and Permian samples. The green box shows depositional constraints and black boxes show constraints related to major unconformities. The middle left box show observed vs model predicted AHe, AFT ages and track lengths. The expected model and max likehood model predicts similar ages for the samples. Middle to lower right: Track length distribution and model fit. Bottom Left: The likehood chain for the model.*

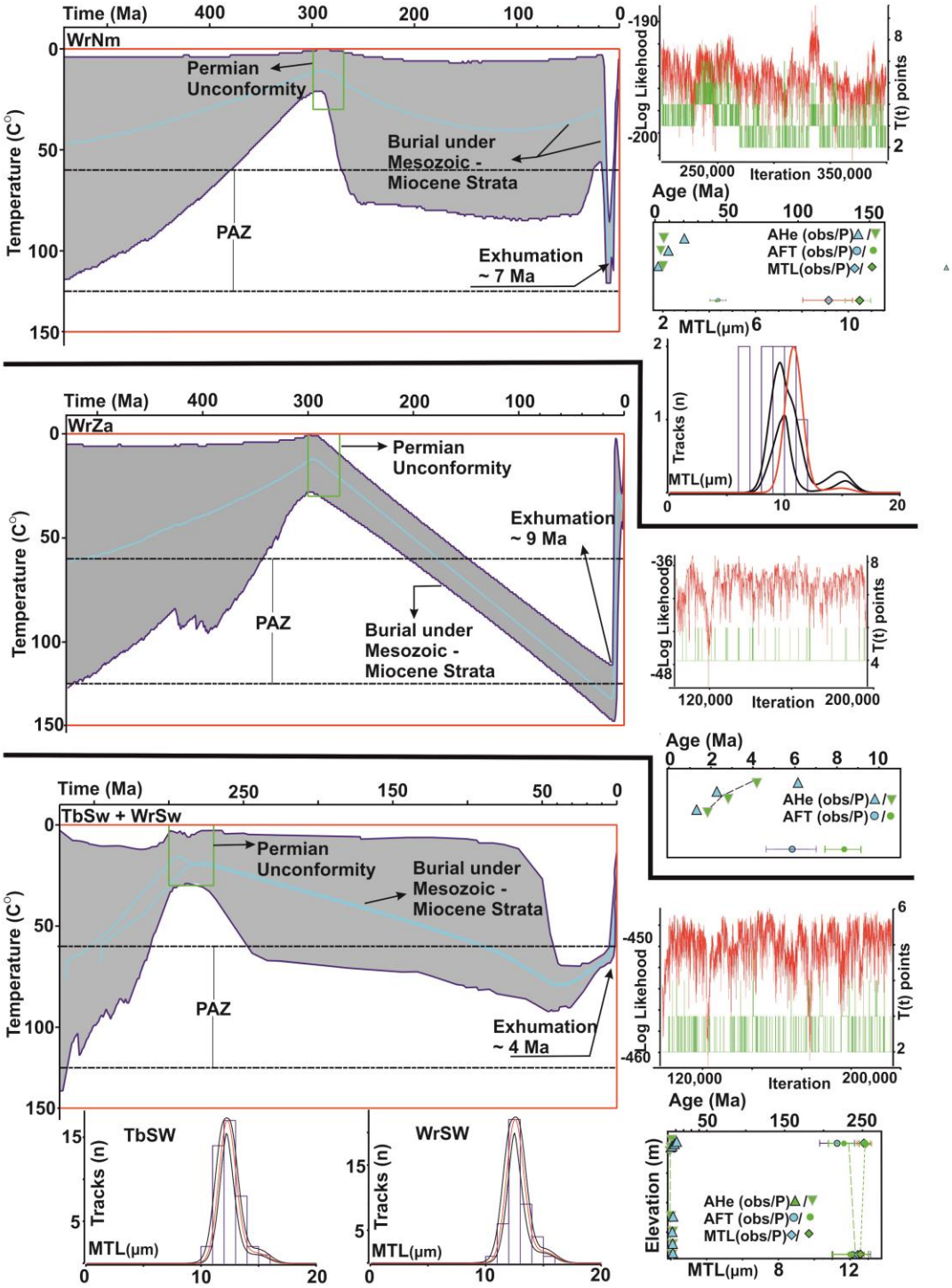

Figure SM 4.7. *Thermal history model and predictions for the Western Salt Range section. Shaded area represents path probability and thick lines represent expected model for Permian samples. The green box shows depositional constraints; other constraints are not used in these models. Model predictions, track length distribution and likelihood chain are presented on the sides of each model. Please use the scheme mention in the earlier figures SM 4.5 – 4.7.*

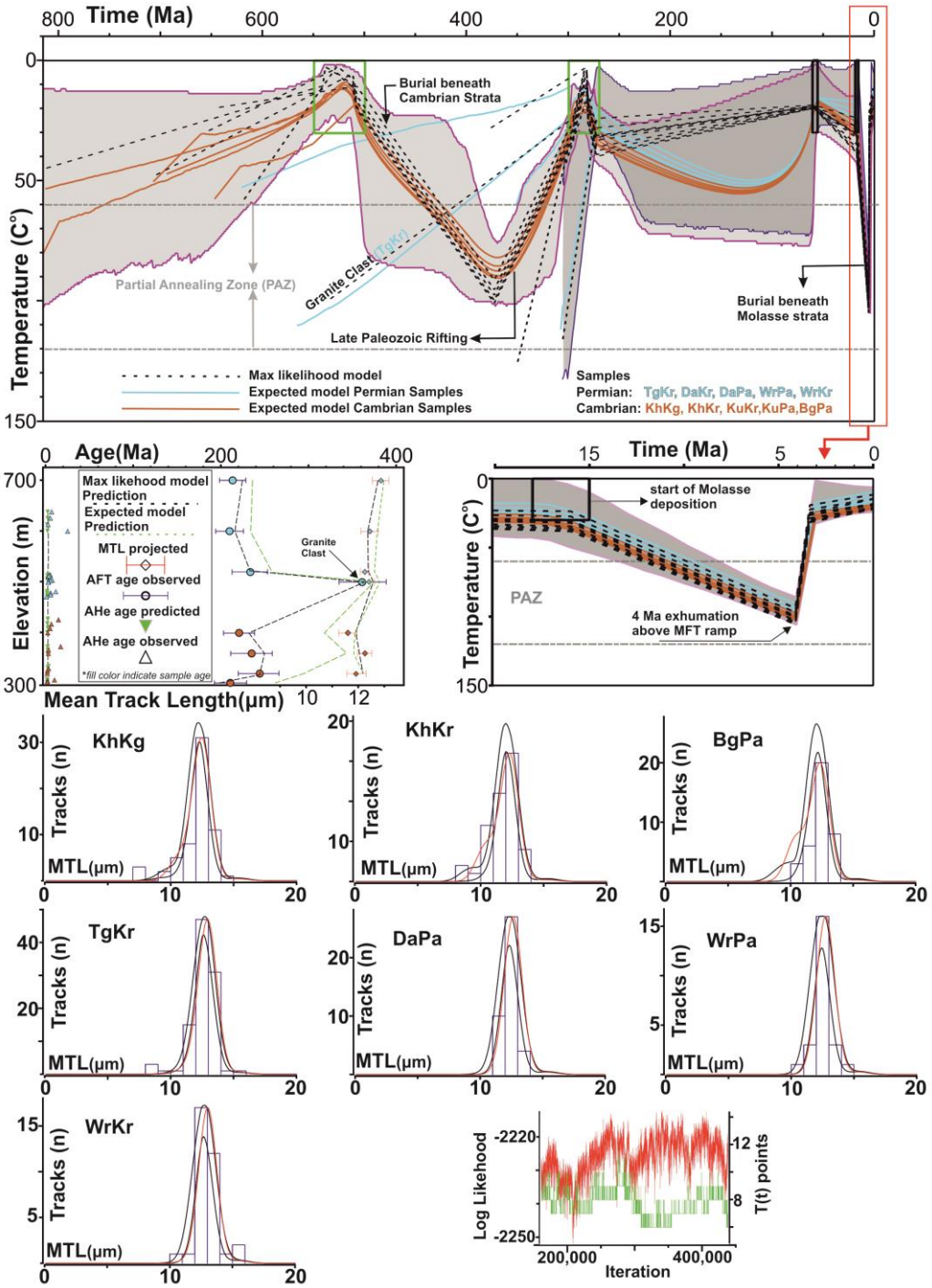

Figure SM 4.8. *Thermal history model and predictions for the combined Khewra, Karoli and Pail sections (model presented in the paper). Shaded area represents path probability and thick lines represent expected model for five Cambrian (brown lines) and five Permian (blue lines) samples. Thick dashed lines represents max likelihood model for the Cambrian and Permian samples. The green box shows depositional constraints and black boxes show constraints related to major unconformities. The middle left box show observed vs model predicted AHe, AFT ages and track lengths. Middle Right: Thermal model of last 25 Ma. Bottom: Track length distribution and model fit. Bottom Right: The likelihood chain for the model.*

Table SM 4.1. *Apatite (U-Th-Sm/He) data*

Sample	Ft corrected Age (Ma)	Weighted 2s analytic error (Ma)	U (ppm)	Th (ppm)	147Sm (ppm)	e[U]	Th/238U	He (nmol/g)	mass (ug)	Ft	ESR (mm)
Khewra Section											
KhKG_1	2.6	0.3	15.9	28.2	18.7	22.6	1.83	0.22	1.99	0.68	46
KhKG_2	5.5	0.6	18.5	39.3	60.7	27.8	2.19	0.47	0.86	0.56	34
KhKG_3	47.3	4.3	0.8	4.6	14.3	1.9	5.84	0.33	1.58	0.64	42
KhKG_4	2.6	0.6	6.5	37.3	25.7	15.3	5.94	0.13	1.19	0.61	38
KhKG_5	81.4	1.6	38.4	125.1	70.1	67.8	3.37	18.70	1.45	0.62	39
Karoli Section											
KhKr_1	19.4	0.4	71.7	38.6	21.1	80.8	0.56	6.13	3.31	0.72	54
KhKr_2	10.1	0.5	24.1	28.7	54.6	30.8	1.23	1.03	1.22	0.61	38
KhKr_3	3.4	0.8	3.6	24.3	18.0	9.3	7.06	0.11	1.58	0.64	42
KhKr_4	6.7	0.2	48.4	133.5	100.6	79.8	2.85	2.12	3.85	0.73	55
KhKr_5	34.9	0.8	25.5	64.2	39.2	40.5	2.60	5.51	2.93	0.71	52
KuKr_1	1.9	0.3	9.0	89.5	48.6	30.0	10.31	0.19	1.03	0.59	37
KuKr_2	20.3	1.1	13.0	109.5	73.7	38.7	8.71	2.37	0.74	0.55	33
KuKr_3	10.0	1.0	7.4	47.9	21.3	18.7	6.67	0.60	1.02	0.59	36
KuKr_4	10.2	0.3	48.1	108.3	12.8	73.6	2.33	2.33	0.95	0.57	35
TgKr_1	17.7	0.7	8.8	35.3	28.3	17.1	4.14	1.06	1.55	0.64	41
TgKr_2	4.9	0.8	6.9	35.4	37.2	15.2	5.31	0.24	0.96	0.57	35
TgKr_3	3.8	0.3	10.3	37.8	29.3	19.2	3.79	0.26	1.86	0.65	43
TgKr_4	9.3	0.3	4.2	15.9	18.3	7.9	3.95	0.30	4.23	0.74	58
TgKr_5	7.7	0.4	6.6	34.4	28.7	14.7	5.37	0.43	2.78	0.69	49
DaKr_1	5.5	0.4	11.6	18.6	9.4	15.9	1.66	0.33	2.49	0.69	48
DaKr_2	4.0	0.1	33.1	52.6	26.7	45.4	1.65	0.75	6.88	0.77	65
DaKr_3	2.9	0.5	1.7	5.4	12.1	3.0	3.27	0.04	5.51	0.76	62
DaKr_4	3.8	0.2	13.2	21.8	37.4	18.3	1.70	0.28	5.10	0.75	59
WrKr_1	70.4	1.5	20.9	44.1	34.0	31.2	2.18	8.15	2.50	0.68	47
WrKr_2	135.9	6.9	3.4	8.8	28.2	5.5	2.63	2.67	1.40	0.63	41
KmKr_1	2.4	0.1	9.7	49.8	11.6	21.5	5.28	0.22	6.10	0.77	65
KmKr_2	1.4	0.1	23.0	105.0	10.1	47.6	4.72	0.28	6.48	0.78	68
KmKr_3	2.2	0.1	13.4	63.8	18.8	28.4	4.93	0.28	12.71	0.82	83
Pail Section											
BgPa_1	0.8	0.1	121.6	156.8	78.2	158.4	1.33	0.41	1.39	0.62	40
BgPa_2	4.1	0.1	10.7	121.9	43.9	39.3	11.78	0.60	2.08	0.68	46
BgPa_3	29.0	2.1	2.5	30.4	24.5	9.6	12.58	0.88	0.83	0.56	34
BgPa_4	4.5	0.7	2.0	32.7	18.7	9.7	16.57	0.14	0.98	0.58	36
KuPa_1	3.1	0.6	5.4	8.8	17.6	7.4	1.68	0.09	2.26	0.69	48

KuPa_2	113.7	1.3	25.1	38.2	19.0	34.1	1.57	14.33	2.30	0.68	47
KuPa_3	3.4	0.7	11.3	34.0	17.9	19.3	3.12	0.21	0.98	0.58	36
KuPa-4	17.1	2.2	8.5	9.8	10.3	10.8	1.20	0.57	0.89	0.57	35
WrPa-2	32.2	1.1	8.2	29.8	87.0	15.2	3.76	2.05	4.37	0.74	58
WrPa-3	51.7	2.7	5.5	29.7	27.3	12.4	5.63	2.17	1.26	0.61	39
KmPa_1	2.3	0.3	4.0	12.5	20.4	6.9	3.24	0.07	5.98	0.76	63
KmPa_2	7.0	0.3	9.6	48.6	30.2	21.0	5.23	0.60	5.01	0.74	58
KmPa_3	2.0	0.2	4.1	11.5	10.4	6.8	2.92	0.06	7.95	0.79	71
KmPa_4	1.6	0.1	4.7	26.3	8.5	10.8	5.82	0.08	7.89	0.79	72
NgPa_1	25.3	0.9	8.0	24.3	23.8	13.7	3.14	1.32	2.40	0.69	49
NgPa_2	7.5	0.4	25.4	89.0	19.3	46.3	3.62	1.18	1.47	0.62	40
NgPa_3	11.4	0.3	22.7	81.6	8.8	41.9	3.71	1.88	3.79	0.73	55
NgPa_4	12.4	0.4	20.6	69.1	9.1	36.9	3.46	1.72	2.64	0.69	49
Western Salt Range											
WrNm_1	2.6	0.2	1.1	21.2	18.3	6.1	19.94	0.07	14.52	0.83	89
WrNm_2	68.3	3.0	0.7	24.0	17.3	6.3	37.32	1.48	1.29	0.62	39
WrNm_3	9.9	0.8	3.9	19.1	8.3	8.4	5.10	0.33	3.10	0.72	54
WrNm_4	24.0	1.1	3.3	16.1	33.8	7.0	5.10	0.79	16.35	0.84	92
WrSw_1	9.6	0.6	3.5	82.8	27.1	22.9	24.67	0.92	5.54	0.77	65
WrSw_2	17.5	0.6	58.7	39.3	40.1	67.9	0.69	3.66	1.01	0.57	35
WrSw_3	5.1	1.2	12.4	23.5	18.9	17.9	1.97	0.27	0.83	0.55	33
WrSw_4	8.0	0.5	8.4	17.8	8.9	12.6	2.19	0.41	4.48	0.75	61
TbSw_1	10.1	1.3	14.8	56.1	11.4	28.0	3.92	0.85	0.80	0.56	34
TbSw_2	6.4	1.1	8.1	32.8	21.4	15.8	4.19	0.34	1.24	0.62	39
TbSw_3	4.3	1.0	3.5	1.6	11.0	3.9	0.48	0.07	3.75	0.73	56
TbSw_4	4.3	0.6	4.7	54.2	13.8	17.4	11.89	0.26	1.62	0.64	42
TbSw_5	70.1	2.8	19.9	29.3	28.4	26.8	1.52	7.32	2.95	0.71	52
WrZa_1	3.0	0.3	5.0	16.9	34.0	8.9	3.5	0.1	7.92	0.79	72
WrZa_2	1.7	0.3	2.4	51.9	20.3	14.6	22.63	0.10	3.70	0.74	57
WrZA_3	7.0	0.3	7.8	48.1	28.9	19.1	6.4	0.6	24.91	0.86	107
TbDk_1	8.8	1.3	6.5	16.0	16.0	10.3	2.55	0.31	1.36	0.63	41
TbDk_2	5.2	0.5	6.5	17.8	14.5	10.7	2.84	0.22	4.21	0.74	58
TbDk_4	17.0	0.4	17.0	5.4	19.1	18.3	0.33	1.40	13.54	0.82	85

*Ages are reported as single grain cooling ages. Ages highlighted in red are not used in the thermal models because of negative Age Vs eU correlation.

Table SM 4.2. *Apatite fission track data*

Sample	(n)	Ns	ρs	Ni	ρi	N d	ρd	P (χ2) %	Age ± 1σ	Populations Age± 1σ (n)	P (χ2) %	No. of tracks (N)	MTL ± 1σ (µm)	STD (µm)	Dpar (µm)	STD (µm)
KhKg	23	1287	17.1	1839	24.5	8035	13.0	0	162 ± 20	249 ± 13 (14)	98	61	9.78	1.5	2.14	0.24
										131 ± 10 (5)	69					
KhKr	22	1425	12.0	1611	13.6	8035	13.0	0.6	196 ± 12	216 ± 10 (17)	98	41	9	1.57	2.2	0.33
										112 ± 13 (5)	90					
KuKr	20	936	14.3	1257	19.2	8035	13.3	0.03	174 ± 13	220 ± 13 (11)	99					
										122 ± 9 (9)	99					
TgKr	22	2021	11.6	1230	7.4	8035	13.1	96	355 ± 15			100	10.59	1.35	2.06	0.21
WrKr	20	1884	15.7	2225	18.6	8035	13.1	0.09	196 ± 10	203 ± 9 (19)	42	34	11	1.5	2.12	0.26
KuPa	20	1443	17.3	2499	30.0	8035	13.1	0	155 ± 18	205 ± 10 (14)	90					
BgPa	20	1033	13.4	1660	21.5	8035	13.0	0	141 ± 21	230. ± 13 (12)	99	37	9.9	1.3	2.25	0.35
										40 ± 4 (6)	83					
DaPa	20	1210	15.9	1327	17.4	8035	13.0	0	200 ± 16	229 ± 11 (17)	99	41	9.5	1.4	1.96	0.24
WrPa	20	1720	14.7	2115	18.1	8035	13.1	0.02	189 ± 11	205 ± 9 (18)	98	24	10.3	1.1	2.33	0.36
KmPa	18	453	2.8	4726	29.1	8035	13.1	0	21 ± 2	28 ± 2 (13)	70	13	12.81	1.5	2.63	0.29
										12 ± 5 (5)	98					
WrNm	25	541	3.8	2384	16.9	7720	12.6	0	53 ± 6	44 ± 3 (20)	99	9	9.1	1.5	2.24	0.22
TbSw	22	903	12.7	1231	17.3	7720	12.6	0	163 ± 25	238 ± 15 (13)	43	44	9.8	1.9	2.54	0.54
										63 ± 6 (7)	47					
WrSw	20	850	9.6	886	10.0	7720	12.6	32	209 ± 12	215 ± 8 (19)	79	43	10.6	1.4	2.57	0.45
WrZa	22	298	2.3	2876	22.4	7720	12.5	0	27 ± 7	6 ± 1 (15)	99	1	7.36			
TbDK	21	29	0.3	1758	19.4	7720	12.6	69	3.7 ± 0.7							

Notations

(n) = Number of grains

Ns: Number of spontaneous tracks

ρs: Spontaneous track density ρs x 10^5 (track/cm2)

ρi: Induced track density ρi x 10^5 (track/cm2)

Nd: Number of tracks counted in dosimetry glass CN5

ρd: Dosimetry track density ρd x 10^5 (track/cm2)

P(χ^2) %: Probability percentage of Chi square value

MTL: Mean Track Length

STD: Standard Deviation

Dpar: Diameter of etch pits parallel to C-axis of the crystal

*Ages are calculated with Zeta (ζ) value = 353 ± 7 (HG). The ages are divided into population passing Chi square test. The Central ages highlighted in blue are used for modeling and reporting in this paper.

4) References

Burtner, R.L., Nigrini, A., Donelick, and R.A. (1994). Thermochronology of lower Cretaceous source rocks in the Idaho-Wyoming thrust belt. American Association of Petroleum Geologist Bulletin, 78, 1613 - 1636.

Carlson, W. D., R. A. Donelick, and R. A. Ketcham. (1999). Variability of apatite fission-track annealing kinetics: I. Experimental results. American Mineralogist, 84, 1213–1223.

Deb, M., Thorpe, R.R.I., Krstic, D.M., Corfu, F., and Davis, D.W. (2001). Zircon U–Pb and galena Pb isotope evidence for an approximate 1.0 Ga terrane constituting the western margin of the Aravalli-Delhi orogenic belt, northwestern India. Precambrian Research, 108, 195–213.

Donelick, R. A. (1991). Crystallographic orientation dependence of mean etchable fission track length in apatite: an empirical model and experimental observations. American Mineralogist,76, 83–91.

Donelick, R. A., R. A. Ketcham, and W. D. Carlson. (1999). Variability of apatite fission-track annealing kinetics: II. Crystallographic orientation effects. American Mineralogist, v. 84, 1224–1234.

Dunkl, I. (2002). Track Key: a window program for calculation and graphical presentation of fission track data. Computer and Geosciences, 28, 3-12.

Farley, K. A. (2000). Helium diffusion from apatite; general behavior as illustrated by Durango fluorapatite. Journal of Geophysical Research, 105, 2903–2914.

Farley, K. A. (2002). (U-Th)/ He dating; techniques, calibrations, and applications, *in* D. Porcelli, C. J. Ballentine, and R. Wieler, eds., Noble gases in geochemistry and cosmochemistry. Reviews in Mineralogy and Cosmochemistry, v. 47, 819–843.

Flowers, R. M., D. L. Shuster, B. P. Wernicke, and K. A. Farley, 2007, Radiation damage control on apatite (U-Th)/He dates from the Grand Canyon region, Colorado Plateau: Geology, v. 35, p. 447–450.

Flowers, R. M. (2009). Exploiting radiation damage control on apatite (U-Th)/He dates in cratonic regions. Earth and Planetary Science Letters, 277, 148–155.

Galbraith, R.F., and Laslett, G.M. (1996). Statistical modelling of thermal annealing of fission tracks in apatite. Geochim. Cosmochim. Acta, 60, 5117-5131.

Gallagher, K. (2012) Transdimensional inverse thermal history modeling for quantitative thermochronology. Journal Geophysical Research, Solid Earth, 117 (B2), B02408.

Gautheron, C., L. Tassan-Got, J. Barbarand, and M. Pagel (2009). Effect of alpha-damage annealing on apatite (U-Th)/He thermochronology. Chemical Geology, 266, 166–179.

Gee, E.R. (1980). Salt Range Series Geological Maps: Directorate of Overseas Surveys,United Kingdom, Government of Pakistan and Pakistan Geological Survey, Scale 1:50,000, 6 Sheets.

Ghani, H., Zeilinger, G., Sobel, E.R., and Heidarzadeh, G. (2018). Structural variation within the Himalayan fold and thrust belt: A case study from the Kohat-Potwar fold thrust belt of Pakistan. Journal of Structural Geology, 116, 34-46.

Ghazi, S., and Mountney, N.P. (2011). Petrography and Provenance of the Early Permian Warcha Sandstone, Salt Range, Pakistan. Sedimentary Geology, 233, 88-110.

Grazanti, E., Angiolini, L., and Sciunnach, D. (1996). The Mid-Carboniferous to Lowermost Permian succession of Spiti (Po Group and Ganmachidam Formation; Tethys Himalaya, Northern India): Gondwana glaciation and rifting of Neo-Tethys. Geodinamica Acta (Paris), 9, 78-100.

Hurford, A.J., and Green, P.F. (1982). A users' guide to fission track dating calibration. Earth and Planetary Science Letters, 59, 343-354.

Hourigan, J. K., P. W. Reiners, and M. T. Brandon. (2005). U-Th zonation-dependent alpha-ejection in (U-Th)/He chronometry. Geochimica et Cosmochimica Acta, 69, 3349–3365.

Kazmi, A.H., and Abbasi, I.A. (2008). Stratigraphy and Historical Geology of Pakistan. National Centre of Excellence in Geology, University of Peshawar, Pakistan.

Ketcham, R. A., R. A. Donelick, and W. D. Carlson. (1999). Variability of apatite fission-track annealing kinetics; III. Extrapolation to geological time scales. American Mineralogist, 84, 1235–1255.

Ketcham, R.A., Carter, A., Donelick, R.A., Barbarand, J., and Hurford, A.J. (2007). Improved modeling of fission-track annealing in apatite. American Mineralogist, 92, 799–810.

Laslett, G.M., Gleadow, A., and Duddy, I.R. (1994). The relationship between fission-track length and track density in apatite. Nuclear Tracks, 9, 29-38.

McKenzie, N.R., Hughes, N.C., Myrow, P.M., Xiao, S., and Sharma, M. (2011). Correlation of Precambrian Cambrian sedimentary successions across northern India and the utility of isotopic signatures of Himalayan lithotectonic zones. Earth and Planetary Science Letters, 312, 471–483.

Pogue, K.R., Wardlaw, B.R., Harris, A. G., and Hussain, A. (1992a). Paleozoic and Mesozoic stratigraphy of the Peshawar basin, Pakistan: correlations and implications. Geological Society of America Bulletin, 104, 915-927.

Reiners, P. W., and K. A. Farley. (2001). Influence of crystal size on apatite (U-Th)/He thermochronology: an example from the Bighorn Mountains, Wyoming. Earth and Planetary Science Letters, 188, 413–420.

Reiners, P. W., S. N. Thompson, B. J. Tipple, S. L. Peyton, J. M. Rahl, and A. Mulch. (2008). Secondary weathering phases and apatite (U-Th)/He ages. Geochimica et Cosmochimica Acta, 72, A784.

Shah, S.M. (1977). Stratigraphy of Pakistan. In: Geological Survey of Pakistan Memoir 12.

Stephenson, M.H., Jan, I.U., and Al-Mashaikie, S.Z.A.K. (2013). Palynology and correlation of Pennsylvanian glacigene rocks in Oman, Yemen and Pakistan. Gondwana Research, 24, 203-211.

Sobel., E.R. and Seward, D. (2010). Influence of etching conditions on apatite fission-track etch pit diameter. Chemical Geology, 271, 59-69.

Vermeesch, P., D. Seward, C. Latkoczy, M. Wipf, D. Guenther, and H. Baur (2007). Alpha-emitting mineral inclusions in apatite, their effect on (U-Th)/He ages, and how to reduce it. Geochimica et Cosmochimica Acta, 71, 1737–1746.

Willett, C.D., Fox, M., and Shuster, D.L. (2017). A helium-based model for the effects of radiation damage annealing on helium diffusion kinetics in apatite. Earth and Planetary Science Letters, 477, 195-204.

Zhou, R., Schoennohm, L. M., Sobel, E. R., Davis, D. W., and Glodny, J. (2017). New constraints on orogenic models of the southern Central Andean Plateau: Cenozoic basin evolution and bedrock exhumation: Geological Society of America Bulletin,129, no. 1/2, 152–170.

Appendix 2 (Chapter 5)

Supplementary material for Chapter 5 **"Structural evolution of the Kohat fold and thrust belt of Pakistan"**

1) **Section SM 5.1.** Sample locations and characteristics

   Table SM 5.1.1. Geographic location of the samples.

   Figure SM 5.1.1. Generalized stratigraphic column of the Kohat and Trans Indus Ranges. Stratigraphic position of the samples used in the study (modified after Meissner et al., (1974); Pivnik and Wells, (1996)).

2) **Section SM 5.2.** Low temperature thermochronology data

   Figure SM 5.2.1. a) AHe age as a function of effective U (eU), b) AHe age versus FT.

   Table SM 5.2.1. Apatite (U-Th-Sm)/He data.

   Table SM 5.2.2. Apatite Fission Track (AFT) data.

   Table SM 5.2.3. Thermal modeling input parameters

1) Section SM 5.1. Sample locations and characteristics

The sedimentary succession of the Kohat and Trans Indus Ranges range from Cambrian to Pliocene age. Thirteen sandstone samples were collected were collected from the hanging wall of major thrusts are shown in the figure SM 5.1.1.

Table SM5.1.1. *Geographic location of the samples*

Sample	Latitude	Longitude
MrdK	33°45'21.97"N	71°29'29.34"E
PleK	33°38'20.08"N	71°28'42.73"E
MrfK	33°37'20.18"N	71°27'35.89"E
KllK	33°26'46.53"N	71°21'49.09"E
KmsH	33°15'19.63"N	71°29'45.26"E
ShkK	33°15'16.13"N	71°31'1.68"E
NgsK	33°13'55.21"N	71°32'19.33"E
ChnK	33° 4'30.64"N	71°32'55.34"E
SncH	33° 0'8.92"N	71°24'17.99"E

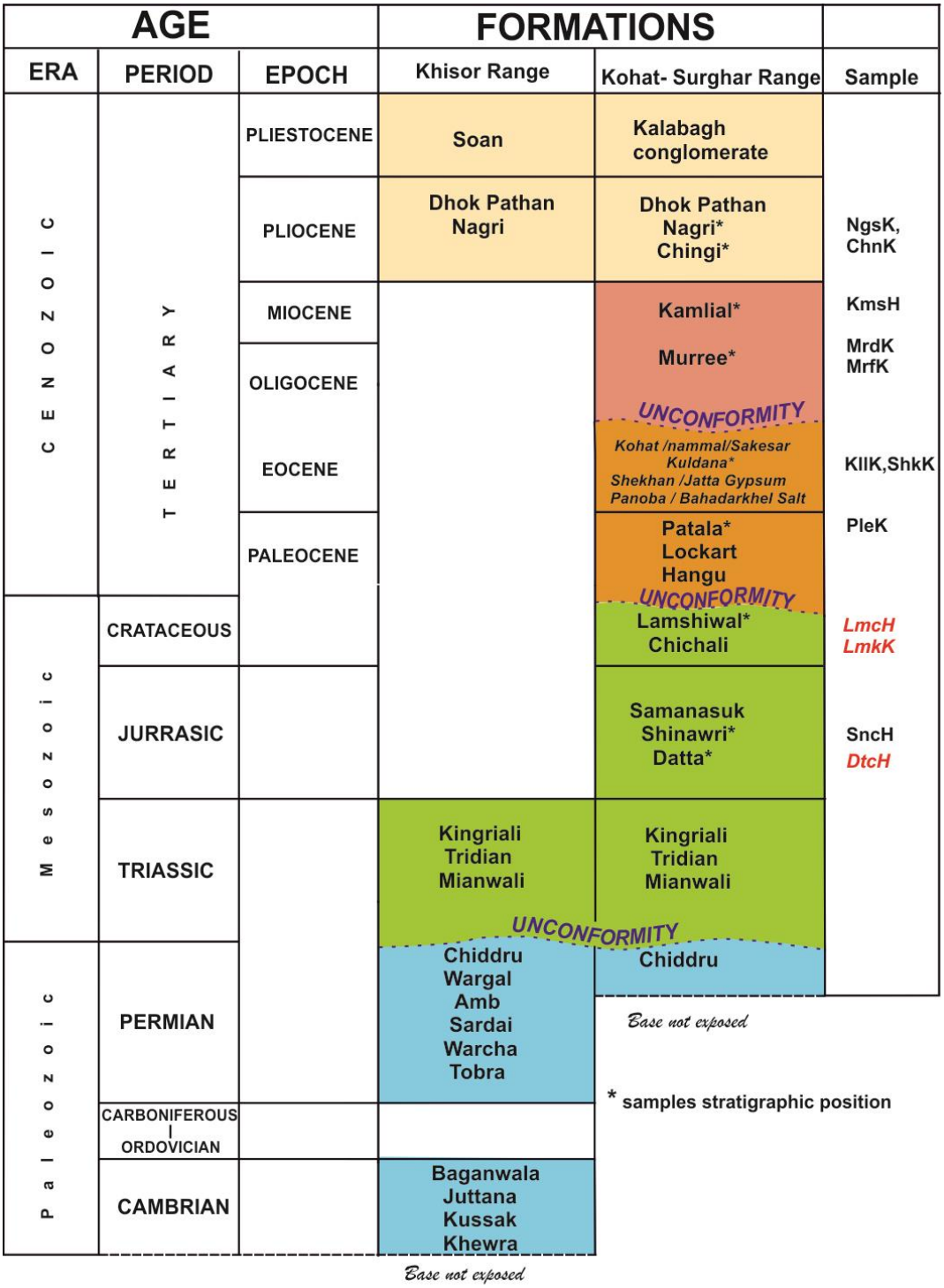

Figure SM 5.1.1. *Generalized stratigraphic column of the Kohat and Trans Indus Ranges. Stratigraphic position of the samples used in the study. Samples labeled with red color were apatite deficient (modified after Meissner et al., (1974); Pivnik and Wells, (1996)).*

2) Section SM 5.2. Low temperature thermochronology data

Thirteen sandstone samples were collected to work out the thermal history of the basin. Only 10 samples produced apatite that are used for AHe and AFT analysis. Details about analytical methods and thermal modelling are provided in the chapter 5 and appendix 1.

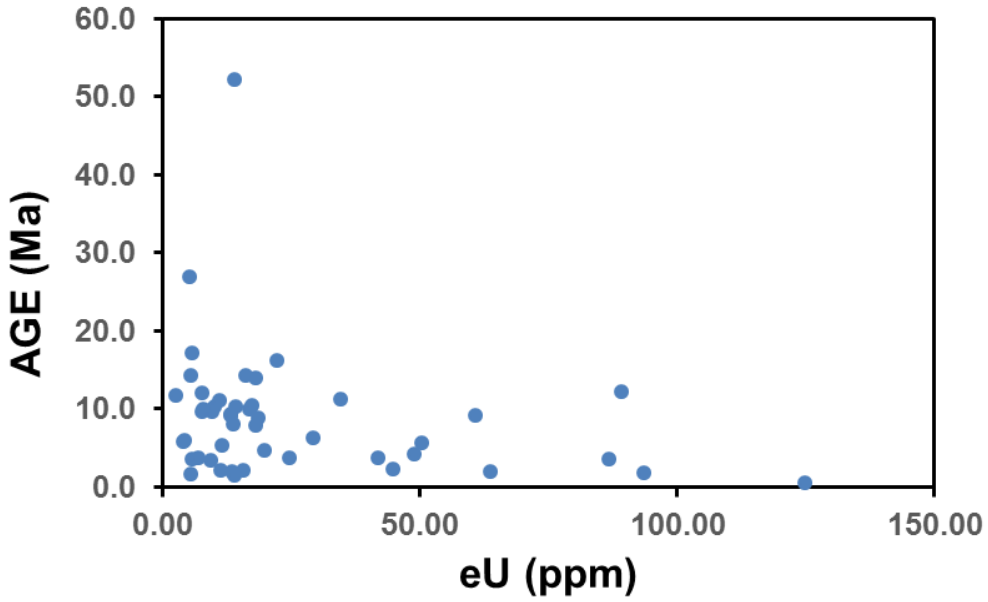

a)

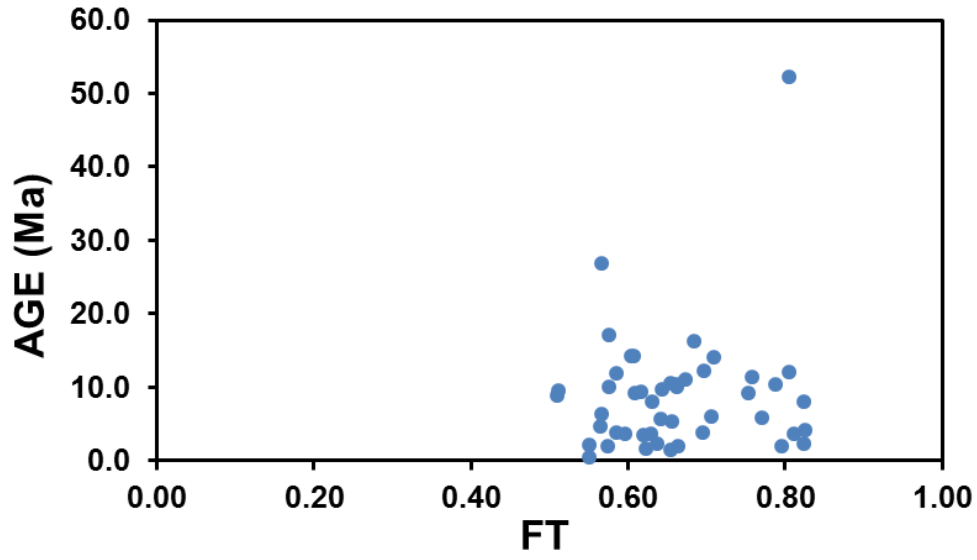

b)

Figure SM 5.2.1. *a) AHe age as a function of effective U (eU), b) AHe age versus FT*

Table SM 5.2.1. *Apatite (U-Th-Sm)/He data*

Sample	Age (Ma)	Error (Ma)	U (ppm)	Th (ppm)	147Sm (ppm)	[U]e	Th/238U	He (nmol/g)	mass (ug)	FT	ESR (mm)	Mean age	error
NgsK-1	2.4	0.1	31.25	57.38	34.70	44.73	1.90	0.48	13.29	0.82	85.2		
NgsK-2	1.9	0.1	60.74	139.48	13.78	93.52	2.37	0.77	8.04	0.80	73.2	**3.2**	**1.0**
NgsK-3	3.8	0.3	11.30	56.56	40.44	24.59	5.17	0.36	2.62	0.69	49.1		
NgsK-4	4.2	0.1	16.07	139.10	19.68	48.76	8.94	0.92	12.51	0.82	85.5		
NgsK-5	3.6	0.1	70.50	69.14	40.39	86.75	1.01	1.36	10.85	0.81	79.6		
SncH-1*	541.6	20.8	0.68	0.50	0.10	0.80	0.75	2.06	20.10	0.85	100.2		
SncH-2	12.2	0.4	66.42	96.27	7.88	89.04	1.50	4.09	2.78	0.70	49.5		
SncH-3	9.4	1.5	6.63	28.44	13.31	13.31	4.44	0.42	1.28	0.62	39.1	**10.6**	**1.4**
SncH-4	10.4	0.3	7.87	27.31	18.72	14.28	3.59	0.64	7.56	0.79	70.7		
KmsH-1*	1472.3	101.4	16.00	16.19	0.09	19.81	1.04	110.65	1.81	0.65	42.9		
KmsH-2*	0.1	0.0	213.30	7137.8	341.03	1890.3	34.57	0.50	2.30	0.68	47.6		
KmsH-3	2.2	0.6	7.67	34.25	17.59	15.72	4.61	0.12	1.64	0.64	41.2		
KmsH-4	2.0	0.6	9.99	14.37	9.21	13.36	1.49	0.09	1.99	0.66	44.6	**1.9**	**0.4**
KmsH-5	1.5	0.4	6.00	33.44	16.04	13.86	5.76	0.08	1.90	0.65	43.3		
PleK-1	11.8	5.1	0.99	6.84	2.82	2.60	7.10	0.10	0.94	0.58	36.1		
PleK-2	10.0	1.1	2.37	61.31	19.52	16.78	26.76	0.53	0.89	0.57	35.3		
PleK-3	10.0	0.7	4.53	14.10	23.49	7.84	3.22	0.29	1.95	0.66	44.4		
PleK-4	17.1	2.5	2.13	14.74	28.46	5.59	7.15	0.31	0.98	0.58	35.4	**11.0**	**2.9**
PleK-5	8.8	1.9	6.66	50.37	9.32	18.50	7.81	0.45	0.57	0.51	30.6		
PleK-6	9.6	3.4	2.85	20.58	16.59	7.69	7.46	0.21	0.60	0.51	30.7		
PleK-7	9.7	1.1	5.21	18.06	26.07	9.45	3.58	0.32	1.53	0.64	41.9		
PleK-8*	26.9	3.4	2.49	11.65	26.05	5.23	4.83	0.45	0.89	0.57	34.6		
MrdK-1*	0.5	0.2	64.76	255.96	128.68	124.91	4.08	0.19	0.78	0.55	33.3		
MrdK-2	14.3	2.6	1.79	15.59	14.00	5.45	9.02	0.26	1.12	0.61	38.2		
MrdK-3	14.0	0.5	5.92	52.05	19.87	18.15	9.08	0.99	2.94	0.71	51.5		
MrdK-4	14.3	1.2	2.99	56.10	26.32	16.17	19.39	0.77	1.09	0.60	37.8	**12.3**	**1.8**
MrdK-5	11.3	0.3	8.74	110.00	25.08	34.59	13.00	1.62	5.18	0.76	61.7		
MrdK-6	10.4	0.8	1.99	33.89	31.95	9.96	17.56	0.38	1.95	0.66	44.4		
MrdK-7	11.1	0.8	3.74	30.86	22.40	10.99	8.53	0.45	2.06	0.67	45.9		
MrdK-8	10.5	0.5	6.90	44.54	20.37	17.37	6.67	0.65	1.68	0.65	43.4		
ShkK-1	2.1	1.1	3.42	32.92	9.32	11.16	9.94	0.07	0.83	0.55	33.4		
ShkK-2	1.6	1.6	2.36	13.32	3.13	5.49	5.83	0.03	1.29	0.62	39.7		

ShkK-3	5.9	0.9	0.60	15.36	16.96	4.21	26.43	0.10	2.63	0.71	50.9		
ShkK-4	5.8	0.3	1.35	11.63	6.06	4.08	8.89	0.10	6.55	0.77	65.3	**3.8**	**1.9**
ShkK-5	5.3	0.7	2.94	36.23	24.54	11.46	12.72	0.22	1.73	0.66	43.5		
ShkK-6	3.5	0.8	1.98	31.02	41.33	9.27	16.18	0.11	1.33	0.62	39.4		
ShkK-7	2.0	0.3	11.24	222.91	52.88	63.63	20.48	0.40	0.90	0.57	35.2		
KllK-1	3.6	1.4	1.35	18.65	9.13	5.73	14.28	0.07	1.04	0.60	37.2		
KllK-2	6.3	0.9	21.76	31.91	6.19	29.26	1.52	0.57	0.88	0.57	34.5		
KllK-3	4.7	0.6	9.73	42.57	17.99	19.73	4.52	0.29	0.82	0.56	34.4	**4.8**	**1.2**
KllK-4	5.7	0.3	27.53	96.52	17.96	50.22	3.62	1.00	1.54	0.64	41.8		
KllK-5	3.8	1.4	2.58	18.85	21.88	7.01	7.55	0.09	0.95	0.58	36.1		
MrfK-1	12.1	0.3	2.21	22.71	4.49	7.55	10.61	0.40	9.61	0.80	76.7		
MrfK-3	8.0	0.3	3.25	44.46	30.02	13.70	14.14	0.50	12.54	0.82	85.0	**10.1**	**2.9**
MrfK-2*	52.3	1.2	3.75	43.28	23.48	13.92	11.93	3.23	9.65	0.81	77.0		
ChnK-1	8.0	0.8	9.12	37.69	32.91	17.97	4.27	0.50	1.34	0.63	40.6		
ChnK-2	9.3	1.2	11.94	5.70	10.24	13.28	0.49	0.41	1.16	0.61	38.3		
ChnK-3	3.7	0.3	25.60	68.93	22.31	41.80	2.78	0.53	1.35	0.63	40.4	**9.3**	**4.5**
ChnK-4	9.2	0.2	24.63	153.57	20.08	60.72	6.44	2.29	4.90	0.75	60.7		
ChnK-5	16.2	0.7	15.24	29.84	10.36	22.25	2.02	1.34	2.16	0.68	47.5		

Note: Average ages and associated errors are calculated as mean and standard deviation of all the aliquots from the same sample.

*Not used for calculating average age.

Table SM 5.2.2. *Apatite Fission Track (AFT) data*

Sample	N	Ns	ρs	Ni	ρi	Nd	ρd	P(χ2)	Age (Ma ± 2σ)
SncH	35	172	1.304	2878	21.823	7720	12.623	91	13.3±1.1
KmsH	22	98	0.978	4953	49.419	5614	13.77	86.6	4.8±0.5
PleK	13	11	0.166	257	3.875	4923	12.01	99	9.1±2.8
MrdK	25	47	0.416	539	4.771	5133	12.498	100	19.2±3.0
ShkK	12	18	0.339	1385	26.091	5614	13.78	98	3.2±0.8
KllK	19	62	1.289	1866	38.782	4923	12.036	99	7.1±0.9
ChnK	23	233	1.964	5800	48.89	4923	12.063	99	8.6±0.6

Notations

(N) = number of grains counted

Ns: Number of spontaneous tracks

ρs: Spontaneous track density ρs x 10^5 (track/cm2)

ρi: Induced track density ρi x 10^5 (track/cm2)

Nd: Number of tracks counted in dosimetry glass CN5

ρd: Dosimetry track density ρd x 10^5 (track/cm2)

P(χ^2): Probability percentage of Chi square value

Age: Pooled ages are calculated with Zeta (ζ) value = 353±7 (HG).

Table SM 5.2.3. *Thermal modeling input parameters*

Sample Name	Time Temperature Box	Low Temperature Constraint	Modern Temperature Constraint	Number of Iterations Pre-Burn in	Post-Burn in
Plek	100-0 Ma 75±75 °C	65-55 Ma 15±15 °C	15±15 °C	200,000	200,000
SncH	300-0 Ma 100±100 °C	200-140 Ma 15±15 °C	15±15 °C	200,000	200,000